SYNTHESIS OF THIOL-FUNCTIONALISED γ-Al_2O_3 AS ADSORBENT FOR Cd^{2+}

NUR IRAIZZATI BINTI SHAIFUDIN

05-4506832 pustaka.upsi.edu.my Perpustakaan Tuanku Bainun Kampus Sultan Abdul Jalil Shah PustakaTBainun ptbupsi

SULTAN IDRIS EDUCATION UNIVERSITY

2025

05-4506832 pustaka.upsi.edu.my Perpustakaan Tuanku Bainun Kampus Sultan Abdul Jalil Shah PustakaTBainun ptbupsi

SYNTHESIS OF THIOL-FUNCTIONALISED γ-Al_2O_3 AS ADSORBENT FOR Cd^{2+}

NUR IRAIZZATI BINTI SHAIFUDIN

DISSERTATION PRESENTED TO QUALIFY FOR A MASTER OF SCIENCE
(RESEARCH MODE)

FACULTY OF SCIENCE AND MATHEMATICS
SULTAN IDRIS EDUCATION UNIVERSITY

2025

UNIVERSITI PENDIDIKAN SULTAN IDRIS
SULTAN IDRIS EDUCATION UNIVERSITY

Please tick (√)
Project Paper ☑
Masters by Research ☐
Master by Mixed Mode ☐
PhD ☐

INSTITUTE OF GRADUATE STUDIES

DECLARATION OF ORIGINAL WORK

This declaration is made on the 22nd day of Sept 2025

i. Student's Declaration:

I, Nur Izzati binti Shaifudin, M20201000752, Faculty of Science and Mathematics (PLEASE INDICATE STUDENT'S NAME, MATRIC NO. AND FACULTY) hereby declare that the work entitled Synthesis of Thiol-Functionalised γ-Al_2O_3 As Adsorbent For Cd^{2+} is my original work. I have not copied from any other students' work or from any other sources except where due reference or acknowledgement is made explicitly in the text, nor has any part been written for me by another person.

Signature of the student

ii. Supervisor's Declaration:

I Ch'm. Dr. Aisyah binti Mohamad Sharif (SUPERVISOR'S NAME) hereby certifies that the work entitled Synthesis of Thiol-Functionalised γ-Al_2O_3 As Adsorbent For Cd^{2+} (TITLE) was prepared by the above named student, and was submitted to the Institute of Graduate Studies as a * partial/full fulfillment for the conferment of Master of Science (Research mode). (PLEASE INDICATE THE DEGREE), and the aforementioned work, to the best of my knowledge, is the said student's work.

22/9/2025
Date

Signature of the Supervisor

DR. AISYAH MOHAMAD SHARIF
Pensyarah Kanan
Jabatan Kimia
Fakulti Sains dan Matematik
Universiti Pendidikan Sultan Idris

UNIVERSITI PENDIDIKAN SULTAN IDRIS
SULTAN IDRIS EDUCATION UNIVERSITY

INSTITUT PENGAJIAN SISWAZAH /
INSTITUTE OF GRADUATE STUDIES

BORANG PENGESAHAN PENYERAHAN TESIS/DISERTASI/LAPORAN KERTAS PROJEK
DECLARATION OF THESIS/DISSERTATION/PROJECT PAPER FORM

Tajuk / *Title*: Synthesis of Thiol-Functionalized γ-Al2O3 As Adsorbent For Cd2+ [redacted]

No. Matrik /*Matric's No.*: M20201000752

Saya / *I* : Nur Iraizzati binti Shaifudin

(Nama pelajar / *Student's Name*)

mengaku membenarkan Tesis/Disertasi/Laporan Kertas Projek (Kedoktoran/Sarjana)* ini disimpan di Universiti Pendidikan Sultan Idris (Perpustakaan Tuanku Bainun) dengan syarat-syarat kegunaan seperti berikut:-
acknowledged that Universiti Pendidikan Sultan Idris (Tuanku Bainun Library) reserves the right as follows:-

1. Tesis/Disertasi/Laporan Kertas Projek ini adalah hak milik UPSI.
   The thesis is the property of Universiti Pendidikan Sultan Idris
2. Perpustakaan Tuanku Bainun dibenarkan membuat salinan untuk tujuan rujukan dan penyelidikan.
   Tuanku Bainun Library has the right to make copies for the purpose of reference and research.
3. Perpustakaan dibenarkan membuat salinan Tesis/Disertasi ini sebagai bahan pertukaran antara Institusi Pengajian Tinggi.
   The Library has the right to make copies of the thesis for academic exchange.
4. Sila tandakan (√) bagi pilihan kategori di bawah */ Please tick (√) for category below:-*

☐ **SULIT/*CONFIDENTIAL***	Mengandungi maklumat yang berdarjah keselamatan atau kepentingan Malaysia seperti yang termaktub dalam Akta Rahsia Rasmi 1972. */ Contains confidential information under the Official Secret Act 1972*
☐ **TERHAD/*RESTRICTED***	Mengandungi maklumat terhad yang telah ditentukan oleh organisasi/badan di mana penyelidikan ini dijalankan. */ Contains restircted information as specified by the organization where research was done.*
☑ **TIDAK TERHAD / *OPEN ACCESS***	

(Tandatangan Pelajar/ Signature)

Tarikh: 22/9/2025

(Tandatangan Penyelia / *Signature of Supervisor*)
& (Nama & Cop Rasmi / *Name & Official Stamp*)
DR. AISYAH MOHAMAD SHARIF
Pensyarah Kanan
Jabatan Kimia
Fakulti Sains dan Matematik
Universiti Pendidikan Sultan Idris

Catatan: Jika Tesis/Disertasi ini **SULIT @ TERHAD**, sila lampirkan surat daripada pihak berkuasa/organisasi berkenaan dengan menyatakan sekali sebab dan tempoh laporan ini perlu dikelaskan sebagai **SULIT** dan **TERHAD**.

Notes: If the thesis is CONFIDENTAL or RESTRICTED, please attach with the letter from the organization with period and reasons for confidentiality or restriction.

ACKNOWLEDGEMENTS

Alhamdulillah, thank you to Allah for His support throughout this journey. My sincerest thanks go to my parents and my brother who supported me. I would like to take this opportunity to express my heartfelt appreciation to ChM. Dr. Aisyah binti Mohamad Sharif, who has been my supervisor and provided me with invaluable guidance, support and encouragement throughout my research. The appreciation also goes to Mrs. Rozita binti Yahaya, my co-supervisor who also provided some of her wisdom and knowledge. I am truly grateful for their expertise and insightful feedback. My heartfelt appreciation goes to Universiti Pendidikan Sultan Idris for their support through the Fundamental University Research Grant Project. Their funding made this research and my study possible. I would like to take this opportunity to thank Professor ChM. Dr. Azlan bin Kamari for allowing me to use his laboratory for adsorption studies, Dr. Yusnita binti Juahir who provided some chemicals for my research, Dr. Nurulsaidah binti Abdul Rahim and Dr. Norlaili binti Abu Bakar who gave me some guidance and ideas. I would like to extend my sincere appreciation to laboratory assistants of the Chemistry Department in the Faculty of Science and Mathematics especially to Mr. Mohd Zurin bin Mahmood who always helped me in my preparations for my experiment, as well as Mrs.Johana, Mr. Ibrahim, Mr. Ahmad Supian, Mr. Mohd Farhan, Ms. Siti Noor Farina, Mrs. Radiah and Mr. Muhammad Yusri of the Department of Biology. I am also grateful for the help received from administrative staff of the faculty and the Institute of Postgraduate Studies. Without them, my journey in finishing my study would be not possible. Lastly, I would like to express my thanks to my fellow lab mates, Amirah, Aidil, Mior and Ong who were always kind and helped me in various ways. I would like to extend my gratitude to my research fellows, Sofiah, Ain, Norlin, Zakiatul, Mira, Dilla, Khaliesa, Aziani, Nabila, Susana, Rusyidah, Fitriani, Tifa, Afiqah, Kamilah, Husna and Wani. May Allah accept this work and grant me success in my future endeavors. I also pray for His blessings upon all those who have contributed to this journey.

ABSTRACT

The modification of gamma alumina (γ-Al_2O_3) derived from used aluminium (Al) beverage cans as an adsorbent for wastewater treatment is an eco-friendly strategy that supports the Al recycling initiative in Malaysia. This research aimed to evaluate the potential of thiol functionalised γ-Al_2O_3 as an adsorbent for Cd^{2+} removal. The research was conducted with three objectives: first the synthesis of γ-Al_2O_3 from Al beverage cans (later named as γ-Al_2O_3(S)) and thiol-functionalised γ-Al_2O_3 (γ-Al_2O_3-BDMT and γ-Al_2O_3-TgA) from both commercial and synthesised γ-Al_2O_3 (named γ-Al_2O_3(C) and γ-Al_2O_3(S) respectively); secondly, the characterisation of the adsorbents and finally the equilibrium adsorption studies in aqueous solution towards Cd^{2+}, which includes adsorption isotherm profile and kinetics. From the adsorption studies, all adsorbents demonstrated an optimum Cd^{2+} removal at pH 6 at an initial Cd^{2+} concentration of 10 mg/L. However, γ-Al_2O_3(C)-BDMT, γ-Al_2O_3(S)-BDMT, γ-Al_2O_3(C)-TgA and γ-Al_2O_3(S)-TgA recorded different equilibrium times (30 min, 20 min, 30 min, and 20 min, respectively). These results indicated that each adsorbent had different performance during the adsorption studies. All the adsorbents were best fitted with the linearised Freundlich isotherm model (regression coefficient, R^2 between 0.991-0.999) and the pseudo-second order adsorption kinetics regression coefficient, R^2 between 0.996-0.999). From the adsorption studies, γ-Al_2O_3(S) was on par with γ-Al_2O_3(C) in removing Cd^{2+}. The characterisation and adsorption studies concluded that the thiol-modified γ-Al_2O_3 demonstrated greater surface characteristics and adsorption capacity towards Cd^{2+} as compared to γ-Al_2O_3, with γ-Al_2O_3(C)-BDMT showing the highest adsorption capacity (463.767 mg/g). These research outcomes could pave the way for the development of cost-effective adsorbents for water treatment using recycled material.

SINTESIS γ-Al_2O_3 BERFUNGSIKAN TIOL SEBAGAI PENYERAP Cd^{2+}

ABSTRAK

Pengubahsuaian gamma alumina (γ-Al_2O_3) yang diperoleh daripada tin minuman aluminium (Al) terpakai sebagai penjerap untuk rawatan air sisa merupakan strategi mesra alam yang menyokong inisiatif kitar semula Al di Malaysia. Penyelidikan ini bertujuan untuk menilai potensi tiol berfungsi γ-Al_2O_3 sebagai penjerap untuk penyingkiran Cd^{2+}. Penyelidikan ini dijalankan dengan tiga objektif: pertama sintesis γ-Al_2O_3 daripada tin minuman Al (kemudian dinamakan sebagai γ-Al_2O_3(S)) dan γ-Al_2O_3 yang difungsikan thiol (γ-Al_2O_3-BDMT dan γ-Al_2O_3-TgA) daripada kedua-dua γ-Al_2O_3 komersial dan sintesis (dinamakan γ-Al_2O_3(C) dan γ-Al_2O_3(S) masing-masing); kedua, pencirian penjerap dan akhirnya kajian penjerapan keseimbangan dalam larutan akueus ke arah Cd^{2+}, yang merangkumi profil isoterma penjerapan dan kinetik. Daripada kajian penjerapan, semua penjerap menunjukkan penyingkiran Cd^{2+} optimum pada pH 6 pada kepekatan Cd^{2+} awal 10 mg/L. Walau bagaimanapun, γ-Al_2O_3(C)-BDMT, γ-Al_2O_3(S)-BDMT, γ-Al_2O_3(C)-TgA dan γ-Al_2O_3(S)-TgA merekodkan masa keseimbangan yang berbeza (30 min, 20 min, 30 min, dan 20 min, masing-masing). Keputusan ini menunjukkan bahawa setiap penjerap mempunyai prestasi yang berbeza semasa kajian penjerapan. Kesemua penjerap paling sesuai dengan model isoterma Freundlich linearis (pekali regresi, R^2 antara 0.991-0.999) dan pekali regresi kinetik penjerapan pseudo-tertib kedua, R^2 antara 0.996 -0.999). Daripada kajian penjerapan, γ-Al_2O_3(S) adalah setanding dengan γ-Al_2O_3(C) dalam mengeluarkan Cd^{2+}. Kajian pencirian dan penjerapan menyimpulkan bahawa γ-Al_2O_3 yang diubah suai tiol menunjukkan ciri permukaan dan kapasiti penjerapan yang lebih besar terhadap Cd^{2+} berbanding dengan γ-Al_2O_3, dengan γ-Al_2O_3(C)-BDMT menunjukkan kapasiti penjerapan tertinggi (463.767 mg/g). Hasil penyelidikan ini boleh membuka jalan kepada pembangunan penjerap yang kos efektif untuk rawatan air menggunakan bahan kitar semula.

CONTENTS

CHAPTER 3 METHODOLOGY

LIST OF TABLES

LIST OF FIGURES

LIST OF ABBREVIATIONS

1,4-BDMT	1,4-Benzenedimethanethiol
3R	Reduces, reuse and recycle
AAS	Atomic Absorption Spectroscopy
ATRP	Atom transfer radical polymerization
ASP	Activated Sludge Process
BCF	Bioconcentration Factor
BET	Brunauer-Emmett-Teller
BJH	Barret-Joyner-Halenda
CNC	Cellulose nanocrystals
EDX	Energy-dispersive X-ray
FAO	Food and Agriculture Organisation
FESEM	Field Emission Scanning Electron Microscopy
FTIR	Fourier-transform Infrared Spectroscopy
KHTP	Kulim Hi Tech Park
MBR	Membrane Bioreactor
MBBR	Moving Red Biofilm Reactor
MOF	metal-organic frameworks
MPTMS	3-mercaptopropyl trimethoxysilane
NWQS	National Water Quality Standards
POME	palm oil mill effluent

SAM	self-assembled monolayer
SDG	Sustainable Development Goals
STP	Sewage treatment plant
TgA	Thioglycolic Acid
TGA	Thermogravimetric Analysis
UiTM	Universiti Teknologi MARA
UN	United Nations
UPSI	Universiti Pendidikan Sultan Idris
USEPA	United States Environmental Protection Agency
WHO	World Health Organisation
XPS	X-ray Photoelectron Spectroscopy
XRD	X-ray diffraction

CHAPTER 1

INTRODUCTION

1.1 Introduction

In this universe, aluminum (Al) beverage cans are commonly used instead of plastic bottles to store beverages. They are utilised due to their low weight, ease of stacking and recycling (The Aluminium Association, 2021). As shown in Figure 1.1, Al beverage cans are among the recycled materials along with papers, plastics and glasses (Sri Priya, 2022).

Figure 1.1

Items that can be recycled

Adapted from Sri Priya (2022)

Cheku et al. (2017) stated that recycling is one of the crucial actions that can have a good impact on the environment. Although Malaysia had launched its recycling program since 1993 (Elias et al., 2016), but only 35.38% of National Recycling Rate in 2023 was achieved. This achievement is still not sufficient to meet the National Recycling Rate target of 40% by 2025 (Zainal, 2024). The 3R program (reduces, reuse and recycle) is essential to implement for increasing the recycle rate and preventing trash from ending up in landfills (Abd Wahab et al., 2014).

Recycling Al is beneficial due to its unique properties, such as high stiffness, high specific strength, lightweight nature, and excellent corrosion resistance (Bhaskar

et al., 2022). These characteristics make Al increasingly valuable across various industries (Brough & Jouhara, 2020). Recycled Al is extensively utilised in multiple sectors, including manufacturing (for producing machining chips, rods, and sheets), construction (for creating window parts and roof covers), food storage and cooking (for making cans, packaging, pans, and ovens), and transportation (for producing cars, aircraft wings, and supporting structures) (Moungomo et al., 2016). The recycling of Al is of critical importance as it contributes significantly to the conservation of Earth's finite resources and offers substantial environmental benefits by reducing energy consumption and minimizing waste (David & Kopac, 2015).

Numerous studies have demonstrated the feasibility of extracting alumina (Al_2O_3) from Al beverage cans as a means of supporting the 3R initiative. Researchers have employed various techniques, including wet-chemical processes (López-Juárez et al., 2018), sol-gel methods (Liu et al., 2011), and precipitation (Adans et al., 2016), to synthesise adsorbents from recycled alumina for the removal of heavy metals from aqueous solutions. This innovative approach not only mitigates the environmental impact of beverage can waste but also contributes to the development of sustainable materials for pollution remediation. In conclusion, recycling represents a cornerstone of sustainable development, offering a viable strategy for waste management, resource conservation, and environmental preservation. By advancing and adopting enhanced recycling practices, society can foster a more sustainable future, ensuring the well-being of both current and future generations while safeguarding the planet's ecological balance.

1.2 Background of Research

Waste generation represents a significant economic and environmental cost associated with globalisation. Among the most concerning forms of waste are chemical byproducts, including heavy metals, heavy-duty liquids (such as oils and greases), fertilisers, and pesticides (Aljamali et al., 2020), which originate from industrial activities and pose severe risks to both human health and ecosystems. Cadmium (Cd), a highly toxic heavy metal, is particularly hazardous, alongside other contaminants such as arsenic (As), copper (Cu), chromium (Cr), lead (Pb), and mercury (Hg) (Ismail et al., 2018). Regulatory bodies, including the World Health Organization (WHO) (Lavado-Meza et al., 2023) and the National Water Quality Standards (NWQS) established by the Department of Environment, Ministry of Natural Resources and Environmental Sustainability of Malaysia (2024), have set stringent limits for Cd concentrations, with a maximum permissible level of 0.003 mg/L for both drinking water and industrial wastewater. Acute exposure to elevated Cd levels can induce immediate adverse health effects, including vomiting, diarrhea, and gastrointestinal distress. Chronic exposure, however, poses even more severe risks, including irreversible lung damage, renal dysfunction due to kidney accumulation, and skeletal weakening, underscoring the critical need for effective waste management and pollution control measures to mitigate these public health and environmental challenges (Yunus et al., 2020).

A prominent example of the detrimental health effects of Cd exposure is the Itai-itai disease, which emerged in Japan during the 1960s. This condition is characterised by osteomalacia, a severe softening of the bones, and was first identified among populations residing near the Jinzu River in Toyama Prefecture, Japan. The

disease predominantly affected women living in proximity to the river, which was contaminated with Cd and used for irrigating rice paddies. By December 28, 1999, a total of 410 individuals had been either officially diagnosed or suspected of suffering from Itai-itai disease due to prolonged Cd exposure. Of these cases, 380 patients had succumbed to the disease, with 85 undergoing autopsies at Toyama University Hospital. As recently as the year 2000, the Toyama local government reported 20 new cases, comprising one man and 19 women, further underscoring the persistent impact of historical environmental Cd contamination. These cases highlight the significant body burden of Cd result (Nishijo et al., 2017).

In Malaysia, a recent incident involving cadmium Cd contamination occurred in Port Dickson, where eight individuals suffered from food poisoning after consuming mussels contaminated with heavy metals (Singh, 2024). This event highlights the ongoing risks posed by Cd pollution in aquatic ecosystems. Furthermore, a study by Ruzi et al. (2023) revealed elevated concentrations of Cd^{2+} in wastewater samples collected from ten selected sewage treatment plant (STP) facilities in Penang, Malaysia. The average Cd concentration across these STPs was measured at 0.13 ± 0.011 mg/L, significantly exceeding the permissible limit of 0.02 mg/L established under Malaysia's Environmental Quality Act. These findings underscore the urgent need for enhanced monitoring and stricter enforcement of environmental regulations to mitigate Cd contamination and safeguard public health and ecosystems from the adverse effects of heavy metal pollution.

Despite the critical need for immediate and stringent measures to address Cd contamination, current practices in Malaysia remain insufficient. According to Ruzi et al. (2023),

the monitoring program for heavy metals in STPs is conducted in an inconsistent and unstructured manner. This inadequacy stems from the primary focus of domestic sewage treatment, which emphasizes biological treatment processes, often neglecting the detection and removal of heavy metals. Consequently, heavy metal contamination may go undetected, leading to the discharge of polluted water from STPs. Furthermore, the adoption of advanced water treatment technologies in Malaysia remains limited. Ab Razak et al. (2015) highlight that Ultra Membrane Filtration, a highly effective method capable of removing Cd and other heavy metals with an efficiency of 92%–100%, is one of the few cutting-edge technologies employed. While this method demonstrates exceptional performance in heavy metal removal, its high operational and maintenance costs pose significant barriers to widespread implementation. These challenges underscore the urgent need for improved regulatory frameworks, enhanced monitoring systems, and cost-effective solutions to mitigate heavy metal contamination and ensure the safety of water resources in Malaysia.

In the recent review written by Kristanti et al. (2023), Malaysia has been implementing some technologies for municipal wastewater treatment to ensure the provision of clean water. These technologies include the Activated Sludge Process (ASP), Membrane Bioreactor (MBR) and Moving Red Biofilm Reactor (MBBR). The ASP uses microorganisms to break down organic matter that exist in wastewater. The process uses a biological reactor that contained microorganisms, oxygen and wastewater. One of the significant advantages of ASP is its low-cost of set-up and maintenance. The MBR technology is a process that merges conventional biological treatment with membrane filtration. Basically, MBR uses a membrane barrier which is made of ultrafiltration or microfiltration membranes. On the other hand, MBBR technology uses biofilm growth on mobile plastic carriers which move freely within the reactor. Generally, this MBBR technology utilised by introducing wastewater into the reactor mentioned

previously. The advantages of using this MBBR technology is that it can remove up to 95% of organic matter as well as can handle fluctuations in flow and organic loading. Malaysia is progressively adopting advanced technologies for water treatment to address its environmental challenges and ensure sustainable water management.

Malaysia is a developing nation, therefore appropriate monitoring heavy metals, especially in wastewater, is needed (Shahbudin & Kamal, 2021). In order to overcome the deficiency of Cd-free water treatment, a low-cost, easily maintained process or product must be developed.

1.3 Problem Statement

According to Okon Recycling (2023), about 65% of Al beverage cans were recycled from over 80 billion cans every year. Even though the number is significant, the fact that the remaining almost 30 billion cans that end up in landfills are still cannot be ignored. The worst part is Al takes around 200-500 years to be fully degraded in landfill conditions, exacerbating its environmental impact. According to Sengupta (2023), Malaysians are among the top consumers of Al beverage scrap, thus the issue with Al is something should be addressed seriously. In 2021, Malaysia emerged as the fourth-largest importer of Al beverage scrap globally, with imports valued at $1.33 billion (Sengupta, 2023). For instance, in August 2023 alone, the United States exported 26,400 tons of Al scrap to Malaysia, highlighting the country's significant reliance on this material

Despite this, public awareness of the benefits of recycling remains low, leading to increased environmental and economic costs. The improper disposal of Al cans not only contributes to landfill waste but also necessitates higher government expenditure on the production of new Al cans, which is both resource-intensive and environmentally damaging. The production of primary Al is associated with the emission of harmful gases, including perfluorocarbons, hydrogen fluoride, polycyclic aromatic hydrocarbons, and sulfur oxides (SOx) (Brough & Jouhara, 2020). Recycling Al, however, can significantly reduce these emissions, offering a more sustainable alternative to primary production. Despite this, the recycling rate in Malaysia remains suboptimal, underscoring the need for greater public and industrial engagement in recycling initiatives.

In addition to Al beverage can waste, industrial activities contribute significantly to environmental pollution in Malaysia. The "Eleventh Malaysia Plan," introduced in 2015 by the Economic Planning Unit of the Prime Minister's Department, identified manufacturing as one of the country's seven primary priority areas (Liao et al., 2018). The manufacturing sector, however, generates substantial amounts of chemical waste, including heavy metals such as Cd, Pb, Hg, and As, which pose serious risks to human health and the environment. Poor industrial waste management can lead to the accumulation of these heavy metals, increasing the risk of cancer and other health issues (Ibrahim et al., 2020).

Malaysia also has problems related to Cd pollution like other countries in the world. According to Ahmed and Mokhtar (2020), the United States Environmental Protection Agency (USEPA) has designated Cd as one of the dangerous metals. In 2019, Astro Awani released

an article detailing the discovery of numerous heavy metals at the harbour and river mouth along the Strait of Malacca. A study conducted by Associate Prof. Dr. Ong Meng Chuan and his team at Universiti Malaysia Terengganu revealed elevated levels of heavy metals, including Cd, in Johor's harbours, Klang Port, and Penang's water mouths. This pollution poses a significant risk to marine life, particularly shellfish, and increases the likelihood of heavy metal poisoning in humans (Bernama, 2019).

Cd contamination is also prevalent in Malaysia's water and soil systems. At Kulim Hi-Tech Park (KHTP), the Cd concentration in tap water was measured at 0.0177 ± 0.0017 mg/L, exceeding the permissible limit of 0.003 mg/L (Zanon et al., 2023). Similarly, a study of the Telibong Water Treatment Plant 2 in Sabah found Cd concentrations as high as 0.846 mg/L in the treated water supply, with Universiti Teknologi MARA (UiTM) Sabah recording the highest Cd concentration at 0.880 mg/L (Aini, 2015). These findings suggest that Cd contamination occurs during the water treatment process, highlighting the need for improved filtration and monitoring systems. The increase in Cd contamination in the water supply after treatment indicates that Cd contamination occurred during the treatment process (Aini, 2015).

In agricultural settings, Cd contamination in soil has been shown to affect crop quality and safety. A study conducted in Jengka, Pahang, revealed that Cd had the highest Bioconcentration Factor (BCF) among the heavy metals studied (Cd, As, and Pb) in three green vegetables: Pak choi, Amaranth, and Caisin (Sulaiman et al., 2020). The BCF values for Cd were particularly high, with Pak choi (leaves-soil = 15.62, root-soil = 76.00), Amaranth (leaves-soil = 33.16, root-soil = 51.88), and Caisin (leaves-soil = 31.21, root-soil = 87.98). These findings indicate that Cd is readily absorbed by plant

roots and accumulated in edible parts, posing a risk to consumers. The high BCF values suggest that Cd contamination in soil and irrigation water may be contributing to this issue, necessitating further investigation and remediation efforts.

Given the dual challenges of rising Al waste and Cd pollution in Malaysia, this study aims to explore the potential of recycled Al beverage cans as a resource for mitigating Cd contamination. Specifically, the study will investigate the synthesis of gamma alumina (γ-Al_2O_3) from recycled Al cans and its functionalisation with 1,4-benzenedimethanethiol (1,4-BDMT) and thioglycolic acid (TgA) to produce adsorbents for Cd^{2+} in aqueous solutions. The proposed adsorbents, γ-Al_2O_3-BDMT and γ-Al_2O_3-TgA, are expected to exhibit high adsorption capacities due to the intercalation of Al atoms in γ-Al_2O_3 with the -SH functional groups of 1,4-BDMT and the -COOH/-SH groups of TgA, respectively. This approach not only addresses the issue of Al waste but also provides a sustainable solution for Cd pollution remediation.

1.4 Purpose of the Research

The goal of this study is to create new Cd^{2+} adsorbents by intercalating between γ-Al_2O_3 and TgA and 1,4-BDMT respectively. γ-Al_2O_3 is created via precipitation process from recycled Al beverage cans. Those new adsorbents are simple, convenient to use and cost effective.

1.5 Objectives of the Research

1. To synthesise and characterise γ-Al_2O_3, γ-Al_2O_3-BDMT and γ-Al_2O_3-TgA adsorbents.
2. To elucidate the adsorption studies of adsorbents γ-Al_2O_3-BDMT and γ-Al_2O_3-TgA as Cd^{2+} absorbent.
3. To investigate the kinetic of adsorption reactions using pseudo first order and second order models.

1.6 Research Questions

1. What are the structural, morphological, and physicochemical characteristics of γ-Al_2O_3, γ-Al_2O_3-BDMT, and γ-Al_2O_3-TgA adsorbents?
2. How effective are γ-Al_2O_3-BDMT and γ-Al_2O_3-TgA in adsorbing Cd^{2+} ions from aqueous solutions?
3. What is the adsorption isotherm of γ-Al_2O_3-BDMT and γ-Al2O3-TgA for the removal of Cd^{2+} ions from aqueous solutions?
4. What are the adsorption kinetics of Cd^{2+} ions onto γ-Al_2O_3-BDMT and γ-Al_2O_3-TgA based on pseudo-first order and pseudo-second order models?

1.7 Research Hypothesis

The three primary phases of this study are depicted in Figure 1.2 below. In stage 1, precipitation method is expected to synthesise γ-Al_2O_3 from Al beverage cans. The synthesis of the γ-Al_2O_3-TgA and γ-Al_2O_3-BDMT adsorbents is also expected to be done in this stage. In stage 2, the characterisations of all the synthesised adsorbents are expected to be conducted.

In Stage 3, both stages' efficacy and processes will be examined using three parameters; pH of Cd^{2+} solution, initial concentration of Cd^{2+} solution and contact time. The stage 3 is expected to successfully get the optimum condition as Cd^{2+} adsorbents. The adsorbents' selectivity and sensitivity will both increase with intercalation. Thus, boost the adsorbents' adsorption capacity and lower Cd^{2+} in an aqueous environment.

Figure 1.2

The conceptual framework of the research

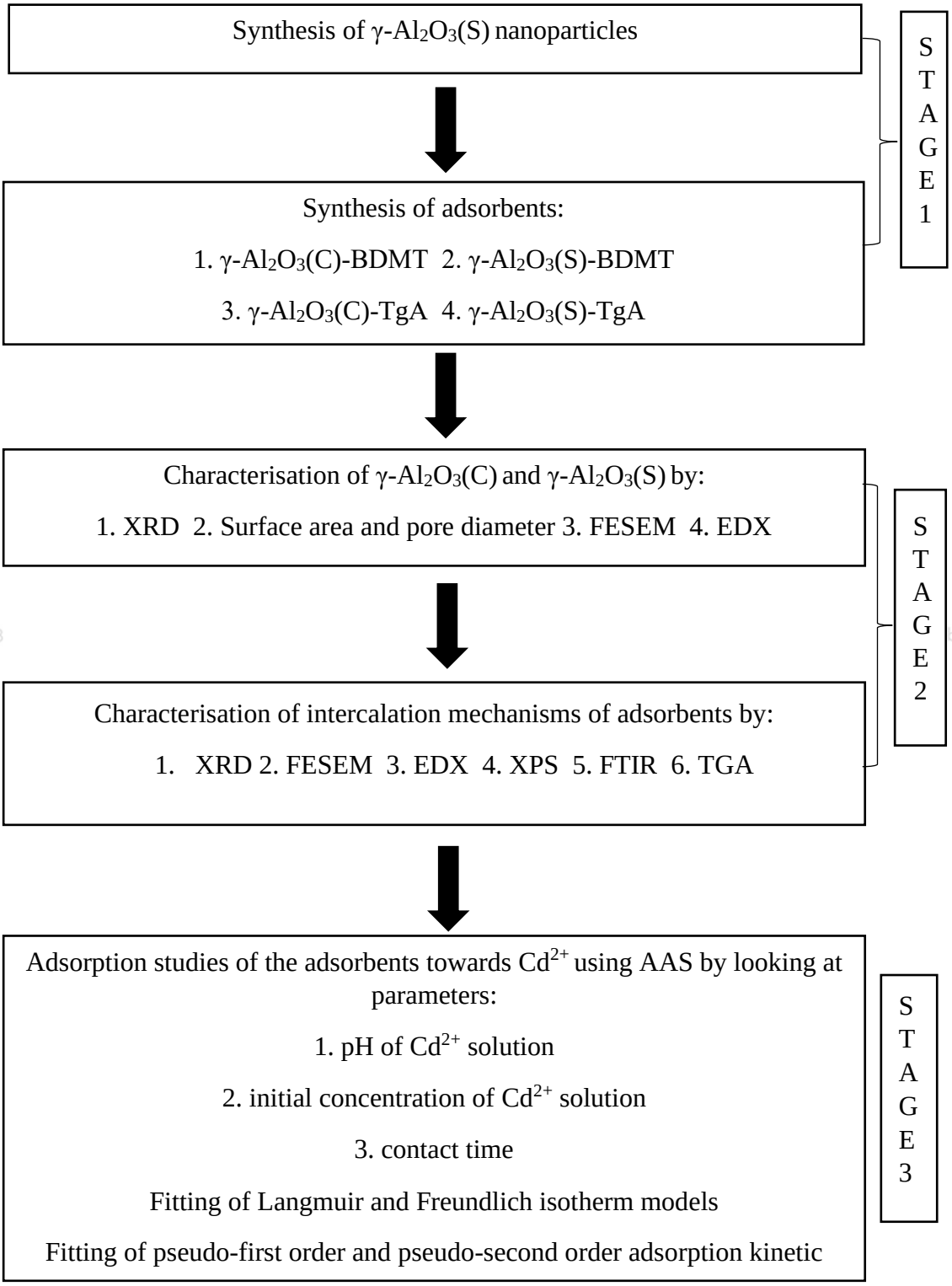

1.8 Research Scopes

This research focuses on a single heavy metal which is Cd. The heavy metal was chosen based on the availability of suitable instruments that can be used in Universiti Pendidikan Sultan Idris (UPSI). The study utilises recycled Al materials, specifically beverage cans, as they represent the most common source of Al scrap (Tabereaux & Peterson, 2024). In addition, this study focuses on the synthesis and characterisation of γ-Al_2O_3 and its functionalised forms, γ-Al_2O_3-BDMT and γ-Al_2O_3-TgA, as potential adsorbents. The adsorption performance of these materials is specifically investigated for the removal of Cd^{2+} ions from aqueous solutions. The study is limited to evaluating adsorption kinetics using pseudo-first order and pseudo-second order models to understand the adsorption mechanism. Experimental conditions are controlled within a laboratory setting, and no real environmental samples are analysed. Additionally, the scope is restricted to Cd^{2+} ions, excluding other heavy metals or contaminants that may coexist in complex environmental systems. These limitations define the study's boundaries while providing a foundation for future research on adsorbent optimization and broader environmental applications.

1.9 Importance of Research

1. The product, γ-Al_2O_3-BDMT and γ-Al_2O_3-TgA will be able to help industry in providing alternative method to reduce Cd contamination in water body. The knowledge of this new adsorbents will be able to help future researchers in researching these adsorbents' capability to find new or better optimum

condition to adsorb Cd^{2+}. The kinetic studies of these adsorbents also will be able to provide information regarding the reaction pathways and the mechanisms involved in the adsorption of sorbate by the sorbent (Mustapha et al., 2019).

2. Production of the adsorbents, which is used γ-Al_2O_3 synthesised from Al beverage cans, will able to help to reduce Al beverage cans wastes in environment. Apart from sending Al beverage cans to landfills and factories to be recycled, the cans also can be reused as materials in water treatment research. In the same time, citizens also provide their contributions in water treatment research by implementing 3R for Al beverage cans.

1.10 Summary

Generally, Al is highly valued for its properties, including high stiffness, high specific strength, light weight and good corrosion resistance. It is also a recyclable material. In Malaysia, Al is widely used in various sectors such as construction, food and cooking and transportation. However, despite being recyclable, many Malaysians choose not to recycle Al. Instead, a significant amount of Al is sent to landfills, even though Malaysia has launched a 3R program.

In addition to Al waste, chemical waste is also a serious problem that needs attention. Chemicals such as Cd can cause pollution in water bodies. Cd has been associated with various cases and diseases, such as Itai-itai disease, which was first

reported in Japan. Many researchers are working on treating and removing Cd from water bodies. This research contributes to the development of adsorbents made from Al beverage cans, which can be used to treat water contaminated with Cd. The hope is that this research will benefit future scholars conducting research in the same field.

CHAPTER 2

LITERATURE REVIEW

2.1 Introduction

The globe has entered the age of technology since the start of the twenty-first century. As the global population is growing, the technological also advancing. In November 2022, there were 8 billion people on the planet. The United Nations (UN) projects that number would rise to approximately 10.4 billion by the 2080s (Norrman, 2023). Billions of people are supported by a multitude of industries. Malaysia, for instance, is one of the nations actively integrating technology into its development strategies to meet the demands of its populace. Malaysia's population has been steadily increasing, with an estimated 33.4 million people in 2023, up from 32.7 million in 2022 (New

Straits Times, 2023). This demographic growth, coupled with rapid urbanisation, has spurred the expansion of industrial activities. However, this industrialisation has also led to unintended environmental consequences, including the release of heavy metals into ecosystems (Saeed et al., 2022).

2.2 Heavy Metals

Heavy metals are ubiquitously present in the environment. Certain substances are hazardous to live cells and exhibit no essential biological functions (Kenawy et al., 2018). Generally, heavy metals can be classified into two categories based on their properties and effects. The first category consists of heavy metals that are essential for human health such as zinc (Zn), iron (Fe), Cr, Cu and cobalt (Co). For instance, Zn can be taken ideally around 15 mg per day and Fe is around 7 mg per day (Zoroddu et al., 2019). The second category consists of heavy metals that are nonessential for human health such as As, Pb, Hg and Cd which are extremely harmful even at low quantities (Saeed et al., 2022). This study focuses on Cd, a heavy metal that will be discussed in detail in section 2.2.1.

Heavy metals are known to pose significant risks to human health and the environment due to their carcinogenic properties, severe toxicity, non-biodegradability, and potential to cause harm (Sulaiman et al., 2020). Heavy metal pollution has been linked to numerous adverse environmental impacts, further exacerbating ecological and public health concerns (Bagheri et al., 2019). Recent research has demonstrated that heavy metals negatively affect microbial populations, exerting selective pressure that

can lead to co-selection mechanisms for antibiotic resistance (Silva-Holguín et al., 2023). This suggests that the emergence of antibiotic-resistant microorganisms is not solely driven by the presence of antibiotics but is also influenced by heavy metal exposure. To mitigate these risks, the World Health Organization (WHO) has established permissible limits for the safe consumption of each heavy metal, as outlined in Table 2.1.

Table 2.1

The limit for heavy metal in drinking water set by WHO

Heavy Metal	mg/L	Reference
Zn	3.000	(Beyene & Berhe, 2015)
Fe	0.300	(Abdulhadi et al., 2021)
Cr	0.050	(Ahmed & Mokhtar, 2020)
Cu	2.000	(Al-Saydeh et al., 2017)
Co	0.005	(Beyene & Berhe, 2015)
As	0.010	(Frisbie & Mitchell, 2022)
Pb	10.000	(Zhang et al., 2016)
Hg	0.001	(Deng et al., 2020)
Cd	0.003	(Pang et al., 2022)

2.2.1 Cadmium

Cadmium, also known as Cd, belongs to Group II B of the periodic table. It is a soft metal with a dazzling silvery-white appearance. It has an atomic number of 48, an atomic weight of 112.41 u, and a density of 8.64 g/cm^3 (Unsal et al., 2020). Cd has an

oxidation state of +2 (Branca et al., 2020) and is classified as a semi-volatile metal (Yu et al., 2021). Its biological half-life ranges from 10 to 35 years, as reported by Ahmed and Mokhtar (2020). Cd ores are not abundant, but Cd may be found in most Zn ores given its isomorphic substitution to Zn (Genchi et al., 2020). Cd is considered one of the most toxic pollutants in the environment and has a tendency to bioaccumulate, posing a serious threat to human health (Mohammadnia et al., 2018). Because of its significant persistence and high solubility in water (Ahmed & Mokhtar, 2020), Cd is a substance that is challenging to be degraded (Zhao et al., 2021). WHO has established a standard stating that the maximum concentration of Cd^{2+} in drinking water should not exceed 0.003 mg/L (Pang et al., 2022). Cd is primarily obtained from industries such as plastics, paint pigments, smelting, electroplating, and batteries, including nickel-cadmium and silver-cadmium batteries (Khan et al., 2020; Sulaiman et al., 2020). Additionally, corroded galvanized pipes (Ahmed & Mokhtar, 2020) and palm oil mill effluent (POME) contribute to the increasing levels of Cd due to the presence of numerous heavy metals (Oyekanmi et al., 2019). The wastewater released by these industries has the potential to contaminate nearby waterways.

Cd can enter our bodies and accumulate in our organs through the food chain (Zhang et al., 2023). Similar to other heavy metals, chronic exposure to Cd can cause serious lung damage, accumulate in the kidneys leading to renal disease and weaken bones. Consuming extremely high levels of Cd can result in vomiting, diarrhea, and stomach discomfort (Yunus et al., 2020). The negative impacts of Cd can also affect microorganisms. If bacteria are used for heavy metal bioremediation, Cd can cause denaturation, oxidative damage, and reduce the microbes' ability to perform this task (Igiri et al., 2018).

The problems associated with Cd should not be ignored because it can have negative impacts on our bodies. Numerous studies have been published on the levels of Cd in water bodies, especially rivers, worldwide. Research has indicated that Cd levels in the Nubui River, Ghana, exceed recommended guideline values, signifying significant pollution. Readings from two out of five sampling stations ranged between 0.0215 mg/L and 0.0383 mg/L (Norvivor et al., 2024). Similarly, the Gomti River in India recorded Cd levels of 0.00554 mg/L, which is twice the permissible limit of 0.003 mg/L (Pandey, 2024, August 26). A study by El-Saadani et al. (2022) revealed alarming levels of Cd contamination in the Nile River, Egypt. Out of 23 sampling locations, seven exceeded the acceptable limits, specifically in Cairo, Giza, Helwan, Beni Suef, Sohag, Qena, and Samalut, with concentrations of 0.009, 0.01, 0.008, 0.007, 0.007, 0.006, and 0.006 mg/L, respectively.

This issue is also present in Malaysia. Salam et al. (2020) conducted a study to determine Cd level in fish samples collected from the Perak River. The study found that consumers of fish in the Perak River would not experience any negative health effects as their estimated daily intakes of Cd (0.0065-0.0085 mg/L/day) were lower than the study's findings 0.16-0.49 mg/L. However, prolonged consumption of fish from that river poses a potential cancer risk due to the carcinogenic hazards associated with Cd. The target risk values for the studied fish species in the range from 4.12×10^{-3} to 5.35×10^{-3} L/kg. The values are within 10^{-3} and 10^{-4}, which is unacceptable. To compare pollution levels in the future, the study recommended conducting regular investigations that also consider other aquatic organisms and different seasons. Recently, researchers have focused on the removal of heavy metals from wastewater due to the aforementioned risks. This study contributes to this trend by treating Cd-contaminated

water and providing valuable references for future scholars.

2.3 Wastewater

Wastewater is one of the main contributors to ecosystem damage (Wahyuhadi et al., 2023) alongside sewage disposal, effluent treatment facilities, and industrial discharge, particularly in rivers systems (Ahmed et al., 2020). Wastewater contains various contaminants such as pesticides, dyes, heavy metals and pharmaceuticals, which are a direct consequence of the growth in the chemical and pharmaceutical industries, as well as agricultural practices (Liu et al., 2021).

2.3.1 Wastewater Treatment

Researchers are currently working on developing advanced technology to meet the increasing demand for clean water (Mahmoud et al., 2021). This is particularly significant because one of the Sustainable Development Goals (SDG) for 2030 is to ensure access to safe drinking water for households (Ahmed & Mokhtar, 2020). As a result, there are various water treatment techniques available. In general, the three stages of wastewater treatment are primary, secondary and tertiary. Table 2.2 provides an overview of the data for each of these steps (Ali et al., 2020).

Table 2.2

Three stages of wastewater treatment

Stages	Techniques	Details
Primary	Screening (first operation in the wastewater treatment), filtration, coagulation-flocculation, centrifugation, gravity and sedimentation.	Safeguard the implement and/or water plant from possible harm or obstruction by removing big non-biodegradable floating solids or sediments in the wastewater (paper, wood, hair, cloth debris, kitchen waste, fibre and faecal solids). In coagulation technique, activated silica, alum or iron materials are used sometimes to remove unsettled solids.
Secondary	Using different biological microbes, normally bacterial and fungal strains to remove different pollutants.	Required for surface water because biological, inorganic and organic are the responsible one to initiate contamination. The microbes reacting with organic pollutants, producing by-products such as water, carbon dioxide and ammonia gas.
Tertiary	Precipitation, oxidation, reverse osmosis, ion exchange, adsorption, etc.	Final treatment for water purification. To get a quality of water that is within the standard of human consumption. Necessary to remove toxic anions and cations. Required for surface water because biological, inorganic and organic are the responsible one to initiate contamination.

Adapted from Ali et al., 2020

From Table 2.2, the primary stage involves the removal of larger contaminants that are visible to the naked eye, while the secondary and tertiary stages address smaller

contaminants that cannot be seen. As noted in Table 2.2, the secondary stage employs biological microbes to treat water contaminated with organic pollutants. The tertiary stage further processes the water by removing cations and anions until it reaches a level safe for human consumption. Hence, tertiary stage is our focus for this research to remove Cd from aqueous solution by using adsorption method.

2.4 Current Methods to Remove Cd^{2+}

There are several methods available for removing Cd^{2+} in contaminated water. Membrane filtration, coagulation, chemical precipitation, ion exchange and adsorption are commonly used techniques in water treatment to remove Cd^{2+} from water (Mohammadnia et al., 2020). The advantages and disadvantages of each method are discussed in the following subtopics.

2.4.1 Membrane Filtration

This method employs several types of filtrations, namely reverse osmosis, nanofiltration, and ultrafiltration (Xia et al., 2017). The choice of filtration method depends on the size of the particles to be removed (Ali et al., 2020). It utilises a semi-permeable membrane to allow only water to pass through (Prabhu & Prabhu, 2018). According to them, this method applies pressure to separate the concentrated side, which contains impurities, from the dilute side, which contains pure water. The advantages of this method include the decolorization and desalination processes, which produce pure water using reverse osmosis (Ali et al., 2020). However, there are several

disadvantages associated with this method, such as high maintenance costs caused by the operational system and the requirement for high pressures, as well as the need for significant capital investment (Xia et al., 2017). Research by Zhang et al. (2011) and Karim et al. (2019) exemplifies the application of this method. Zhang et al. (2011) investigated the use of 5,10,15,20-Tetrakis (1-methyl-4-pyridinio) porphyrin tetra (p-toluenesulfonate), an optical indicator ligand for Cd^{2+}. They immobilised the ligand onto a porous chitosan/cellulose acetate blend membrane through polymer brushes that were grafted onto the membrane surface using a surface-initiated atom transfer radical polymerisation (ATRP) method. In contrast, Karim et al. (2019) focused on nanofiber membranes fabricated from poly (vinyl alcohol)/chitosan (PVA/Chi) using an electrospinning technique. Their research aimed at achieving selective and high adsorption of Cd^{2+} and Pb^{2+}, contingent upon the acidity of the solution. Both researches removed Cd^{2+} in aqueous solution.

2.4.2 Coagulation

According to Prabhu and Prabhu (2018), this method, also known as flocculation, uses certain chemicals to form flocs. The flocs are formed when finely divided particles combine together to form larger particles and settle out. Ren et al. (2022) also mentioned that coagulation is one of the most recognized water treatment techniques. Although it is usually the first step in the drinking water treatment process, it has several disadvantages that have prompted researchers to explore this method further in order to overcome its weaknesses. As mentioned earlier, the formation of flocs or sludge is a byproduct of this method. Treating and disposing of the flocs or sludge adds to the overall cost. Additionally, this method requires a large amount of coagulants, especially

for water contaminated with algae. A large amount of coagulants results in a significant quantity of sludge. Furthermore, this method involves complex variables that need to be considered, such as water matrices and operating conditions. Figure 2.1 shows a general view of how coagulation-flocculation process works.

Figure 2.1

Coagulation-flocculation process in turbid water treatment

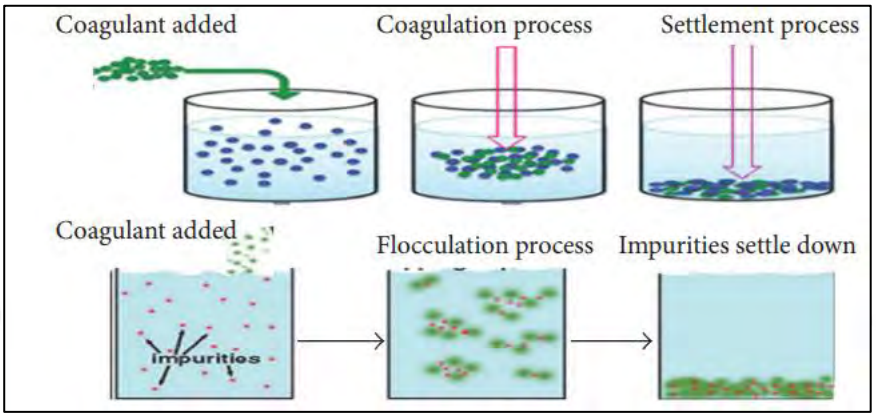

Adapted from Beyene et al., 2016

Examples of research utilising this method include a study by Oyewo et al. (2019), which modified and utilised cellulose nanocrystals (CNC) derived from sawdust as coagulants for the removal of Cd^{2+} and Ni^{2} from water and another by Malakootian et al. (2017), which employed ferric chloride as a coagulant.

2.4.3 Chemical Precipitation

Generally, this method uses separation as a principle by first separating contaminants from the solution as sediment, before being filtered or centrifuged. The precipitate is

formed from a complex between heavy metal ions and the precipitation agent. One of the most important parameters to be regulated in this method is pH. The success of this method also depends on factors such as the type and concentration of the heavy metal ions in the solution, the presence of other compounds, the precipitation reagent used and the reaction conditions. There are several factors that make the calculation of chemicals used in this method difficult, including mixing modes, pH and alkalinity of the wastewater, point of injection and phosphate level (Pohl, 2020). This method has a simple operation and low capital cost, but it has drawbacks such as the formation of sludge and the need for additional operational costs for sludge disposal (Al-Ghouti et al., 2019). Examples of research employing this method include a study conducted by Loughlaımı et al. (2024) which utilised calcium oxide as a precipitating agent. Additionally, Abu-El-Halawa and Zabin (2017) focused on preparing two types of dithiocarbamate ligands; one aliphatic (diethyldithiocarbamate) and one aromatic (diphenyldithiocarbamate) to act as chelators for removing Cd^{2+} from contaminated water.

2.4.4 Ion Exchange

The method relies on resin for ion exchange between Cd^{2+} in water and ions on the resin (Xia et al., 2017). There are two types of ion exchange membranes in this method; anion and cation exchangers (Ali et al., 2020). Ali et al. (2020) explained that anion exchangers are membranes charged with positively charged ions like NH^{3+}, NH^{2+}, and NR^{3+}. These membranes allow anions to pass through but not cations. On the other hand, cation membranes are charged with negatively charged ions like SO_3^{2-}, $RCOO^-$, and PO_3^{3-}. These membranes only allow cations to pass through but not anions. In 1990,

the removal of heavy metals from wastewater using clinoptilolite, one of natural zeolite species was studied. The results indicated that the ion exchange loading values could range from 1.6 mg/g for Pb^{2+} to 0 mg/g for Cr^{3+}. The selectivity of the heavy metals examined is ranked as follows: $Pb^{2+} > Cd^{2+} > Cu^{2+} > Co^{2+} > Cr^{3+} > Zn^{2+} > Ni^{2+} > Hg^{2+}$ (Babel & Kurniawan, 2003). The research showed that the ion exchange method also has the potential to remove Cd^{2+} from wastewater. This method has fast kinetics, high removal efficiency, and treatment capacity. However, it has some disadvantages, including low selectivity, high cost of synthetic resins, and the formation of serious secondary pollution during resin regeneration (Al-Ghouti et al., 2019). Figure 2.2 shows a general view of ion exchange method.

Figure 2.2

Ion exchange method

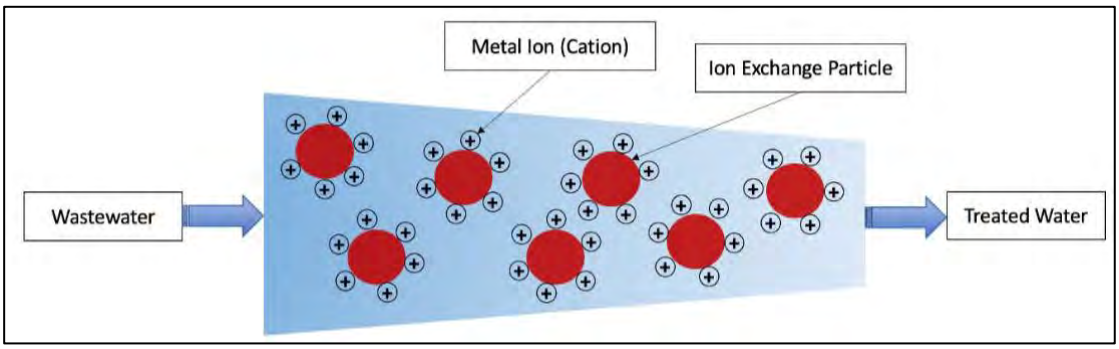

Adapted from Muhaidin et al., 2024

Some research that utilised this method includes a study by Elfeghe et al. (2022), which used 22 ion exchange resins with different functional groups which were among the resins, the Dowex G-26 resin, featuring a sulfonic functional group, and the Puromet™ MTS9570 resin, which contains both sulfonic and phosphonic functional groups, demonstrated exceptional efficacy in the removal of Cd^{2+}. Maximum Cd

removal rates of 99.2% and 98.9% were achieved for the G-26 and MTS9570 resins, respectively, under the following conditions: an initial cadmium concentration of 1000 mg/L, an initial solution pH of 5.0, an adsorption duration of 30 minutes, with a resin dosage of 0.01 mg/L for G-26 and 0.025 mg/L for MTS9570. This is in addition to a study by Wong et al. (2014), which utilised chelating resin D-401. Within the pH range of 2.5 to 5.5, the resin exhibits its maximum sorption capacity of 2.18 mmoles of Cd per gram of resin at pH 5.

2.5 Adsorption

Adsorption is the most promising technique among the previously mentioned ones due to its high efficiency, affordability and ease of use (Zhao, 2021).

Adsorption is generally defined as the process of allowing a fluid to pass through an adsorbent, which is a porous substance, in order to change the concentration of the fluid at the end (Yusuff et al., 2019). The choice of adsorption materials plays a crucial role in this process (Zhang et al., 2023). Therefore, the adsorbent is a key component of this procedure.

Adsorption processes can be classified into two categories; chemical adsorption and physical adsorption (Chen et al., 2022). The chemisorption process involves the formation of a chemical bond, usually a covalent bond, between an adsorbate and an adsorbent, while the physisorption process involves weak interactions, often Van der Waals forces, between an adsorbate (metal ions) and an adsorbent (Velempini & Pillay,

2019). Sahmoune (2019) states that while chemisorption is irreversible, physisorption is reversible. Figure 2.3 provides a simplified overview of chemical and physical adsorption.

This method is affected by six factors, namely the ionic strength effect, initial ion concentration effect, temperature effect, contact time effect, adsorbent dosage effect and pH effect (Tahoon et al., 2020). The study explains that extra ions existing in a solution play a very important role in the adsorption efficiency. Occasionally, the effect of ionic strength on the adsorption process is neglected due to the weak attraction of the adsorbent to the extra ions, compared to the desired metal ions. Meanwhile, it is a commonly known fact that increasing the concentration of target metal ions will increase the adsorption process until a certain point, after which the process will decrease because the target metal ions reach the optimum concentration.

Small concentrations of toxic metals will result in lower removal efficiency, while higher concentrations of toxic metals will enhance adsorption efficiency. However, at a certain initial concentration, when the metal ions reach the same amount as the available adsorption sites, the adsorption efficiency will decrease as the initial concentration increases beyond this threshold.

For the temperature effect, when the temperature of a solution is increased, the viscosity of the solution decreases, resulting in improved diffusion of ions. This, in turn, enhances the adsorption process. Therefore, by raising the temperature of the solution, the mobility of ions to reach the binding sites increases.

At the same time, the increase in contact time also affects the efficiency of adsorption. This is because a longer interaction time allows for a greater interaction between the active sites and the metal ions. Usually, at the beginning of the adsorption process, the efficiency increases rapidly before gradually levelling off. This is because the available active sites become gradually occupied over time.

Another important factor in the adsorption process is the dosage of the adsorbent. Increasing the dosage of the adsorbent increases the number of active sites, thus enhancing the adsorption capacity. However, despite increasing the dosage to increase the active sites, there are instances when the adsorption capacity decreases due to the agglomeration of the adsorbent. This is because the surface area and the active sites of the adsorbent decreases, resulting in a decrease in active sites and ultimately leading to a decrease in adsorption efficiency.

The study also mentions the pH effect as a crucial factor. When the pH of the solution is low, the functional groups on the surface of the adsorbent will become protonated. This protonation leads to electrostatic repulsion, preventing the adsorption of metal ions on the active sites. Additionally, there will be a competition between the metal ions and H_3O^+ at the same time. Conversely, when the pH of the solution is high, the metal ions species and OH groups will form various complexes that block the active sites, thereby reducing their adsorption capacity.

Figure 2.3

Depiction of physisorption and chemisorption

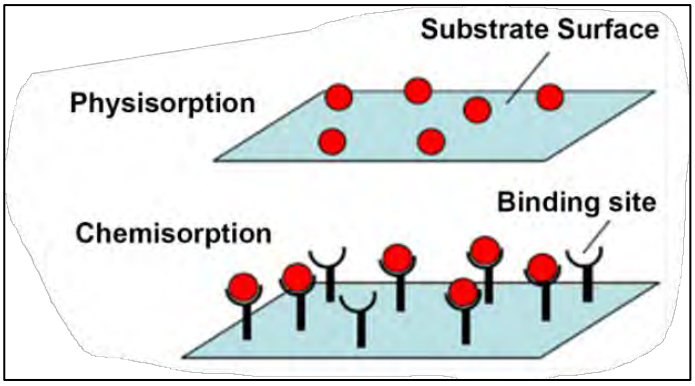

Adapted from Kennedy et al., 2018

2.5.1 Adsorbent of Cd^{2+}

Cd^{2+} can be extracted from contaminated water using adsorbent substances (Ochedi et al., 2020). A good adsorbent should possess the following qualities; high hydrothermal stability, a large surface area with active binding sites, the ability to withstand harsh environments, and a strong affinity for its target (Shaifudin et al., 2023). Over the years, many adsorbents have been produced, such as biochar, zeolite, composite materials (Zhang et al., 2023), food wastes like banana peel (Memon et al., 2008), garlic peel (Sun et al., 2018), and orange peel (Tran et al., 2016). In addition, chitosan, alkalised alumina, activated carbon, silica gel, bauxite, lignin, bentonite, iron oxide, porous pellets of NaF and dolomite (Prabhu & Prabhu, 2018) have been used as starting materials for the production of unmodified adsorbents for the adsorption of Cd^{2+} in wastewater.

Santamoorthy et al. (2023) found that adsorbents with higher functional ligand content had better adsorption capability compared to unmodified adsorbents. Despite the frequent use of natural and raw sorbents like clays and silica in pollutant removal, these materials have several drawbacks, including low removal capacity, poor selectivity and weak binding strength between the sorbent and the pollutant. To address these limitations, the development of inorganic-organic hybrid materials has been a significant advancement in more effective adsorbents in recent years (Tonlé et al., 2008). According to García-Martínez and Collar (2020), organic-inorganic materials are compounds with multiple components, where at least one component is inorganic or organic and has a nanometric size. These materials generally exhibit better performance compared to non-hybrid counterparts. Some recent hybrid materials used as adsorbents include metal-organic frameworks (MOF) (Li et al., 2020), carboxymethyl-chitosan-montmorillonite (Zhang et al., 2020), and chemically modified silica with porphyrin (Radi et al., 2019). According to Kayan (2019), hybrid materials combine the advantageous qualities of light-stable and less-soluble inorganic compounds with the functional properties of organic chemicals.

Consequently, these hybrid materials exhibit strong binding affinities towards heavy metal ions, both chemically and physically, along with large adsorption capabilities. The type of inorganic-organic hybrid material used in this study is γ-Al_2O_3-thiol hybrid. By incorporating thiol into the adsorbent material, the hybrid increases the amount of thiol, thereby enhancing the efficacy of adsorption (Santhamoorthy et al., 2022).

Before discussing the suggested hybrid in a later section, Table 2.3 provides a list of some previous studies on the adsorption of Cd^{2+} in aqueous solution.

Table 2.3

Past researches of adsorption of Cd^{2+}

Adsorbents	Explanations	Outcomes	References
Natural zeolite (NZ) Modified zeolite: NaOH modification (JZ) High-temperature modification (HZ) Humic acid modification (FZ) Na_2S modification (SZ) Ultrasonic modification (CZ)	NZ that was used was natural clinoptilolite. The modified zeolites were then compared with NZ in removing Cd^{2+} in aqueous solution.	Adsorption capacity of JZ was improved by 68.87% and SZ was 32.06% as comparison to natural zeolite. But for HZ, FZ and CZ have decreased adsorption capacity. At initial Cd concentration of 100 mg/L: JZ adsorbed 99.90% while SZ was 93.44% JZ has maximum adsorption capacity of 9.74 mg/g while SZ has 7.62 mg/g	(Zhang et al., 2023)
NaOH-treated oil palm empty fruit bunch (NaOH-treated OPEFB)	The OPEFB fibre was acquired from a palm oil mill before treated with NaOH solution to remove Cd^{2+} in aqueous solution.	Maximum removal of Cd^{2+} was 88.07% at pH 6, 150 rpm of stirring speed, 45 ^{o}C of temperature, 5 mg/L of initial Cd^{2+} concentration and 0.030 g of adsorbent dosage.	(Naihi et al., 2022)

Adsorbents	Explanations	Outcomes	References
Rice husk biochar	Preparation of activated biochar used physicochemical activation method, which consisted of NaOH pre-impregnation and nitrogen (N_2) pyrolysis to remove Cd^{2+} in aqueous solution.	The optimal biochar obtained was consisting of 34.5% biochar yield, 72% Cd removal and 17.8 mg/g adsorption capacity on Cd using 458^{o}C, 120 min reaction time and 3 NaOH impregnation ratio.	(Saeed et al., 2022)
Modified granular activated carbon (Modified GAC)	GAC was modified by impregnating sodium lauryl sulfoacetate (SLSA), a plant-based anionic surfactant into it to remove Cd^{2+} in aqueous solution.	Maximum Cd^{2+} removal was 37.87% at 125 ppm while the minimum Cd^{2+} removal was 7.70% at 10 ppm.	(Jundam et al., 2020)
Sulfuric acid-treated cottonseed cake (SCSC)	The cottonseed cake was obtained from cottonseed oil factory before treat it with sulphuric acid to remove Cd^{2+} from aqueous solution and electroplating wastewater.	Maximum Cd^{2+} removal was 99.9%±0.1% in 3 h and pH 4.0-8.0 with SCSC dose of 150 mg.	(Malathi et al., 2020)

Adsorbents	Explanations	Outcomes	References
Copper-based metal organic framework (Cu-MOF)	The Cu-MOF was synthesised by using solvothermal method, to remove Cd^{2+} from aqueous solution.	The removal efficiency of Cd^{2+} was 98.62% while the equilibrium adsorption capacity was 1.924 mg/g at initial Cd^{2+} concentration of 20 mg/L, adsorbent dosage of 0.5 g and contact time of 60 min.	(Yusuff et al., 2019)
Saponified garlic peel (SGP)	The SGP was being used to remove Cd from model solution and samples of soil washing effluent.	Removal of Cd^{2+} reached 100% for pH below 8 and above 4 during the absence of tartaric acid due to the dominance of Cd^{2+} (presence of tartaric acid can change Cd nature in the model solution, and tartaric acid was used in the research to mimic the function of it as a soil-washing reagent). Adsorption of Cd from the soil washing effluent was 48% (100 % for Pb, 91% for Cu and 93% of Zn) for once time adsorption and removed all the heavy metals during third time adsorption.	(Sun et al., 2018)

Adsorbents	Explanations	Outcomes	References
Banana peel	The surface of the banana peel was modified with carboxylic group using acidic methanol to remove Cd^{2+} from aqueous solution.	~97% in 10 min	(Memon et al., 2008)

Table 2.3 presents a compilation of past research focused on the removal of Cd^{2+} from aqueous solutions, highlighting various adsorbent materials and their corresponding results. Prior to this, the discussion emphasized inorganic-organic hybrid adsorbents, particularly their enhanced adsorption efficacy. It was noted that hybrid adsorbents can outperform non-hybrid counterparts in terms of adsorption capacity. For instance, research conducted by Zhang et al. (2023) indicates that the adsorption capacity of modified zeolite increases by 68.87% for JZ and 32.06% for SZ compared to natural zeolite. This enhanced adsorption capacity is crucial for effectively removing Cd^{2+} from aqueous solutions. Furthermore, all studies listed in Table 2.2 utilised hybrid adsorbents by transforming an existing adsorbent into an upgraded version. Examples include modifications from natural zeolite to modified zeolite, OPEFB to NaOH-treated OPEFB, biochar to rice husk biochar, GAC to modified GAC, cottonseed cake to SCSC, MOF to Cu-MOF, garlic peel to SGP, and banana peel to modified banana peel. Building on these previous studies, the current research also employs a hybrid adsorbent by modifying γ-Al_2O_3 into thiol-functionalised γ-Al_2O_3 for the removal of Cd^{2+} from aqueous solutions.

2.5.2 Alumina as Cd^{2+} Adsorbent

Al is a crucial component of Al_2O_3 and cannot be disregarded when discussing Al_2O_3. According to Capuzzi and Timelli (2018), Al is the second most abundant metallic element on Earth. However, it is highly reactive and does not exist naturally in its pure form. It is commonly found in the Earth's crust and has an atomic number of 13. Al has a density of 2.70 g/cm^3 and is an excellent conductor of heat and electricity. Additionally, it has a silvery-white appearance (Rahman & Upadhyaya, 2021). Due to

its strong affinity for oxygen, Al can only exist as Al_2O_3, with bauxite ore being its primary source. Through additional reactions with atmospheric water, the oxide form can become hydrated, resulting in the formation of surface hydroxyls and various hydrated forms such as boehmite (γ-AlO(OH)) and bayerite ($Al(OH)_3$) (Ludwig, 2022).

The terms "alumina" and "aluminum oxide" (Al_2O_3) can sometimes be used interchangeably (Sheel et al., 2016). However, there are also other less common names for it, such as "aloxide," "alundum" and "aloxite" (Salahudeen et al, 2015). It is worth noting that heat treatment can cause Al_2O_3 to undergo various phase changes (Osman et al., 2012). This is why Al_2O_3 is sometimes referred to as "Transition Alumina" (Kiyohara et al., 2000).

Al_2O_3 is a solid white ceramic material with a molecular weight of 101.96 g/mol, a density of 3.9 g/mL, and melting and boiling points of 2320°C and 3600°C, respectively. It is insoluble in water and partially soluble in ethanol. Additionally, Al_2O_3 is chemically stable, considered inert, and does not easily oxidize, corrode, or react within biological systems. Its resistance to fracture is relatively low (2-4 MPa $m^{1/2}$), so to be effective, it must be compacted to a high density, with an average size close to 4 μm per gram and a purity of at least 99.5%. Due to these properties, Al_2O_3 is widely used as an adsorbent (Aguirre-Terrazas et al., 2021).

Al_2O_3 is one of the most widely used metal oxides, with applications spanning chemistry, electronics, medicine, physics, and material sciences (Gholizadeh et al., 2023). It is found in natural sources such as kaolin (Chargui et al., 2018) and can also be derived from anthropogenic materials, including Al foil waste and beverage cans

(Adans et al., 2016). Furthermore, Al_2O_3 can be synthesised through chemical experiments in laboratory settings (Urbonavicius et al., 2020) or extracted from secondary Al dross (Mahinroosta & Allahverdi, 2018). These diverse sources can be processed to obtain specific phases of Al_2O_3. For instance, Hosseini et al. (2011) demonstrated the synthesis of γ-Al_2O_3 using kaolin as a precursor through a precipitation method.

In various studies, Al beverage cans have been synthesised using different methods and then calcined to obtain the required Al_2O_3 phase (γ, η, θ, χ, δ, κ and α) (Urbonavicius et al., 2020). Researchers such as Matori et al. (2012), Ahmedzeki et al. (2017), and Lopez-Juarez et al. (2018) have used Al beverage cans as raw materials in their investigations. There are many advantages to using Al_2O_3 synthesised from beverage cans. It mainly consists of Al_2O_3(~ 99.51%) with a minute quantity of other oxide contents, demonstrating a high level of purity in the extracted Al_2O_3 powder. Additionally, it has a lower production cost compared to commercially available options. The approximate cost of synthesised Al_2O_3 powders (~0.29μm average-sized Al_2O_3 particles) ranges between 84.47 and 87.45 USD per kg. In contrast, the market price of commercially available Al_2O_3 powder varies between 140 and 7000 USD per kg, depending on the purity level, specific surface area, application grade, and size of the alumina particles. Moreover, H_2 gas collected during the synthesis process can be utilised for other purposes (Rahman et al., 2023). The main objective of this research is to replace expensive commercial raw materials with alternative options, such as Al beverage cans, in order to develop a cost-effective adsorbent (How et al., 2017).

Al_2O_3 production in the laboratory can also be carried out by using appropriate precursors. Several common precursors used to produce Al_2O_3 include aluminum isopropoxide, aluminum nitrate, and aluminum chloride (Urbonavicius et al., 2020). For example, mesoporous γ-Al_2O_3 was synthesised using aluminum 2-butoxide as a precursor (Derakhshani et al., 2018). Additionally, Sifontes et al. (2014) synthesised γ-Al_2O_3 by employing carboxylate alumoxane as a precursor derived from the oleoresin of the Pinus caribaea plant species.

Among the various sources of Al, this study specifically chose Al beverage cans. This decision was motivated by the need to address the issue of waste generated by Al beverage cans in the environment, as opposed to utilizing natural sources such as kaolin, which do not contribute to waste accumulation.

The γ- Al_2O_3 can be synthesised by calcining Al_2O_3 at temperatures ranging from 700-800 ^oC. Subsequently, the temperature can be increased to 800-900 ^oC to obtain the delta (δ) phase, followed by the theta (θ) phase at 900-1100 ^oC. The α- Al_2O_3 phase is at approximately 1150 ^oC, which is the most stable phase out of all phases (Kaunisto et al., 2023).

Among these phases, the α and γ phases of Al_2O_3 are widely studied in research on water treatment applications. Table 2.4 summarises the key characteristics differences between α-Al_2O_3 and γ- Al_2O_3.

Table 2.4

Some characteristics differences between α-Al_2O_3 and γ-Al_2O_3

	α-Al_2O_3	γ-Al_2O_3	Reference
Crystal structure	Hexagonal crystal structure with the R-3c space group	Cubic crystal structure with the Fd-3m space group	(Fatimah et al., 2021)
Specific surface area	Around 15.396 m^2/g	Around 96-196 m^2/g	(Fatimah et al., 2021)
Pore volume	0.0453 mL/g	0.294-0.327 mL/g	(Fatimah et al., 2021)
Characteristics	• Has low specific area • Has almost no catalytic activity • Resist to high temperature	• Has high specific area • Has high catalytic activity • Resist to high temperature • High purity • Has excellent dispersion	(Shaifudin et al., 2023)

Table 2.4 indicates that the γ phase of Al_2O_3 exhibits a higher level of catalytic activity than the α phase, suggesting that the γ phase is a better choice as an adsorbent and catalyst support. While α-Al_2O_3 is the most stable phase, γ- Al_2O_3 can also approach critical surface area and be thermodynamically stable, comparable to α-Al_2O_3 (Wang et al., 2008). Patterns from X-ray diffraction (XRD) can be used to confirm phases α and γ (Dey, 2014). The γ phase was chosen as part of this research.

The γ-Al_2O_3 has high mechanical strength, low production cost, and ease of preparation with large surface area, for instance, 126.76 m^2/g (Singh et al., 2014) and 214 m^2/g (Benu et al., 2021). Additionally, it has a melting point up to 2050 ^oC (Liu et al., 2011) and can be converted into ultrafine powders (Dynys & Halloran, 1982). These

properties are influenced by various factors, including reaction time, material ratios and solution pH (Kim et al., 2001).

Many methods and routes can be used to synthesise γ-Al_2O_3, such as hydrolysis (Wang et al., 2009), freeze drying (Nieto et al., 2006), solvothermal (Meor & Masliana, 2007), sol-gel, hydrothermal and precipitation (Parida et al., 2009).

The hydrolysis method primarily involves the addition of water to aluminum phosphide. This reaction occurs in a reactor where a specific temperature must be maintained. Following the reaction, a suspension is obtained, which is then filtered and washed. The resultant sample is dried and calcined at the desired temperature to produce γ-Al_2O_3 (Wang et al., 2009). The sol-gel method involves the hydrolysis of aluminum alkoxide, which results in a suspension. After peptizing, this sol or colloidal suspension transforms into a gel upon evaporation, hence the name "sol-gel." This gel subsequently converts into a metal oxide after calcination (Perez-Catán & Guraya, 2015). The freeze-drying method relies on the rapid freezing of an aqueous solution containing the desired cation or cations, followed by the sublimation of ice under vacuum conditions. To ensure solution homogeneity, freezing must occur as quickly as possible. The most common approach involves spraying the solution into liquid nitrogen (Nieto et al., 2006). Hydrothermal and solvothermal methods employ water and organic solvents, respectively, for the synthesis of nanomaterials. Both methods operate under similar principles, with the key difference being the use of water in hydrothermal processes and organic solvents in solvothermal processes. These processes take place in an autoclave (Zheng et al., 2019).

However, each method has its advantages and disadvantages. The hydrolysis method requires high-purity aluminium, such as aluminium isopropoxide, which can be costly to obtain. Additionally, this method has a complicated product line (Yi et al., 2009). The freeze-drying method necessitates special equipment to prevent the loss of volatile compounds (Luque de Castro & Luque García, 2002). Conversely, the solvothermal method involves solvents that are harmful to the environment. This method is also time-consuming, requiring anywhere from 4 to 72 hours, and operates at high temperatures ranging from 80 to 400 °C (González et al., 2021). Similarly, the hydrothermal method also demands a significant amount of time (Kaur et al., 2020). Lastly, the sol-gel method often experiences substantial volume shrinkage and cracking during the drying process (Carter & Norton, 2007).

This research employed the precipitation method as the main research method mainly due to its simple route as depicted in Figure 2.4. Moreover, the production of hydrogen gas, an eco-friendly fuel can be collected during the reaction between Al with HCl as written in Equation 2.1 (Adans et al., 2016). Based on research by Adans et al. (2016), this research used NaOH as precipitant. Besides NaOH, Na_2CO_3, $(NH_4)_2CO_3$, ammonium bicarbonate, ammonium carbonate, sodium bicarbonate and sodium carbonate also can be used as precipitants (Parida et al., 2009). γ-Al_2O_3, which was used in this research, generally unreactive to other elements (Yahaya et al., 2013) and has high porosity (Yahaya et al., n.d.), such as 0.99 cm^3/g (Benu et al., 2021).

Figure 2.4

Flow chart of preparation of nanometer powder by precipitation method

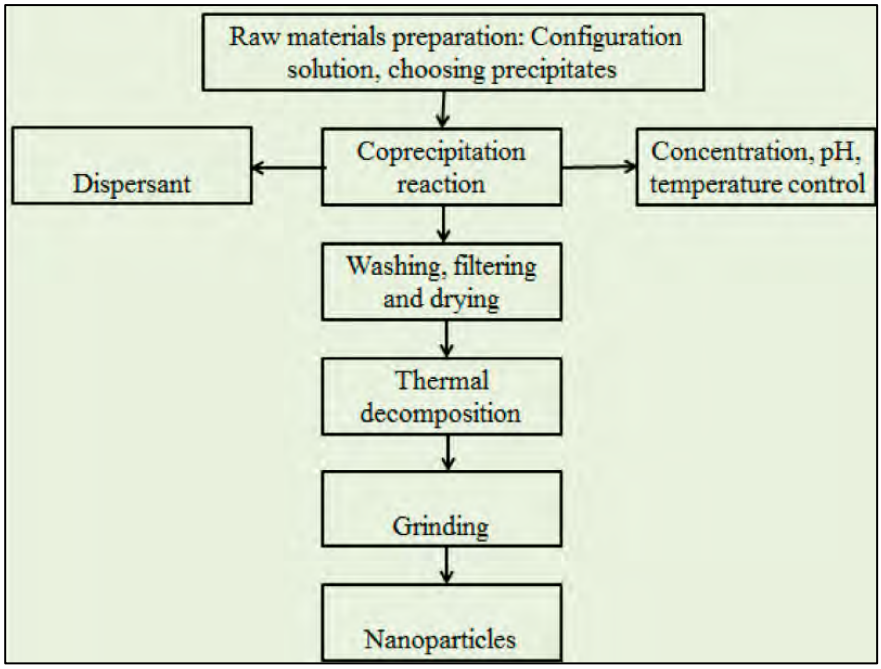

Adapted from Li et al., 2023

$$2Al + 6HCl \rightarrow 2AlCl_3 + 3H_2 \quad (2.1)$$

According to Mayordomo et al. (2023), amphoteric surface sites such as in γ-Al_2O_3 can undergo protonation and deprotonation reactions depending on the pH value. These reactions can be represented as in equation 2.2 and 2.3.

$$XOH + H^+ \rightleftarrows XOH_2^+ \quad (2.2)$$

$$XOH \rightleftarrows XO^- + H^+ \quad (2.3)$$

In general, Cd sorption on surface sites can be described by the following reaction in equation 2.4.

$$XOH + Cd^{2+} \rightleftarrows XOCd^{+} + H^{+} \quad 2.4$$

From the information cited by Mayordomo et al. (2023), the anticipated structure of γ-Al_2O_3 when binding Cd can be illustrated in Figure 2.5.

Figure 2.5

Expected structure of γ-Al_2O_3 when binding Cd

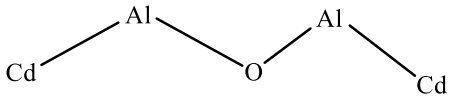

The functionalisation of Al_2O_3 has received significant attention because Al_2O_3 alone is not efficient at absorbing positively charged pollutants. However, after surface modification, it can effectively remove a large amount of water-soluble contaminants from aqueous media (Sadraei, 2020). Al_2O_3 also has hydrophilic surfaces, which lead to high chemical activity. Additionally, their large surface area and high surface energies can cause them to aggregate in order to minimise these energies. To mitigate these issues, Al_2O_3 surface functionalisation is employed. Surfactants containing both polar and non-polar functional groups can reduce the surface forces of hydroxyl groups. Consequently, the organic chains that adsorb or bond to the particle surfaces help prevent the formation of oxygen bridge bonds and the agglomeration of Al_2O_3 nanoparticles (Said et al., 2020).

2.5.3 Thiol as Cd^{2+} Adsorbent

Thiol is sulfur-containing molecules that has SH functional group in its chemical structure. It has a pungent odor, acidic and strong antioxidant activity (Vermeulen et al., 2005). Thiol also is one of the active groups to be attached to surface of adsorbents to improve adsorption capacity along with amino ($-NH_2$), carboxyl (-COOH) and sulfonic acid ($-SO_3H$) (Liu & Xie, 2021). For decades, thiol has been used in adsorption and self-assembly on various metal substrates (Grimm et al., 2021).

Thiol has been employed as a molecule to produce an adsorbent for heavy metals in aqueous media especially Cd, which can be seen in Table 2.5.

Table 2.5

Past researches of adsorption of Cd^{2+} involving thiol

Adsorbents	Thiols's Source	Explanation	Outcomes	References
Thiol functionalised silica microspheres loaded alginate hydrogel beads (SH-SiO_2MS-Ca-Alg)	3-mercaptopropyl trimethoxysilane (MPTMS)	The SH-SiO_2MS-Ca-Alg was prepared stepwise: Synthesis of polyvinylpyrrolidone (PVP) functionalised polystyrene particles by preparing monodispersed polystyrene (PS) first. Synthesis of polystyrene-silica core-shell particles by reacting tetraethyl orthosilicate (TEOS) with PVP functionalised PS latexe particles (from first step). Synthesis of hollow silica microspheres from second step by drying in oven. Synthesis of thiol functionalised silica microspheres (SH-SiO_2MS) by treating the product from third step with MPTMS Synthesis of SH-SiO_2MS-Ca-Alg by adding SH-SiO_2MS to sodium alginate solution and homogenised before adding the mixture to calcium chloride solution.	Removal of Cd: 60-85% at concentration ranged 0.1-100 µg/mL and pH 5-7. The sorption capacity from Langmuir isotherm was 70.68 mg/g.	(Singh et al., 2022)

Adsorbents	Thiols's Source	Explanation	Outcomes	References
DMSNs-TESPA (to adsorb Cd^{2+} and as support for the dispersion of Ag, Pd and Ni NPs)	6-(3-triethoxysilylpropyl)amino-1,3,5-triazine-2,24-dithiol (TESPA)	Other than DMSNs-TESPA, there were also DMSNs-MPTES and DMSNs-APTES that being prepared. 3-(aminopropyl)triethoxysilane (APTES), 3-(mercaptopropyl)triethoxysilane (MPTES) and TESPA have been chemically anchored onto cutting-edge dendritic mesoporous silica nanospheres (DMSNs) to produce DMSNs-APTES, DMSNs-MPTES and DMSNs-TESPA respectively.	DMSNs-TESPA was the most powerful other than the two adsorbents with q_e value of 1280 mg/g while DMSNs-MPTES was 816 mg/g and DMSNs-APTES was 900 mg/g.	(Wang et al., 2022)
Thiol-modified rice straw biochar (RS)	β-mercaptoethanol	Rice straw biochar (RB) was modified with the thiol, named as RS. The RS was tested in batch sorption experiment (aqueous solution of Cd^{2+}) and soil incubation experiments.	Maximum adsorption capacity for Cd^{2+} in single-metal system was 45.1 mg/g while in binary-metal system (consisted of Cd^{2+} and Pb^{2+}) the RS selectively adsorbed Cd^{2+} over Pb^{2+}. For soil incubation experiment, in 28 days, the RS effectively reduce available Cd by 34.8-39.2%.	(Fan et al, 2020)

Adsorbents	Thiols's Source	Explanation	Outcomes	References
3-(trimethoxysilyl)-1-propanethiol functionalised mesoporous silica (KIT-6-SH)	3-(trimethoxysilyl)-1-propanethiol	Synthesised KIT-6 mesoporous silica was then modified with 3-(trimethoxysilyl)-1-propanethiol, later named as KIT-6-SH (a novel sorbent). Other sorbents which were SBA-15-SH and MCM-41-SH, also being studied to compare their performance with the novel sorbent.	Maximum adsorption capacity for Cd by KIT-6-SH was 85 mg/g while MCM-41-SH and SBA-15-SH were 61 mg/g and 60 mg/g respectively.	(Bagheri et al., 2019)
Thioglycolic acid modified mesoporous silica nanoparticles (MCM-41-TgA)	TgA	The MCM-41-TgA was prepared by using sol-gel procedure, where the modification part used microwave irradiation to adsorb Cd^{2+} from aqueous solution.	Has maximum adsorption capacity of 91.3 mg/g at pH 6.	(Kenawy et al., 2018)
Thiol-functionalised metal organic framework material (HS-mSi@MOF-5)	MPTMS	Zinc based metal organic framework (MOF-5) was synthesised by hydro-thermal method, which was then modified with silica gel and thiol.	Saturated adsorption capacity of HS-mSi@MOF-5 was 98 mg/g while MOF-5 was 3.6 mg/g. Adsorption capacity of HS-mSi@MOF-5 was 312 mg g^{-1} while MOF-5 was 211 mg/g.	(Zhang et al., 2016)

Table 2.5 compiles past research that used thiol as a material modified with other substances. The compilation shows the adsorption of Cd^{2+} from aqueous solutions. Various thiol compounds were used to functionalise adsorbents, such as MPTMS with silica microspheres, TESPA with DMSN, β-mercaptoethanol with RB, 3-(trimethoxysilyl)-1-propanethiol with KIT-6 mesoporous silica, TgA with mesoporous silica nanoparticles, and MPTMS with zinc-based MOF. All the mentioned thiols and their unmodified adsorbents have been used to adsorb Cd^{2+} in the past and have shown satisfactory results. The performance of SH-SiO_2MS-Ca-Alg was optimized at pH 5-7, with Cd^{2+} uptake ranging from 60-85% at a concentration of 0.1-100 µg/mL. DMSNs-TESPA had adsorption capacity of 1280 mg/g, which was the most powerful compared to other two adsorbents; DMSNs-MPTES was 816 mg/g and DMSNs-APTES was 900 mg/g. Meanwhile, RS demonstrated a higher affinity for Cd^{2+} over Pb^{2+} when tested in a binary-metal system. A novel adsorbent KIT-6-SH demonstrated maximum adsorption capacity for Cd which was 85 mg/g while for reference MCM-41-SH and SBA-15-SH were 61 mg/g and 60 mg/g respectively. Mesoporous silica nanoparticles also can be functionalised with TgA (named as MCM-41-TgA) which showed adsorption capacity of 91.3 mg/g at pH 6. For HS-mSi@MOF-5, its performance was outstanding compared to MOF-5 (the adsorbent before functionalisation with MPTMS). The saturated adsorption capacity of HS-mSi@MOF-5 was 98 mg/g, while that of MOF-5 was 3.6 mg/g. Additionally, the adsorption capacity of HS-mSi@MOF-5 was 312 mg/g, compared to 211 mg g^{-1} for MOF-5, and the adsorption rate of HS-mSi@MOF-5 was 65.2 g/mg·$min^{0.5}$, while for MOF-5 it was 4.2 g/mg·$min^{0.5}$. The thiol functional group acts as an active site, enhancing the adsorption of Cd^{2+} by functionalising it with other inorganic compounds, as shown in Table 2.5. Figure 2.6 below depicts the thiol compounds mentioned in Table 2.5.

Figure 2.6

Structures of (a) MPTMS, (b) TESPA (c) β-mercaptoethanol (d) 3-(trimethoxysilyl)-1-propanethiol and (e) TgA

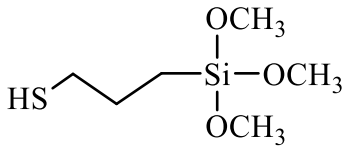

(a)

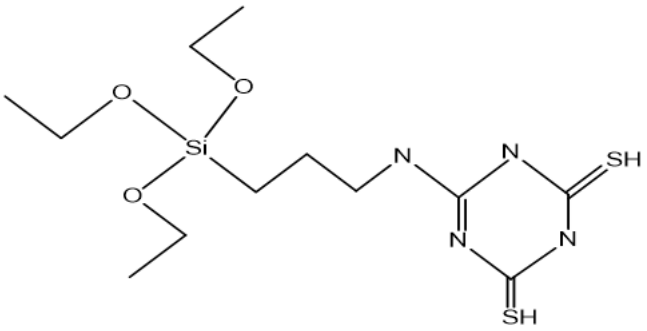

(b)

(c)

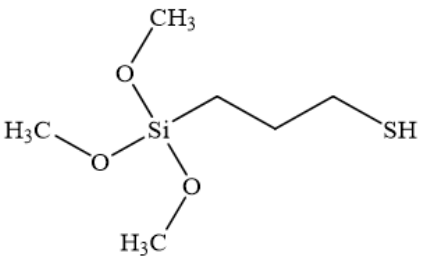

(d)

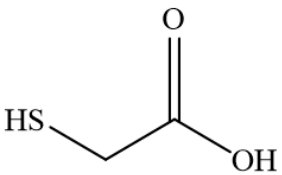

(e)

According to the theory of Pearson's hard soft acid-base, a soft acid and a soft Lewis base can create extremely strong bonds. In particular, Cd^{2+} is categorised as a soft acid and thiol groups as soft Lewis bases (Liu & Xie, 2021). Thiol groups are particularly useful for capturing Cd^{2+} from wastewater. A stable complex with a high reaction rate will be formed by the two bonded soft acid and Lewis base (Shen et al.,

2018). For this reason, a lot of researchers are interested in enhancing their adsorbents for the removal of Cd^{2+} in aqueous environments by adding the thiol group to other inorganic materials.

Moreover, thiol groups alone cannot be adsorbent because thiol groups are readily oxidised to form disulfide bonds, which are unable to engage in ion-exchange interactions. This alteration results in a decreased sorption capacity for various metal ions (Melnyk et al., 2018). This research aims to functionalise thiol with γ-Al_2O_3 to leverage thiol's affinity for Cd^{2+} while addressing the limitations of unmodified thiol groups as adsorbents.

2.5.4 Intercalation Between γ-Al_2O_3 and 1,4-BDMT for Potential Adsorption of Cd

Previous studies have successfully employed thiol and examined γ-Al_2O_3. Thus, this investigation employs dithiol compound 1,4-BDMT which illustrated in Figure 2.7 (for the thiol component) in conjunction with γ-Al_2O_3 to create an adsorbent that is intended to remove Cd. To our knowledge, there have been no published studies on the intercalation of γ-Al_2O_3 with 1,4-BDMT to date. Generally, the thiol group is influenced by pH. At lower pH, the thiol group tends to undergo a protonation process, and the abundance of H^+ ions makes it difficult to bond with Hg^{2+}. The suitable pH for the thiol group is pH 7 and pH 8, according to the pKa value for thiols, which is at ~10. As pH increases, the amount of OH^- increases, and the thiol undergoes a deprotonation process. This process forms RS^- and allows it to interact with Hg^{2+} ions to form the complex S-Hg thiolate (Sharif et al., 2018). As a fellow heavy metal ion, Cd^{2+} is

expected to be able to bond with S from 1,4-BDMT and form the complex S-Cd thiolate as well. Salazar Alarcón et al. (2010) state that the research of dithiols with aromatic rings (Pasquali et al., 2017) has become a "hot issue" in recent years because of the possibility for dithiols to act as linkers between two metallic identities. The dithiols' two ends can bind to the electrode of metals (Salazar Alarcón et al., 2017). Having two ends S-H in 1,4-BDMT can increase the probability of having one end bind with γ-Al_2O_3 while the other end bind to Cd^{2+}, meaning that only one thiol proton is lost (Murty et al., 1998). Furthermore, Pawlas et al. (2019) state that 1,4-BDMT is the most effective thiol for eliminating hazardous contaminants. For references, Table 2.6 demonstrates several researches of adsorption of Cd^{2+} involving metal oxide functionalised with thiol. These researches demonstrated that thiol is likewise a suitable adsorbent material for heavy metals. There were no 1,4-BDMT used for adsorption of heavy metal in aqueous solution especially its functionalisation with γ-Al_2O_3. In fact, there were many researches regarding 1,4-BDMT especially in self-assembled monolayer (SAM) study such as by Hong et al. (2019), Salazar Alarcón et al. (2017), Jia et al. (2015) etc.

Figure 2.7

Structure of 1,4-BDMT

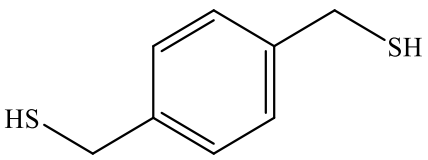

Table 2.6

Past researches of adsorption of Cd^{2+} involving metal oxide functionalised with thiol

Adsorbents	Tthiol's Source	Explanation	Outcome	Reference
Thiol-methyl-modified magnetic microspheres	MPTMS	Submicron Fe_2O_3 was prepared by solvothermal method. Core/shell structured Fe_2O_3@SiO_2 microspheres were prepared by Stöber method. Thiol group-protected and unprotected Fe_2O_3@SiO_2-SH were prepared: • Fe_2O_3@SiO_2-SH protected (preparation included MPTMS and MTES) • Fe_2O_3@SiO_2-SH unprotected (preparation only included MPTMS)	Exhibited adsorption capacity of 27.5 mg/g for Fe_2O_3@SiO_2-SH protected and 7.80 mg/g for Fe_2O_3@SiO_2-SH unprotected at pH 7 and 25 ^oC.	(Liu & Xie, 2021)
Thiol-functionalised magnetic sawdust	MPTMS	γ-Fe_2O_3 was precipitated on the sawdust surface before modified with MPTMS layers.	The equilibrium was reached within 20 min and had adsorption capacity of 3.80 mg/g.	(Gan et al., 2016)

Adsorbents	Tthiol's Source	Explanation	Outcome	Reference
γ-Al_2O_3 nanofibers grafted with thiol	MPTMS	Two types of γ-Al_2O_3 nanofibers were prepared via hydrothermal method: Smaller fibers (FA(S)) which had 5-7 nm thickness and 40-60 nm long. Larger fibers (FA(L)) which had ~10 nm thickness and 300 nm long. Both nanofibers were then grafted with thiol group (MPTMS) and renamed as SH-FA(S)-1 and SH-FA(L)-1 (0.6 mL MPTMS) as well as SH-FA(S)-2 and SH-FA(L)-2 (0.9 mL MPTMS).	~43%, 45% and 50% for SH-FA(S)-1 at 10, 5 and 3 mL/min of flux respectively. ~70%, 75% and 80% for SH-FA(S)-2 at 10, 5 and 3 mL/min of flux respectively. ~40%, 43% and 45% for SH-FA(L)-1 at 10, 5 and 3 mL/min of flux respectively. ~48%, 50% and 53% for SH-FA(L)-2 at 10, 5 and 3 mL/min of flux respectively. ~20% for FA(S) at all 10, 5 and 3 mL/min of flux. ~5%, 7% and 10% for FA(L) at 10, 5 and 3 mL/min of flux respectively.	(Yang et al., 2010)

2.5.5 Intercalation Between γ-Al_2O_3 and TgA for Potential Adsorption of Cd

This research used TgA to intercalate with γ-Al_2O_3 as there was no published papers reported the said intercalation. The product then will be used as an adsorbent to remove Cd^{2+} from aqueous solution.

TgA is a bifunctional molecule made up of carboxylic acid and thiol groups. Carboxylic acid is commonly used either to be directly attached ligand or subsequently modified by using “clickable” chemistry (Grimm et al., 2021). A few potential configurations can be inferred from the fact that both groups can be adsorbed on Ag surfaces to create a monolayer (Chung & Lee, 2004). In general, carboxyl/hydroxyl groups are recognized functional groups with the highest adsorption capacity, according to Kayranli (2022). The hydroxyl group (-OH) in the adsorbents' shells participated in their binding with heavy metals, whereas the carboxyl group underwent a transformation to –COO- at a specific pK, which significantly assisted in the reduction of heavy metals. Figure 2.8 shows several illustrations of how the carboxyl group is expected to bind Cd^{2+}, referred from Azócar et al. (2014) which have several coordination of carboxylate ion, RCO^{2-} ; as a monodentate ligand, bridging bidentate ligand, bidentate symmetric: isobidentate, or as a bidentate unsymmetric: anisobidentate. According to the previously stated studies by Chung & Lee (2004) and Kayranli (2022), TgA is anticipated to assist in the removal of Cd^{2+} from water through intercalation with γ-Al_2O_3.

Same as discussed about the intercalation between γ-Al_2O_3 and 1,4-BDMT previously, the intercalation between γ-Al_2O_3 and TgA will form expected product

complex γ-Al_2O_3-TgA to remove Cd^{2+} as illustrated in Figure 2.9. The adsorbents will be tested on deionised water containing Cd^{2+} in batch experiments.

Figure 2.8

Illustrations of how the carboxyl group in TgA is expected to bind Cd^{2+} which have several coordination of carboxylate ion, RCO^{2-} ; as a (a) monodentate ligand, (b) bridging bidentate ligand, (c) bidentate symmetric: isobidentate, or as a (d) bidentate unsymmetric: anisobidentate

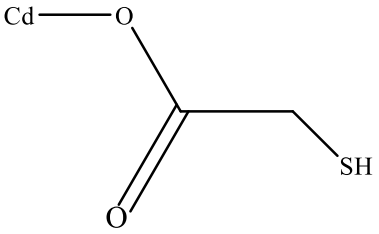

(a)

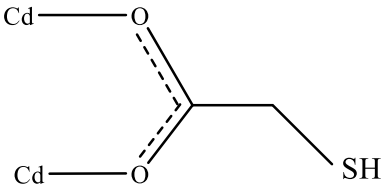

(b)

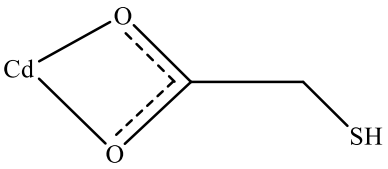

(c)

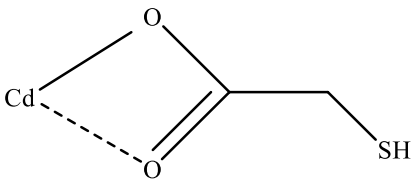

(d)

Figure 2.9

Expected product complex γ-Al_2O_3-TgA to remove Cd^2

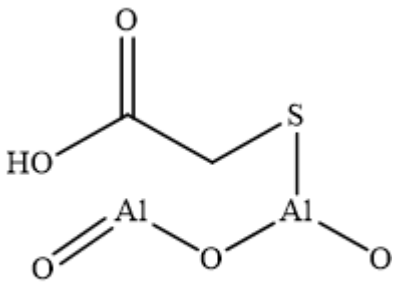

CHAPTER 3

METHODOLOGY

3.1 Introduction

This chapter describes the materials and instruments used in this research. The study consists of three parts in the methodology. The first part examines the fundamental adsorption studies on the adsorbents for Cd^{2+}. The second part discusses the characterisation of the adsorbents to analyse their morphology and potential structures after functionalisation. The final part focuses on the evaluation of the adsorbents for removing Cd^{2+} from aqueous solutions and explores their potential mechanism.

3.2 Materials

3.2.1 List of Chemicals

The chemicals, reagents and instruments used in this research are listed in Table 3.1. Deionised water and analytical grade chemicals were used for this study. Glassware was thoroughly washed with soap and tap water and rinsed with deionised water.

Table 3.1

List of chemicals

Chemical	Chemical Formula	Purity	Manufacturer
1,4-benzenedimethanethiol	$C_8H_{10}S_2$	98 %	Sigma-Aldrich
Acetone	$(CH_3)_2CO$	≥99.5 %	Systerm
Aluminium oxide	Al_2O_3	≤100 %	Sigma-Aldrich
Ammonium hydroxide (Ammonia solution)	NH_4OH	25 %	Supelco
Cadmium acetate dehydrate	$(CH_3COO)_2Cd.H_2O$	98 %	Sigma-Aldrich
Cadmium standard metal solution for AAS	CdH_2N2O_6	1000 ppm	Thermo Fisher Scientific

Chemical	Chemical Formula	Purity	Manufacturer
Ethanol absolute	CH_3CH_2OH	≤100 %	SAFC (Sigma-Aldrich Fine Chemicals)
Hydrochloric acid	HCl	37 %	Sigma-Aldrich
Sodium hydroxide pellets	NaOH	≤100 %	Sigma-Aldrich
Toluene (anhydrous)	$C_6H_5CH_3$	≤100 %	Sigma-Aldrich
Thioglycolic acid	$HSCH_2COOH$	98 %	Sigma-Aldrich

3.3 Stage 1: Preparation of Adsorbents

The preparation of adsorbents was divided into two procedures. The first procedure involved the synthesis of γ-Al_2O_3, while the second procedure included the synthesis of γ- Al_2O_3-BDMT and γ- Al_2O_3-TgA.

3.3.1 The First Procedure: Synthesis of γ-Al_2O_3

The method used for this analysis was adapted from Adans et al. (2016) with some modifications. Al beverage cans were collected from a recycling centre in Tanjung Malim, Perak, without any dents to make it easier to remove the ink on the cans by polishing them with sandpaper before washing with tap water to ensure no dust from polished ink remains. The centre was selected because it has a huge number of undented cans. The cans were then cut into small pieces (1 cm x 1 cm) by using an Al cutter. Only the cylindrical part of the can was taken for the process since it can be cut more easily. From here on out, all steps were performed in a fume hood to ensure that no harmful gases were released elsewhere because according to Equation 3.1, hydrogen gas was released during the formation of aluminium chloride. A solvent was prepared by adding hydrochloric acid solution (6 mol L^{-1}, 100 mL) drop by drop (at a rate of 3.0 mL min^{-1} due to the large amounts of heat and hydrogen released) to deionised water (100 mL) while continuously stirring with a magnetic stirrer (colourless solution can be seen during this time). Then, 4 g of the Al beverage can pieces were placed into the previously prepared solvent and set aside for 20 minutes to allow the pieces to react with the solvent completely (a pilot study revealed it took 20 minutes to allow the reaction to complete). The reaction took place in 500 mL beaker. During the 20 minutes,

the solution transformed into a gray-coloured mixture with hydrogen gas being released, and bubbles were formed. The Al beverage can piece and the solvent were considered complete when no gas was released and no bubbles were seen anymore. The solution harboured a colourless solution at this point. The reaction up to this point can be described by Equation 3.1 below (Adans et al., 2016).

$$2Al(s) + 6HCl(l) \rightarrow 2AlCl_3(l) + 3H_2(g) \quad (3.1)$$

After that, sodium hydroxide solution (6 mol L^{-1}, 75 mL) was added drop-to-drop (8.0 mL min^{-1}) under constant stirring. The solution then transformed into a milky white-coloured mixture. The reaction can be described through Equation 3.2.

$$AlCl_3(l) + 3NaOH(l) \rightarrow Al(OH)3(s) + 3NaCl(l) \quad (3.2)$$

The mixture was left to mature under constant stirring for 24 hours before being separated by centrifugation using centrifuge (Sigma / 1-6). The mixture obtained was transferred into 13 mL centrifuge tube before centrifugation without any modification. The centrifugation lasted for 10 minutes at 4500 rpm. The solid obtained (gel-like pink-coloured) from the separation was washed with a 1% (v/v) ammonium hydroxide solution. The washing was to ensure the sample synthesised came with high purity (Muhammad et al., 2007). A pink gel formed instead of the commonly observed white colour for aluminium hydroxide. The gel obtained which pink in colour was due to the presence of manganese, iron and potassium as confirmed by EDX, reported by Adans et al. (2016). All the processes were carried out at room temperature. The gel was then dried at 110 ^{o}C for 24 hours in a laboratory oven (Constance FCH9076 Series), ground

using a laboratory mortar and pestle, and sieved to obtain particles of 100 mesh in size. Finally, the resulting material was calcined at 800 ^{o}C for 4 hours using furnace (to transform it into the γ phase of Al_2O_3). The calcined sample was brown in colour as mentioned by Adans et al. (2016). To confirm the phase, an XRD instrument (Rigaku, model MiniFlex 600-C) was utilised. Once the phase was confirmed, the γ-Al_2O_3 was subjected to analysis using the surface area and porosity instrument, Field Emission Scanning Electron Microscopy (FESEM), and Energy-dispersive X-ray (EDX) instruments (Hitachi, model SU 8020). The product was denoted as γ-Al_2O_3(S). The simplified procedure is illustrated in Figure 3.1.

Figure 3.1

Diagram of The First Procedure: Synthesis of γ-Al_2O_3

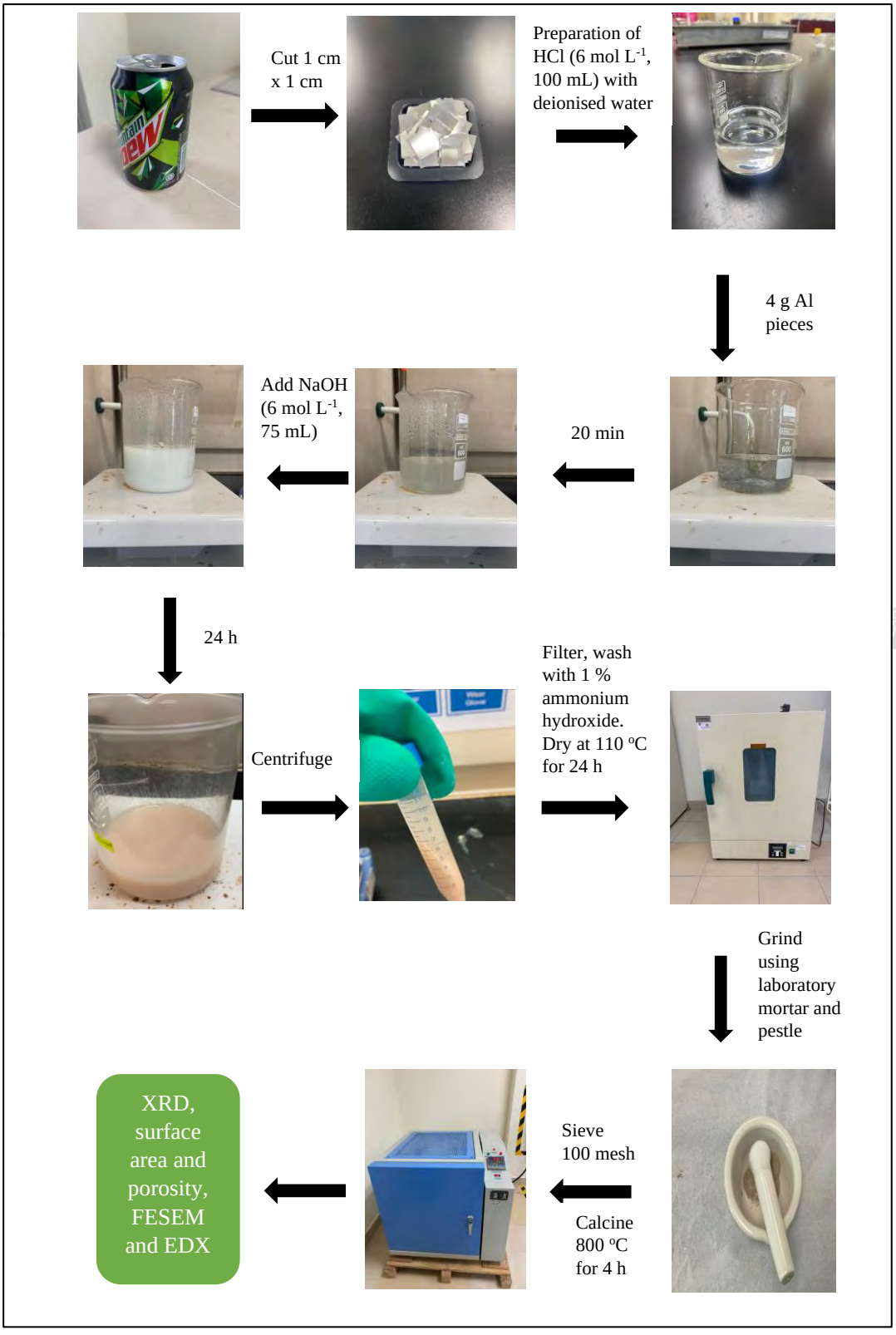

3.3.2 The Second Procedure: Synthesis of γ-Al_2O_3-BDMT and γ-Al_2O_3–TgA

The γ-Al_2O_3(S) and the commercial γ-Al_2O_3 (denoted as γ-Al_2O_3(C)) were subjected to this step to functionalise them with thiol groups obtained from 1,4-BDMT and TgA. The intercalation of γ-Al_2O_3 with 1,4-BDMT was based on the method described by Xia et al. (2017), while the intercalation of γ-Al_2O_3 with TgA was based on the method described by Alexander et al., (2016), with some modifications.

First, γ-Al_2O_3 was functionalised with 1,4-BDMT. To do this, 0.85 g of 1,4-BDMT was added to 5 mL of anhydrous toluene and allowed to dissolve. Next, 0.034 g of synthesised γ-Al_2O_3 was added to the solution. The mixture was stirred continuously using a magnetic stirrer at room temperature for 24 hours. Brown-coloured suspension had been seen during the reaction. After 24 hours, the mixture was filtered using Buchner funnel filtration and washed with 5 mL each of anhydrous toluene and acetone. The washing process was conducted on the mixture to achieve high purity of the sample (Muhammad et al., 2007). The functionalised γ-Al_2O_3 was then dried under room temperature (De Paoli et al., 2021) before being used for Cd removal studies. The same process was also carried out for the commercial γ-Al_2O_3 and during the stirring process, white-coloured suspension had been seen. The commercial γ-Al_2O_3 was renamed as γ-Al_2O_3(C). γ-Al_2O_3(C) was added as research's material to become a milestone for γ-Al_2O_3(S). By comparing both of them as adsorbents, the ability of γ-Al_2O_3(S) can be determined or compared with γ-Al_2O_3(C). The products then named as γ-Al_2O_3(C)-BDMT and γ-Al_2O_3(S)-BDMT which were white and brown in colour respectively. The sample underwent grinding and sieving processes, like in

the first procedure, before being taken for analysis by instruments. The overview of this procedure is illustrated in Figure 3.2.

Next, the functionalisation of γ-Al_2O_3 with TgA was performed. A total of 2.48 g of synthesised γ-Al_2O_3 was added to a 10 mL aqueous solution of TgA and refluxed overnight. The ratio of synthesised γ-Al_2O_3 to TgA was 1:6 in terms of mole equivalence. Continuous stirring was maintained using a magnetic stirrer throughout the process. After refluxing, the functionalised particles were filtered and washed three times with deionised water and absolute ethanol (10 mL each) to remove any unreacted TgA. Subsequently, the functionalised particles were dried overnight at 80°C in an oven. The same procedure was also conducted for commercial γ-Al_2O_3.

The resulting adsorbents, γ-Al_2O_3(C)-BDMT, γ-Al_2O_3(S)-BDMT, γ-Al_2O_3(C)-TgA, and γ-Al_2O_3(S)-TgA, were then analysed using Fourier-transform Infrared Spectroscopy (FTIR) (Perkin Elmer, model Spectra3), FESEM, EDX, X-ray Photoelectron Spectroscopy (XPS) (Shimadzu, model Axis Ultra DLD) and Thermogravimetric Analysis (TGA) (Perkin Elmer, model Pyris1) instruments. The summarised procedure is depicted in Figure 3.3.

Figure 3.2

Diagram of The Second Procedure: Synthesis of γ-Al_2O_3-BDMT

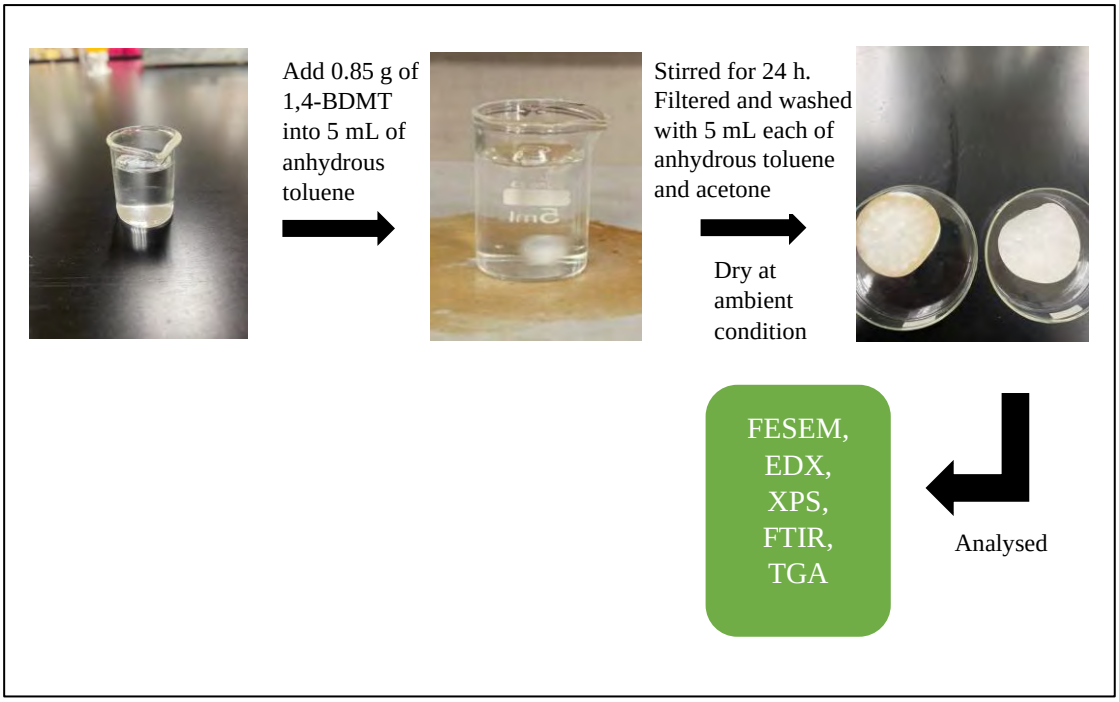

Figure 3.3

Diagram of The Second Procedure: Synthesis of γ-Al_2O_3-TgA

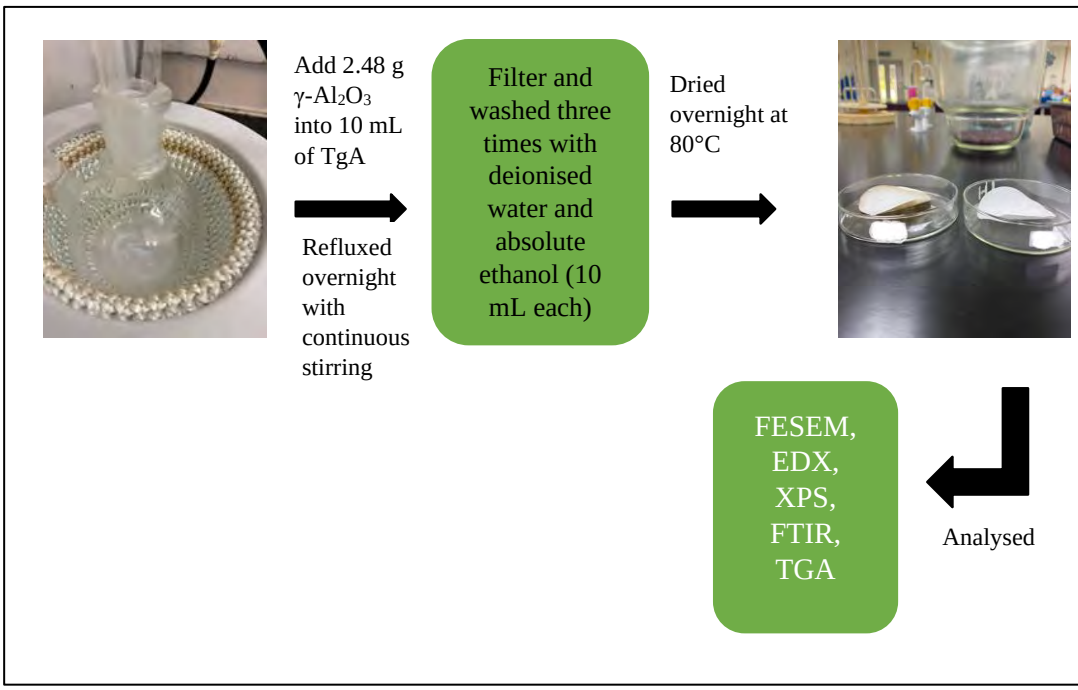

3.4 Stage 2: Characterisation Studies on γ-Al_2O_3(S), γ-Al_2O_3(C)-BDMT, γ-Al_2O_3(S)-BDMT, γ-Al_2O_3(C)-TGA and γ-Al_2O_3(S)-TgA

The study further characterised γ-Al_2O_3(S), γ-Al_2O_3(C)-BDMT, γ-Al_2O_3(S)-BDMT, γ-Al_2O_3(C)-TgA, and γ-Al_2O_3(S)-TgA using seven multiple analytical techniques: XRD to determine phase purity and crystallinity; Brunauer-Emmett-Teller (BET) analysis to measure specific surface area, critical for porous adsorbents; Field Emission Scanning Electron Microscopy (FESEM) for morphological evaluation; Energy-Dispersive X-ray Spectroscopy (EDX) coupled with FESEM for elemental composition; Fourier Transform Infrared Spectroscopy (FTIR) to identify functional groups; X-ray Photoelectron Spectroscopy (XPS) for surface chemical state analysis via binding energies; and Thermogravimetric Analysis (TGA) to assess thermal stability and mass loss profiles. These methods collectively elucidated the structural, textural, and chemical modifications induced by thiol functionalisation, enabling comparative analysis between pristine and modified γ-Al_2O_3 adsorbents.

3.4.1 X-ray Diffraction (XRD)

XRD was used to determine the phase and crystallinity of calcined materials (Parida et al., 2009). It is a non-destructive testing technique that can determine the arrangement of atoms in each unit cell, the position of atoms and the spacing between the atomic planes (Ali et al., 2022). Meanwhile, Epp (2016) explained that this instrument is so powerful that it can obtain chemical composition, qualitative phase analysis, space group, or lattice parameters through the peak position. Approximately 95% of solid materials are crystalline, and for information on crystals and powders can refer to the International Centre for Diffraction Data (ICDD), which has over 51,400 organic and

460,900 inorganic entries (Ali et al., 2022). XRD and ICDD are closely related, and their relationship will be explored further in Chapter 4. Generally, XRD starts working when X-rays strike a solid material. The X-rays are then scattered by the electrons revolving around the nucleus of the atom. Interference occurs when the scattered X-rays are emitted in multiple directions and interfere with each other. Diffraction is the constructive interference of the scattered X-rays. It is important to note that constructive interference is caused by the orderly arrangement (periodicity) of atomic structures in solids. As a result, the XRD graphs of crystalline materials can be interpreted. From the graph, the intensity of diffraction peaks can determine the atomic number and atomic position, while the shape of the diffraction peak can provide information about the size and shape of the unit cell. In a single graph, XRD can identify several minerals present in a sample (Ali et al., 2022). Figure 3.4 shows an illustration of XRD analysis.

Figure 3.4

Basic illustration of XRD analysis

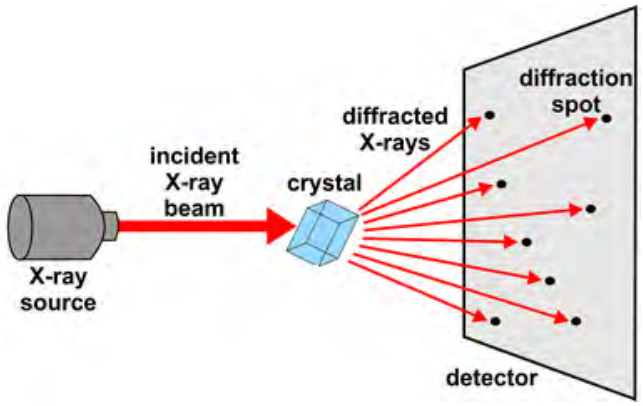

Adapted from Bijelic and Rompel, 2018

The analysis used Rigaku brand (model Miniflex 600) with Cu Kα radiation at scanning rate of 3° per minute. The data collected for 2θ was set at range 3°-80° so that all necessary diffraction peaks for the crystal structures can be covered (Rozita et al., 2010). The desired phase for Al_2O_3 was γ phase. From this analysis, crystallite size (D) can be calculated by employing Scherrer equation as shown in Equation 3.3 below:

$$D = \frac{k\lambda}{\beta \cos \theta} \tag{3.3}$$

Where k is a constant valued 0.9, λ is the wavelength of X-rays, β is the full width of diffraction peak at half maximum intensity and θ is the Bragg angle in radian (Alamouti et al., 2021). Before the analysis, the sample was taken as it was, without modification, onto a sample holder (Figure 3.5(a)). The sample had to be placed on the rough surface of the holder, indicated with a black arrow, and carefully flattened without any voids using a glass slide (Figure 3.5(a)). Figure 3.5(b) presents the XRD instrument utilised for phase identification and crystallinity determination in this research.

Figure 3.5

Sample preparation of XRD analysis. (a) glass slide and sample holder for XRD analysis and (b) XRD instrument

(a) (b)

3.4.2 Surface Area and Average Pore Diameter

Specific surface area is closely related to applications involving porous structures. Pores can be classified into a few categories based on their diameter; micropores (< 2 nm), mesopores (2-50 nm), and macropores (> 50 nm). Within the micropores category, there are several subcategories; ultra-micropores (< 0.7 nm), medium-sized micropores (0.7-0.9 nm) and super-micropores (> 0.9 nm).

The most reliable methods for measuring specific surface area, pore size distribution, average pore diameter and volume of porous materials involve using gas physisorption equilibrium isotherms of nitrogen, argon or carbon dioxide adsorbates. The interaction between gas molecules and surfaces is dominated by Van der Waals forces, with an adsorption heat lower than 4 kJ/mol at temperatures below 100 K. This

force leads to the formation of multiple layers of reversible physisorption of gas molecules on the material's surface. In contrast, chemisorption occurs in a monolayer and is irreversible at higher temperatures. The calculation of surface area (S_{BET}) extends the Langmuir theory of monolayer adsorption to include multiple layers, with only adjacent layers of gas molecules interacting. For pore size, the Barret-Joyner-Halenda (BJH) method was introduced using the Kelvin equation (Bardestani et al., 2019).

Among the gas physisorption equilibrium isotherms mentioned earlier, nitrogen is the most preferred gas adsorbate. This is because nitrogen is inert, inexpensive, available in high purity and can interact with most solids. The nitrogen physisorption analyser consists of two main components; the degassing station and the adsorption station. The process begins with the calibration of a quartz cell used for gas adsorption. This cell is evacuated under high vacuum (< Pa) for 2 hours at 300°C, a process known as degassing. Then, the cell is loaded with a sample (50-150 mg) and connected to the degassing unit. Degassing is necessary to remove any physically adsorbed water and volatiles that may have accumulated during storage. For thermally sensitive solids, a mild degassing temperature is used. For porous materials that are mechanically fragile, a stream of inert gas is used instead of a vacuum. This inert gas is connected to the degassing unit via the adsorbate path. Once degassing is complete, the cell is transferred to the adsorption unit and evacuated. The adsorption cycle is performed by incrementally introducing the adsorbate gas using the calibration volume connected to the adsorption unit. The number of moles of adsorbed nitrogen can be determined by comparing the pressure difference between the empty cell and the measured pressure. During the measurement, a Dewar flask filled with liquid nitrogen is used to maintain the cell at the boiling point of liquid nitrogen (Bardestani et al., 2019).

There are six types of nitrogen physisorption isotherms exist, which are:

- Type I – Langmuir isotherms. Mainly, these materials have narrow micropores, such as zeolites and certain types of activated carbon. These pores have a high affinity for adsorption, leading to a rapid uptake of gas at very low relative pressures. The limited amount of gas adsorbed is determined by the volume of the accessible micropores, rather than the overall internal surface area.
- Type II – reversible isotherms. Involving non-porous materials and those with mainly macropores yields. Nitrogen gas molecules are being adsorbed in a mono/multi-layer manner without limit. At point B in Figure 3.5, it is the beginning of the transition from monolayer coverage to multi-layer coverage.
- Type III – This kind of isotherm makes it impossible to estimate the monolayer capacity and hence, the specific surface area due to weak adsorbate-adsorbent interactions at low relative pressure. For instance, nitrogen adsorption on polyethylene exhibits a zero slope at the beginning.
- Type IV – involving solids with micro and mesopores. Capillary condensation happens here due to the interactions between gas molecules and adsorbent mesopore surface.
- Type V – This isotherm type is observed when water is adsorbed onto different types of zeolites. The curve of this isotherm is characterised by an initial low uptake, which is attributed to the adsorption onto non-polar or weakly polar pore surfaces. This is followed by a sudden increase in adsorption, which is due to the hydrophilic nature of the adsorbent allowing for the filling of micropores with condensed water. After a certain threshold of adsorption is reached, the rate of uptake rise decreases (Muttakin et al., 2018).

- Type VI – stepwise multilayer adsorption. Involving adsorption on a uniform non-porous surface. Usually happens to an adsorption of Ar or Kr on graphitised carbon black at liquid nitrogen temperature.

The surface area of γ-Al_2O_3(S) was estimated using the BET method, while the pore size was determined using the BJH method (Pang et al., 2022). To determine the surface area and pore size of the y-Al_2O_3(S), a N_2 adsorption-desorption isotherm was employed using Micromeritics TriStar II 3020 Version 3.02 at 77.350 K under N_2 gas.

Before running the analysis, around 0.2-0.3 g of sample was taken into a sample tube (Figure 3.7(a)) before being put into degassing chamber at 350 ^oC under vacuum condition. The process was called as degassing, which was to remove any adsorbed moisture and contaminant from the sample surface. Figure 3.7(b) presents the analytical instrumentation employed for surface area and porosity characterisation in this study.

Figure 3.6

Diagram of nitrogen adsorption-desorption isotherms

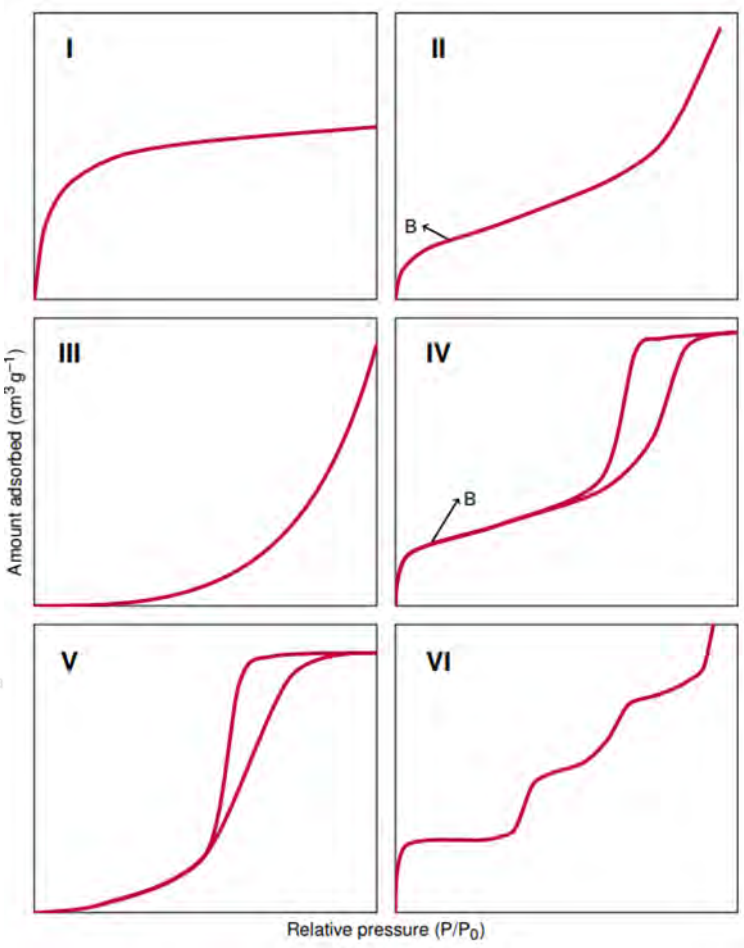

Adapted from Bardestani et al., 2019

Figure 3.7

Sample preparation of Surface Area and Average Pore Diameter analysis. (a) sample in sample tube and (b) the instrument for the analysis

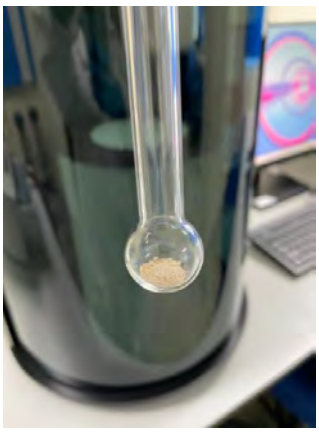

(a)

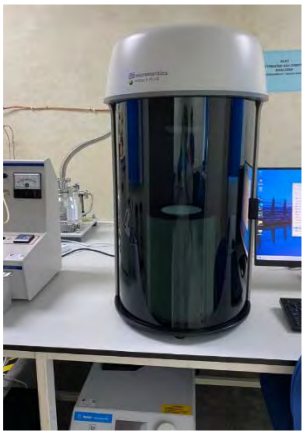

(b)

3.4.3 Field Emission Scanning Electron Microscopy (FESEM)

Electron microscopy is the fundamental concept behind FESEM, which is a technique for imaging the surface of a specimen (Abd Mutalib et al., 2017). This technique involves the interaction between electrons and the specimen, resulting in the generation of topological images. Electron microscopy enables researchers to observe matter at a level of detail that is not visible to the naked eye, surpassing the capabilities of a light microscope.

The beam of electrons produces secondary electrons, backscattered electrons and characteristic X-rays when it contacts the sample. These secondary electrons, backscattered electrons and characteristic X-rays are then detected using their respective detectors and displayed on the monitor. In a typical scanning electron microscope (SEM), there are several main components, including the electron source,

electron detector, column (which contains electromagnetic lenses) and the computer display. In general, image formation in an SEM is mainly based on the signals detected from the interactions between the scanned sample and the electron signals.

SEM utilises a focused beam of electrons emitted from a thermionic electron source, whereas FESEM employs a field emission electron source and emits electron beams through a potential gradient. Hence, FESEM offers superior resolution compared to SEM.

In this research, FESEM was employed to study the morphologies (Alamouti et al., 2021) of adsorbents which are γ-Al_2O_3(S), γ-Al_2O_3(C)-BDMT, γ-Al_2O_3(S)-BDMT, γ-Al_2O_3(C)-TgA and γ-Al_2O_3(S)-TgA. Before proceeding with the analysis, the samples must be prepared according to the right procedures. First, a small cut of conductive tape (Figure 3.8(a)) was attached to the stub (Figure 3.8(b)). Then, a sample was put on the tape to ensure that the sample was on the stub when running the analysis later. The sample was put in sputter coater machine (Figure 3.8(c)) to coat the sample with platinum coating. After that the stub that contained platinum-coated sample was put with stub holder (Figure 3.8(d)) for analysis. The images of surface morphologies of those samples were captured at an accelerating voltage of 10 kV to ensure a good resolution. The images captured before and after thiol intercalation of the samples can determine whether the surface morphologies change. This, in turn, determines the success of the intercalation process. Figure 3.8(e) illustrates the FESEM instrument employed for morphological characterisation in this research.

Figure 3.8

Sample preparation of FESEM analysis. (a) conductive tape, (b) stub with attached tape on it, (c) sputter coater machine for FESEM analysis (d) stub holder and (e) FESEM instrument

(a)

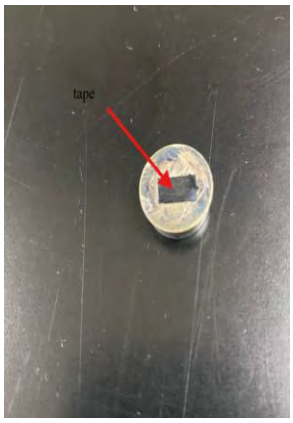

(b)

(c)

(d)

(e)

3.4.4 Energy Dispersive X-Ray (EDX)

EDX is an extension of FESEM that is used for detecting elemental composition. It can detect elements with higher atomic numbers than boron (atomic number = 5) and can also detect elements at a concentration of at least 0.1%. When the electron beam collides with the sample in SEM, characteristic X-rays are produced. Each element has its own unique X-ray emission spectrum, which allows for the measurement of element concentrations. The main electron beam contacts the nucleus of the sample atom, causing the emission of X-rays. An excited electron within the atom's nucleus is ejected, leaving behind an electron hole. The missing electron is replaced by an electron from the outer shell or a higher energy level, resulting in the release of X-rays. These X-rays consist of a continuum spectrum generated by the deceleration of electrons, as well as characteristic X-rays generated when higher shell electrons fill the electron hole in the nucleus. The elemental composition of a specimen is determined by measuring the characteristic X-rays using an energy dispersive spectrometer (Abd Mutalib et al., 2017). Figure 3.9 illustrates the principle of EDX analysis.

Figure 3.9

An illustration of how energy dispersive X-ray analysis works

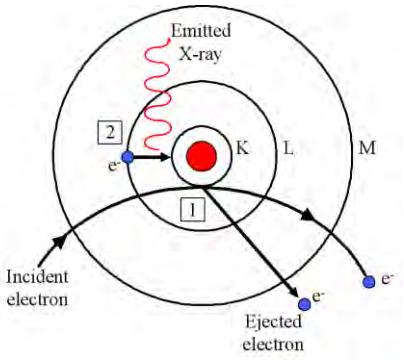

Adapted from McAneney, 2005

EDX, coupled with FESEM was employed in this research to determine the elemental composition of γ-Al_2O_3(S), γ-Al_2O_3(C)-BDMT, γ-Al_2O_3(S)-BDMT, γ-Al_2O_3(C)-TgA and γ-Al_2O_3(S)-TgA. When the samples were irradiated with a high-energy primary electron beam, characteristic X-rays were emitted, enabling elemental analysis (Naihi et al., 2022). This characterisation verified the successful thiol functionalization or intercalation with γ-Al_2O_3. Figure 3.10 presents the EDX instrument utilised for elemental analysis in this research.

Figure 3.10

EDX instrument (red arrow) which integrated with FESEM instrument

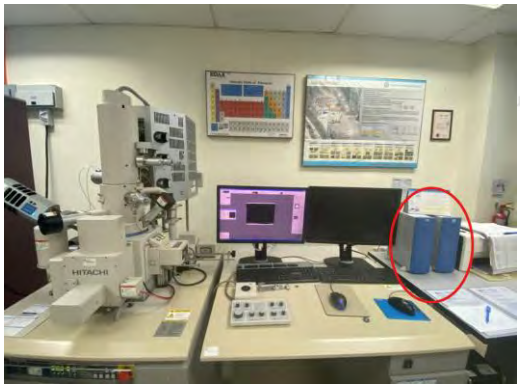

3.4.5 Fourier Transform Infrared (FTIR)

FTIR was employed to identify the major functional groups that exist in molecules (Sun et al., 2018). Chen et al. (2015) explained that this instrument is a non-destructive technique that provides fundamental information about the molecular structure of inorganic and organic compounds. In the FTIR instrument, a photon interacts with a molecule and excites it to a higher energy state, resulting in the absorption of IR

radiation. This absorption leads to vibrations in molecular bonds, such as bending, stretching, rocking, wagging, twisting and out-of-plane deformation, occurring at different wavenumbers or frequencies in the IR region of the light spectrum. The wavenumber of each IR absorbance peak is determined by the intrinsic physicochemical properties of the corresponding molecule, allowing for the identification of specific functional groups, such as C-H, C=O, and O-H. The absorbance of each vibrational band can be measured by the maximum height or the integrated area between the peak and a baseline. The absorbances of molecular vibrations under IR radiation correspond to the abundance of functional groups.

In this study, the Perkin Elmer Spectrum 3 Tri-range model employed as the FTIR instrument. The wavenumber range set for analysis was 4000-400 cm^{-1} to determine the functional groups before and after the intercalation between γ-Al_2O_3 and thiol. Since the instrument is an Attenuated Total Reflectance (ATR) type, a sample was simply placed directly on a special crystal as in Figure 3.11(a) (indicated with red arrow). The FTIR instrument allowed us to predict the mechanisms (Pang et al., 2022) between γ-Al_2O_3 and thiol. Figure 3.11(b) displays the FTIR instrument utilised in this research.

Figure 3.11

FTIR analysis which consisted of (a) special crystal (red arrow) on the sample holder for FTIR instrument and (b)FTIR instrument

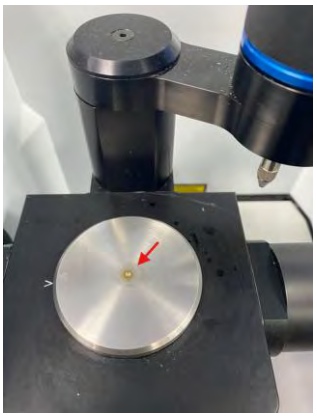

(a)

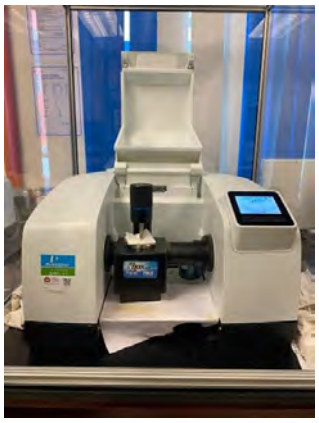

(b)

3.4.6 X-ray Photoelectron Spectroscopy (XPS)

XPS was used to analyse the surface properties of the samples by examining specific binding energies (Pang et al., 2022). XPS has been applied in various fields, including nanomaterials, mineral processing, electronics, corrosion, catalysis, biomedicine, aerospace and automotive (Krishna & Philip, 2022). This instrument provides information on the chemical composition, surface functionalisation, layer thickness and sometimes even particle size of nanomaterials. Theoretically, when materials are exposed to X-rays, photoelectrons are ejected from different energy levels of the material's surface atoms. Changes in the element's chemical bonding and the environment surrounding it, which result from variations in its oxidation state or electronic charge distribution around the nucleus, cause a shift in the binding energy (BE) of an electron in a particular energy level of an element (atom). The kinetic energies of the photoelectrons are then measured by a hemispherical analyser. The BE of an energy level can be determined from the photoelectron's kinetic energy obtained

from that particular level, according to Koopman's theorem. Figure 3.12 shows the principle of XPS generally by an energy level diagram, accompanied by a typical XPS spectrum. In the diagram, the blue circles represent electrons in the core levels, which are labeled using standard spectroscopic notation. The valence band is denoted as VB. The work functions of the spectrometer (XPS) and the sample under analysis are represented as φ and φ_s, respectively. The kinetic energy apparent to the spectrometer is labeled as E_K, while the energy acquired after emission is labeled as E'_K. The vacuum level is denoted as E_V, and the Fermi level as E_F. X-ray photon energy is represented by hν (Krishna & Philip, 2022).

The preparation of the sample was almost the same as in the FESEM analysis. The sample was placed onto a piece of conductive carbon tape. The sample was ensured to be distributed evenly on the surface of the tape. This was to ensure that the sample was in the proper position to withstand the vacuum environment in the instrument.

Figure 3.12

Schematic illustration of the principle behind XPS

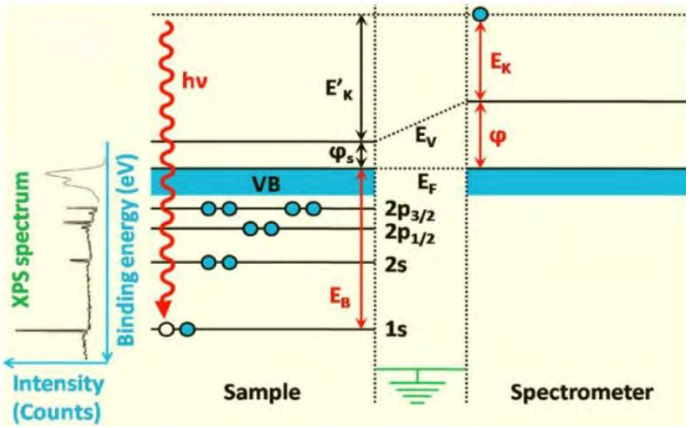

Adapted from Krishna & Philip, 2022

This instrument can verify the intercalation between γ-Al_2O_3 and thiol by looking at a specific binding energy and predict the mechanism between them. The analysis employed brand of Kratos/Shimadzu with Axis Ultra DLD model as shown in Figure 3.13. The energies were referred to aluminium, carbon, sulphur and oxygen peaks.

Figure 3.13

XPS instrument

3.4.7 Thermogravimetric Analyser (TGA)

TGA is a quantitative analytical method that measures the mass of a sample (ranging from 1 mg to a few g) as temperature increases in a furnace up to 1600 ^oC, while controlling the gas flow. This tool accurately monitors and records the temperature, time and mass of the sample. The temperature program can include cooling, heating, isothermal holds or a combination of these. The instrument itself consists of a precise microbalance that is connected to a sample pan inside a closed furnace, which is

equipped with a temperature programmer and controller, or a thermo balance (Saadatkhah et al., 2020).

Theoretically, a thermogravimetric thermal curve or thermogram is a plotted graph version of the sample mass change vs time or temperature. A common thermogram will has several sections, which are:

- Below 150^{o}C – physisorbed water, volatile compound with low molecular weight and trapped gas evolved.
- Between 150^{o}C-250^{o}C – mass lose due to chemisorbed water and volatile decomposition products as well as compounds with low molecular weight such as additives.
- Above 250^{o}C – beginning of the decomposition of compounds between onset and endset temperature. It is also possible to have several onset and endset temperatures for multi-component systems and for reactions with intermediate steps.
- Above endset temperature – the remaining material including non-volatile inorganic ashes and metals.
- Metallic compounds acquire mass and increase in oxidation state in an oxidizing environment.

The schematic figure of a thermobalance, which can be considered as the heart of a TGA instrument, is shown in Figure 3.14. It consists of several subunits, including a furnace, temperature programmer, electronic microbalance, recorder and sample holder. The thermobalance features a clamp that is used to secure the arm of the microbalance. It is important to note that when the clamp is released, the balance should

be returned to the zero position. If the thermobalance, which holds the arm of the microbalance, is moved, the zero position will be affected. It is recommended to allow the thermobalance to stabilise for 15-20 minutes after placing the sample.

TGA was employed to evaluate the thermal stability of γ-Al_2O_3, γ-Al_2O_3(C)-BDMT, γ-Al_2O_3(S)-BDMT, γ-Al_2O_3(C)-TgA and γ-Al_2O_3(S)-TgA using model Netzsch TG 200 F3 Tarsus. It was performed under N_2 atmosphere by heating up to 900 ^oC at a heating rate of 10 ^oC min^{-1}. Before began the analysis, a sample was placed on a balance (Figure 3.15(a)) weighing ~7.5 mg. This method measures the mass change over time as the temperature change. Figure 3.15(b) shows the TGA instrument utilised for thermal stability study in this research.

Figure 3.14

Schematic figure of a thermobalance in TGA

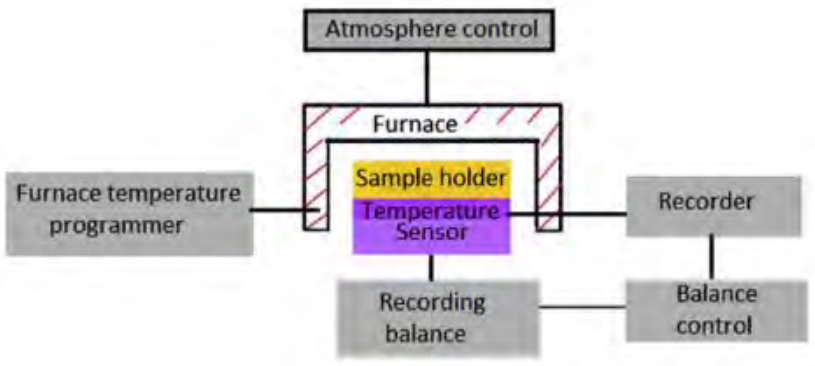

Adapted from Loganathan et al, 2017

Figure 3.15

TGA analysis which consisted of (a) balance of sample in TGA instrument and (b) TGA instrument

(a)

(b)

3.5 Stage 3: Adsorption Studies of γ-Al_2O_3(C)-BDMT, γ-Al_2O_3(S)-BDMT, γ-Al_2O_3(C)-TgA and γ-Al_2O_3(S)-TgA

The potential of the adsorbents to adsorb Cd^{2+} was investigated through batch experiments. The next subsections detail the procedures for preparing Cd solutions, conducting batch adsorption studies and evaluating γ-Al_2O_3(C)-BDMT, γ-Al_2O_3(S)-BDMT, γ-Al_2O_3(C)-TgA and γ-Al_2O_3(S)-TgA as adsorbents.

3.5.1 Preparation of Cd^{2+} Solution

A stock solution of 100 mg/L was prepared by dissolving a specific amount of cadmium acetate dihydrate in deionised water. The stock solution was then diluted to the desired concentrations prior to proceeding with the adsorption studies.

3.5.2 Batch Adsorption Studies

Several parameters were studied to determine the effect of various factors on the adsorption tests of Cd^{2+}. These tests were conducted in batch experiments. The parameters included the pH of the Cd^{2+} solution, the initial Cd^{2+} concentration and the contact time.

3.5.2.1 pH of Cd^{2+} Solution Effect

The effect of the Cd^{2+} solution's pH was studied within the range of pH 2.0 to 8.0. In order to achieve the desired pH level, a few drops of either 1 mol/L or 0.1 mol/L HCl and 1 mol/L or 0.1 mol/L NaOH were added to the 10.0 mg/L aqueous Cd^{2+} solution. The pH was measured using pH meter (Thermo Scientific, model Orion 2-Star) and 5 mg of adsorbents were used.

3.5.2.2 Initial Cd^{2+} Concentration Effect

The study examined the initial concentration of Cd^{2+} which were 5, 10, 20, 30, 40 and 50 mg/L, using 5 mg of adsorbents. The pH of the aqueous solution containing Cd^{2+} was determined based on the optimal result from the pH study.

3.5.2.3 Contact Time Effect

The contact time between adsorbents and a Cd^{2+} solution was studied at different time intervals, ranging from 0.5 to 40 minutes, using 5 mg of adsorbent.

3.5.3 Procedures for Evaluation of γ-Al_2O_3(C)-BDMT, γ-Al_2O_3(S)-BDMT, γ-Al_2O_3(C)-TgA and γ-Al_2O_3(S)-TgA as Adsorbents

In the adsorption studies, three conditions were set as constant; rotation speed (220 rpm), volume of Cd^{2+} solution (100 mL) and amount of adsorbent (5 mg). The ideal shaking speed for the adsorption process is 100-200 rpm (Naihi et al., 2022) and the rotation speed of 220 rpm was chosen to replicate the study by Zhang et al. (2023). The Cd^{2+} solution was agitated using a Protech Orbital Shaker 720 (distributed by Tech-Lab Scientific Sdn. Bhd.) in 250 mL conical flask. Temperature was not considered as a variable, so the study was conducted under ambient conditions (open space room condition) to mimic real-world scenario. Babel and Kurniawan (2003) cited that various adsorbent, including activated carbon and natural materials, effectively remove heavy metals at room temperature under typical wastewater treatment conditions. The amount of adsorbent used for each study was fixed at 5 mg. During pilot study, the solid to liquid ratio (S:L) was at 0.05 with percentage of removal (%) exceed 80 %. The S:L ratio was used in this research since the % was in the good range. Furthermore, the little number of adsorbents used during the study can help to achieve one of good characteristics of adsorbent which is can remove huge amount of adsorbate.

The adsorption experiment was investigated by agitating eight 100 mL solutions, each containing 5 mg of adsorbent and a predetermined concentration of Cd^{2+}, in conical flasks placed on an orbital shaker. 20 mL of the Cd^{2+} solution was collected at varying time intervals (0.5, 1, 2, 5, 10, 20, 30, and 40 minutes) from each flask, after which was filtered through filter paper to separate the adsorbent. The residual Cd^{2+} concentration in the filtrate was quantified using Atomic Absorption Spectroscopy (AAS; PerkinElmer, Analyst 400). The obtained data were analysed to

evaluate the adsorption isotherm and kinetics, with detailed results and discussions presented in Chapter 4.

3.5.4 Adsorption Isotherm Models

Adsorption isotherms were utilised to determine the adsorption between the contaminants (liquid phase) and the adsorbents (solid phase) (Shamsudin, 2016). The adsorption capacity of γ-Al_2O_3(C)-BDMT, γ-Al_2O_3(S)-BDMT, γ-Al_2O_3(C)-TgA and γ-Al_2O_3(S)-TgA was analysed using linearised Langmuir and Freundlich isotherm models.

The adsorption capacity of γ-Al_2O_3(C)-BDMT, γ-Al_2O_3(S)-BDMT, γ-Al_2O_3(C)-TgA, and γ-Al_2O_3(S)-TgA towards Cd^{2+} was calculated using Equation 3.4:

$$q_e = \left(\frac{C_o - C_e}{W}\right) V \tag{3.4}$$

Where q_e is the amount of Cd^{2+} adsorbed by γ-Al_2O_3(C)-BDMT, γ-Al_2O_3(S)-BDMT, γ-Al_2O_3(C)-TgA and γ-Al_2O_3(S)-TgA (mg/g), C_o is the initial concentration of Cd^{2+} (mg/L), C_e is the equilibrium concentration of Cd^{2+} (mg/L), W is the weight of the γ-Al_2O_3(C)-BDMT, γ-Al_2O_3(S)-BDMT, γ-Al_2O_3(C)-TgA and γ-Al_2O_3(S)-TgA (g) and V is the volume of Cd^{2+} solution (L). Meanwhile, the percentage of removal (%) was determined using the formula Equation (3.5) below:

$$\text{Percentage of removal (\%)} = \left(\frac{C_o - C_e}{C_o}\right) \text{x } 100 \tag{3.5}$$

Where C_o is the initial concentration of Cd^{2+} solution (mg/L) and C_e is the final equilibrium concentration of Cd^{2+} solution (mg/L). The results of the isotherm analysis are reported in Chapter 4.

3.5.4.1 Langmuir Isotherm

The linearised Langmuir isotherm is employed to assess whether the adsorbents used have a homogeneous surface, ensuring that the bound Cd^{2+} remains constant across all directions on the surface of the adsorbents (Wahyuhadi et al., 2023). In general, the linearised Langmuir isotherm indicates a uniform surface, where adsorption ceases once all the available adsorption sites are occupied. The model for the linearised Langmuir isotherm model is presented in Equation 3.6 below (Mahmoud et al., 2021).

$$\frac{C_e}{q_e} = \frac{1}{q_{max} K_L} + \frac{C_e}{q_{max}} \tag{3.6}$$

Where C_e is the concentration at equilibrium (mg/L), q_e is the adsorption capacity of Cd^{2+} on the adsorbent at equilibrium (mg/g), q_{max} is the saturated adsorption capacity based on the linearised Langmuir theory and K_L is the linearised Langmuir adsorption constant (L/mg). To plot the linearised Langmuir isotherm, the values obtained from the AAS instrument were labeled as C_e (mg/L) which served as the x-axis of the graph. Then, q_e (mg/g) values were calculated based on Equation 3.4. y-axis of this isotherm took C_e/q_e (g/L) as its component.

3.5.4.2 Freundlich Isotherm

Meanwhile, the linearised Freundlich isotherm suggests that adsorption occurs in multiple layers on the surface of the adsorbents. As the concentration increases, the adsorption also increases (Wahyuhadi et al., 2023). Generally, if the adsorption leans towards the linearised Freundlich isotherm, it indicates that the adsorbents have a heterogeneous surface (Mahmoud et al., 2021). The model of the linearised Freundlich isotherm is expressed through Equation 3.7, as shown below (Liang & Zou, 2020).

$$\log q_e = \log K_f + \frac{1}{n} \log C_e \tag{3.7}$$

Where C_e is the concentration at equilibrium (mg/L), q_e is the adsorption capacity of Cd^{2+} on the adsorbent at equilibrium (mg/g), n is the linearised Freundlich constant associated with adsorption intensity and K_f is the linearised Freundlich constant associated with adsorption capacity. For the Freundlich isotherm, the x-axis was labeled as log C_e while log q_e served as the y-axis.

3.5.5 Adsorption Kinetics

In this research, the adsorption kinetics employed were pseudo-first order and pseudo-second order models. The best fitting model chosen from both models was based on the linear correlation coefficient, R^2 (Yusuff, 2019). The pseudo-first order and pseudo-second order models can be calculated using Equation 3.8 and 3.9 respectively.

$$\text{Log}\,(q_e - q_t) = \log q_e - (K_1/2.303)\,t \tag{3.8}$$

$$t/q_t = \frac{1}{K_2 q_e^2} + \left(\frac{1}{q_e}\right) t \tag{3.9}$$

Where q_t is adsorption capacity at contact time (t), K_1 is the pseudo-first order rate constant (min^{-1}) and K_2 is the pseudo-second order rate constant ($g\ mg^{-1}\ min^{-1}$). For the pseudo-first order, the x-axis was labeled as $\log (q_e - q_t)$ while x-axis for the pseudo-second order was labeled as t/q_t. Both kinetic models have contact time (min) as y-axis.

The pseudo-first-order adsorption kinetic model posits that the rate of adsorption is primarily governed by the diffusion of the adsorbate across the adsorbent surface. In contrast, the pseudo-second-order adsorption kinetics applies to processes that take longer to fill the adsorption sites. This model assumes that the adsorption rate is influenced by the interactions between the adsorption sites on the adsorbent surface and the adsorbate throughout the adsorption process (Wang et al., 2022).

3.5.6 Measurement of Cd

3.5.6.1 Atomic Absorption Spectroscopy (AAS)

The AAS instrument was used to measure the concentration of Cd^{2+} in the solution (Yusuff et al., 2019) after batch adsorption, specifically using the Perkin-Elmer PinAAcle 900F. AAS generally consists of five basic components; a light source, absorption cell, monochromator, detector and a display (Figure 3.16). Essentially, a sample atom in a "ground state" absorbs specific wavelengths and energy emitted by a hollow cathode lamp (Figure 3.17). For this research, a Cd hollow cathode lamp was employed. If there are more atoms in the sample that intersect the light path, more light

will be absorbed. In conclusion, the concentration of absorbed light energy corresponds to the amount of analyte present in the sample (Shamsudin, 2016).

Figure 3.16

AAS instrumentation and interference

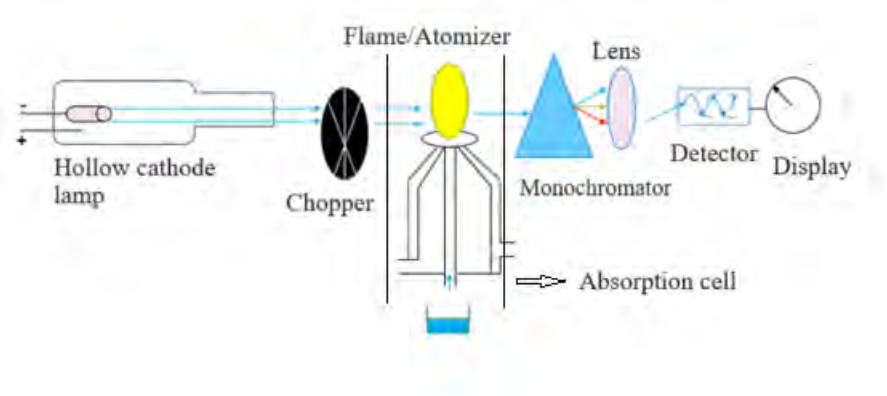

Figure 3.17

Hollow cathode lamps

Before measuring the concentration of Cd^{2+} using AAS, it is necessary to prepare standard solutions for plotting the calibration curve (Appendix 1). The standard solutions were prepared by diluting the desired AAS standard solution, which in this

case was Cd. The stock AAS standard solution had a concentration of 1000 mg/L. The dilutions were prepared at concentrations of 1, 2, 3, 4, and 5 mg/L. Additionally, a quality control (QC) sample was run at a concentration of 3 mg/L. During the analysis, each sample underwent triplicate readings and the mean of the readings was taken into calculation. Figure 3.18 depicts the AAS instrument, including its hollow cathode lamps.

Figure 3.18

AAS instrument

3.6 Summary

In this chapter, the methodology applied to investigate and counter the issue of rising Al waste and Cd pollution in Malaysia by synthesising new adsorbents (γ-Al_2O_3(C)-BDMT, γ-Al_2O_3(S)-BDMT, γ-Al_2O_3(C)-TgA and γ-Al_2O_3(S)-TgA) has been comprehensively described. The research adopted an experimental approach, utilising XRD, FESEM, EDX, surface area and pore diameter, XPS, FTIR, TGA and AAS analysis to obtain data under controlled laboratory conditions. The choice of methods

was informed by their suitability for accurately measuring phase of Al_2O_3, topography of compounds, composition of elements in compounds, bonds available in compounds, size and pore diameter of particle in compounds, thermal properties and concentration of Cd^{2+} in solutions. Details regarding sample preparation, material specifications, instrument calibration, and procedural protocols have been provided to ensure reproducibility. The methods of data analysis were also outlined to validate the experimental results and ensure the accuracy of conclusions drawn. Ethical considerations and safety protocols were strictly adhered to throughout all stages of the experimental work. This methodological framework sets the foundation for the presentation and discussion of the experimental findings, which will be explored in the following chapter.

CHAPTER 4

RESULTS AND DISCUSSION

4.1 Introduction

Synthesis of γ-Al_2O_3(S) nanoparticles and synthesis of adsorbents in this research; γ-Al_2O_3(C)-BDMT, γ-Al_2O_3(S)-BDMT, γ-Al_2O_3(C)-TgA and γ-Al_2O_3(S)-TgA were discussed in Chapter 3. This chapter will discuss the findings of both Stage 2 (characterisation study) and Stage 3 (adsorption study).

4.2 Characterisation Study

In this section, the surface morphology, surface area and pore size, thermal properties, as well as the surface chemistry between molecules, are discussed to predict the intercalation mechanism before proceeding to adsorption studies. This characterisation study is in Stage 2 of this research's framework. The Stage 2 is divided into two sections. Section 1 is dedicated to the characterisation for synthesis of γ-Al_2O_3. This section provides information on the surface morphology, surface area and pore size of the synthesised γ-Al_2O_3. Next is Section 2, which is the characterisation for synthesis of γ-Al_2O_3-BDMT and γ-Al_2O_3-TgA. This stage provides information on the surface chemistry between γ-Al_2O_3, 1,4-BDMT and TgA molecules to predict the intercalation mechanism between them.

4.3 Stage 2, Section 1: Characterisation of γ-Al_2O_3(C) and γ-Al_2O_3(S)

The analysis results for γ-Al_2O_3 (named as γ-Al_2O_3(S) using XRD, BET, FESEM and EDX are discussed in this section. These findings validate the production of γ-Al_2O_3(S). The identification of the crystal lattice, reflecting the phase of the investigated unknown phase of Al_2O_3 (later proven to be γ-Al_2O_3), was confirmed by XRD examination. The surface area and pore size values of γ-Al_2O_3(S) were obtained through surface area and porosity analysis. The surface shape of γ-Al_2O_3(S) was examined using FESEM analysis and its elemental composition was determined using EDX. The same analysis also applied to γ-Al_2O_3(C). The comparison between γ-Al_2O_3(S) and γ-Al_2O_3(C) was

analysed to see if γ-Al_2O_3(S) exhibited the same or almost same characteristics as γ-Al_2O_3(C), a commercial γ-Al_2O_3 which purchased from the market.

4.3.1 XRD Analysis

X-ray Diffraction (XRD) analysis was conducted exclusively on γ-Al_2O_3(C) and γ-Al_2O_3(S) to confirm the phase of these compounds. Figure 4.1(a) shows the XRD analysis results for γ-Al_2O_3(C), which displayed characteristic diffraction peaks at 2 theta values of 32.09°, 37.82°, 46.01°, and 67.12°. These peaks correspond to the planes (2 2 0), (3 1 1), (4 0 0), and (4 4 0) planes, respectively, indicative of the γ-Al_2O_3 (Prins, 2020). Confirmation of γ-Al_2O_3(C) was obtained by referring to JCPDS-ICDD file No. 00-050-0741, consistent with the findings reported by Maldonado et al. (2017). The crystallite size of γ-Al_2O_3(C) was calculated using the Scherrer equation, yielding a value of 2.9 nm, which is comparatively smaller than that of γ-Al_2O_3(S).

Subsequently, Figure 4.1(b) presents the XRD analysis results for the γ-Al_2O_3(S). The γ-Al_2O_3(S) exhibited diffraction peaks at 2 theta values of 31.83°, 37.52°, 45.64°, and 66.52°, corresponding to the (2 2 0), (3 1 1), (4 0 0), and (4 4 0) planes respectively, confirming its γ-Al_2O_3 characteristic (Prins, 2020). The identification of γ-Al_2O_3(S) was also confirmed by referring to JCPDS-ICDD files, No. 00-050-0741, consistent with the result of Maldonado et al. (2017). The crystallite size of this γ-Al_2O_3(S), calculated via the Scherrer equation, was determined to be 16.3 nm. This size is comparable to that of the commercial γ-Al_2O_3 reported by Rozita et al.

(2010) (16 nm), and the synthesised γ-Al_2O_3 from Li et al. (2013) (14.9 nm) and Mahinroosta and Allahverdi (2018) (15.90 nm). Table 4.1 summarises the characterisation of γ-Al_2O_3(C) and γ-Al_2O_3(S), detailing parameters such as pore volume and pore size. Table 4.2 indicates that γ-Al_2O_3(S) exhibits larger crystallite sizes than previously reported synthesised γ-Al_2O_3 samples. Thus, γ-Al_2O_3(S) may not exhibit nano-sized characteristics, as Parida et al. (2009) noted that small particle sizes indicate a nano-sized nature due to reduced crystallite size. Additionally, Wang et al. (2013) observed that adsorption capacity decreases as crystallite size increases. It is anticipated that γ-Al_2O_3(S) may exhibit a slightly lower adsorption capacity than γ-Al_2O_3(C), although further results will be featured in subsequent sections detailing adsorption studies for γ-Al_2O_3(C)-BDMT, γ-Al_2O_3(S)-BDMT, γ-Al_2O_3(C)-TgA and γ-Al_2O_3(S)-TgA.

Figure 4.1

XRD pattern of (a) γ-Al_2O_3(C) and (b) γ-Al_2O_3(S)

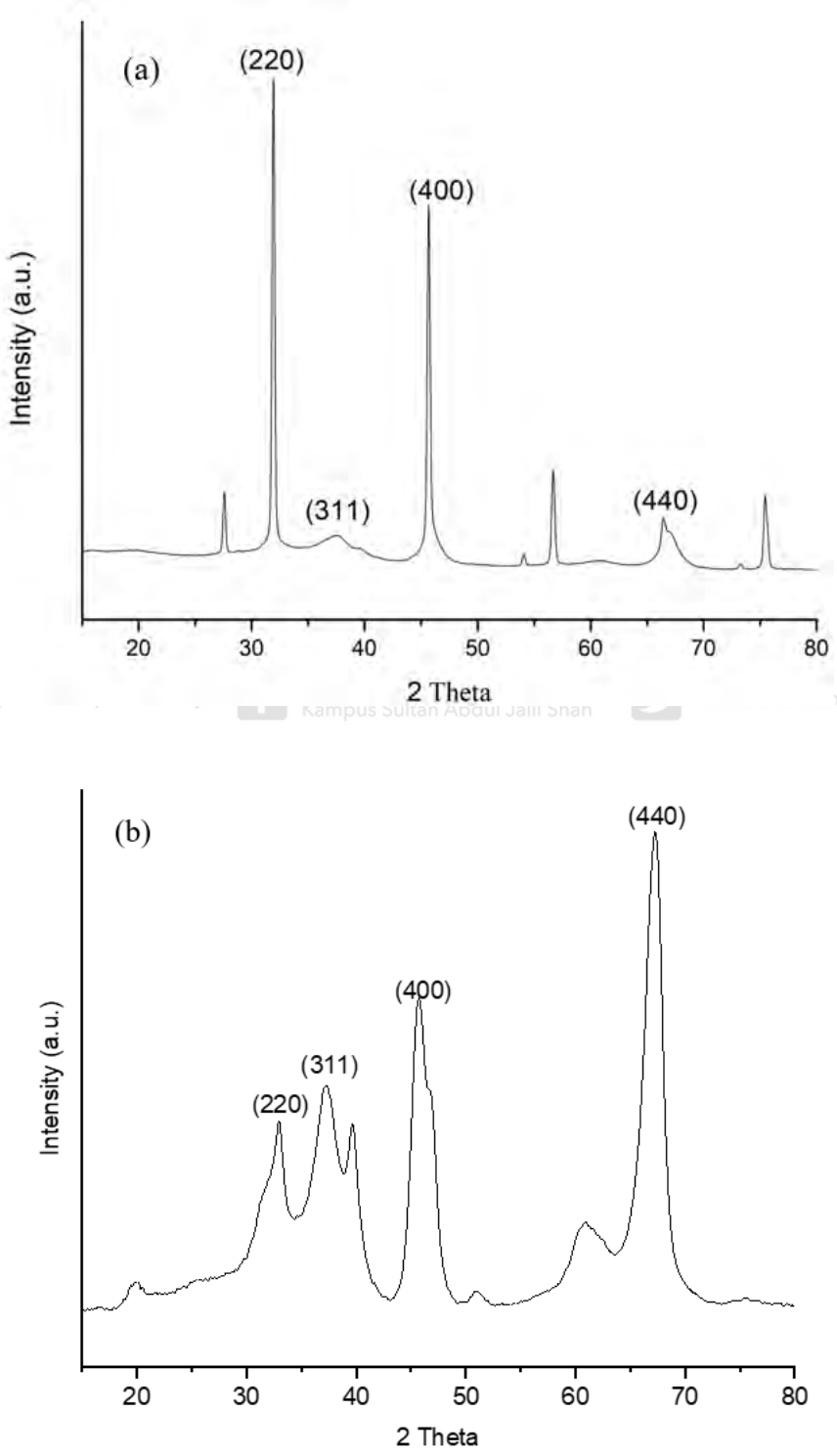

4.3.2 Surface Area and Pore Diameter Analysis

In this study, BET surface area and BJH pore size methods were employed utilizing nitrogen (N_2) adsorption-desorption isotherm.

Table 4.1 shows the characterisation of γ-Al_2O_3(C) and γ-Al_2O_3(S). The pore diameter of γ-Al_2O_3(C) was determined to be 28.40 nm, whereas γ-Al_2O_3(S) exhibited a pore diameter of 4.47 nm. According to a review by AlOthman (2012), mesoporous materials have pore sizes ranging from 2.0-50.0 nm, which is consistent with findings from Liu et al. (2021) and Fatimah et al. (2021). Thus, both compounds are classified as mesoporous material. Mesoporous compounds are characterised by a regular microstructure consisting of pores with similar diameters (Bednarska & Koniorczyk, 2019). The BET surface area for γ-Al_2O_3(C) was measured at 137.44 m2/g, while γ-Al_2O_3(S) was significantly lower at 78.08 m^2/g. The pore volume for both γ-Al_2O_3(C) and γ-Al_2O_3(S) were 0.95 cm^3/g and 0.1 cm^3/g respectively. Compared to other studies, the surface area for γ-Al_2O_3(S) was very low compared to other researches; >200 m^2/g (Shahidian et al., 2020), 126.76 m^2/g (Singh et al., 2014), and 214 m^2/g (Benu et al., 2021). A material is characterised as having high surface area if its surface area exceeds 100 m^2/g, thereby indicating potential suitability as a catalyst support material (Yahaya et al., 2021). It can be confidently stated that the maximum specific surface area should be exceeds 100 m^2/g, which only applied to γ-Al_2O_3(C). The lower surface area of γ-Al_2O_3(S) compared to previous research implies that it may exhibit reduced adsorption capacity, as noted by Liu et al. (2021). Mustapha et al. (2019) indicated that a larger surface area corresponds to more unoccupied spaces adsorption sites, potentially leading to an increased percentage removal of pollutants. Furthermore, as the adsorbent

dosage increases, the removal efficiency of metal ions tends to rise due to enhanced adsorbent surface area, pore size, and volume (Mustapha et al., 2019).

The pore volume of γ-Al_2O_3(S), at 0.10 cm^3/g, is lower when compared to other researches; 0.99 cm^3/g (Benu et al., 2021), 0.697 cm^3/g and 0.256 cm^3/g (Sharma et al., 2022). This diminished pore volume may suggest that γ-Al_2O_3 could facilitate slower removal of Cd^{2+} ions, as posited by Kumar et al. (2019). In contrast, γ-Al_2O_3(C) with a pore volume of 0.95 cm^3/g, may afford faster removal of Cd^{2+} ions. These considerations represent preliminary assumptions that warrant further investigation. A compilation of specific surface area, pore sizes, and pore volume from past studies is provided in Table 4.2.

Table 4.1

Characterisation of γ-Al_2O_3(C) and γ-Al_2O_3(S)

	BET Specific Surface Area (m^2/g)	**Pore Volume (cm^3/g)**	**Pore Size (nm)**
γ-Al_2O_3(C)	137.44	0.95	28.40
γ-Al_2O_3(S)	78.08	0.1	4.47

Table 4.2

The compilation of crystallite sizes, specific surface area, pore size and pore volumes of synthesised γ- Al_2O_3 from current and previous researches

Crystallite Sizes (nm)	Specific Surface Area (m^2/g)	Pore Size (nm)	Pore Volumes (cm^3/g)	Reference
2.86	78.08	4.47	0.1	Current research
3.51, 4.16, 4.56 and 5.07	317, 168, 264 and 225	NM	NM	(Gholizadeh et al., 2023)
8	NM	NM	NM	(Alamouti et al., 2021)
NM	112.9	4.13	NM	(Ali et al., 2019)
4.54	311.15	5.25	0.36	(Ahmedzaki et al., 2018)
NM	203, 204 and 174	NM	0.32, 0.35 and 0.33	(Adans et al., 2016)
10	102.6	0.0305	1.189	(Salahudeen et al., 2015)

6.8, 7.2, 5.3 and 6.1	NM	NM	NM	(Dey, 2014)
4.7-5.7	190 (average)	2.41 (average)	~0.467 (average)	(Parida et al., 2009)
~14.53	269.9	NM	0.57	(Yi et al., 2009)
NM	120-180	NM	NM	(Nieto et al., 2006)

*NM = Not Mentioned

Figure 4.2 present the isotherm obtained for the γ-Al_2O_3(C) and γ-Al_2O_3(S), showing a type IV adsorption pattern which initially, a rounded knee was observed, indicating the formation of a monolayer. As the adsorption progresses to multilayers, the amount of adsorbate continues to increase (Kumari et al., 2024). According to Bardestani et al., 2019, type IV adsorption pattern belongs to solids with micro and mesopores. Thus, the pattern exhibited by both γ-Al_2O_3(C) and γ-Al_2O_3(S) showed the compounds were indeed mesoporous as mentioned in Surface Area and Pore Diameter analysis section.

Figure 4.2

N_2 adsorption-desorption isotherm of (a) γ-Al_2O_3(C) and (b) γ-Al_2O_3(S)

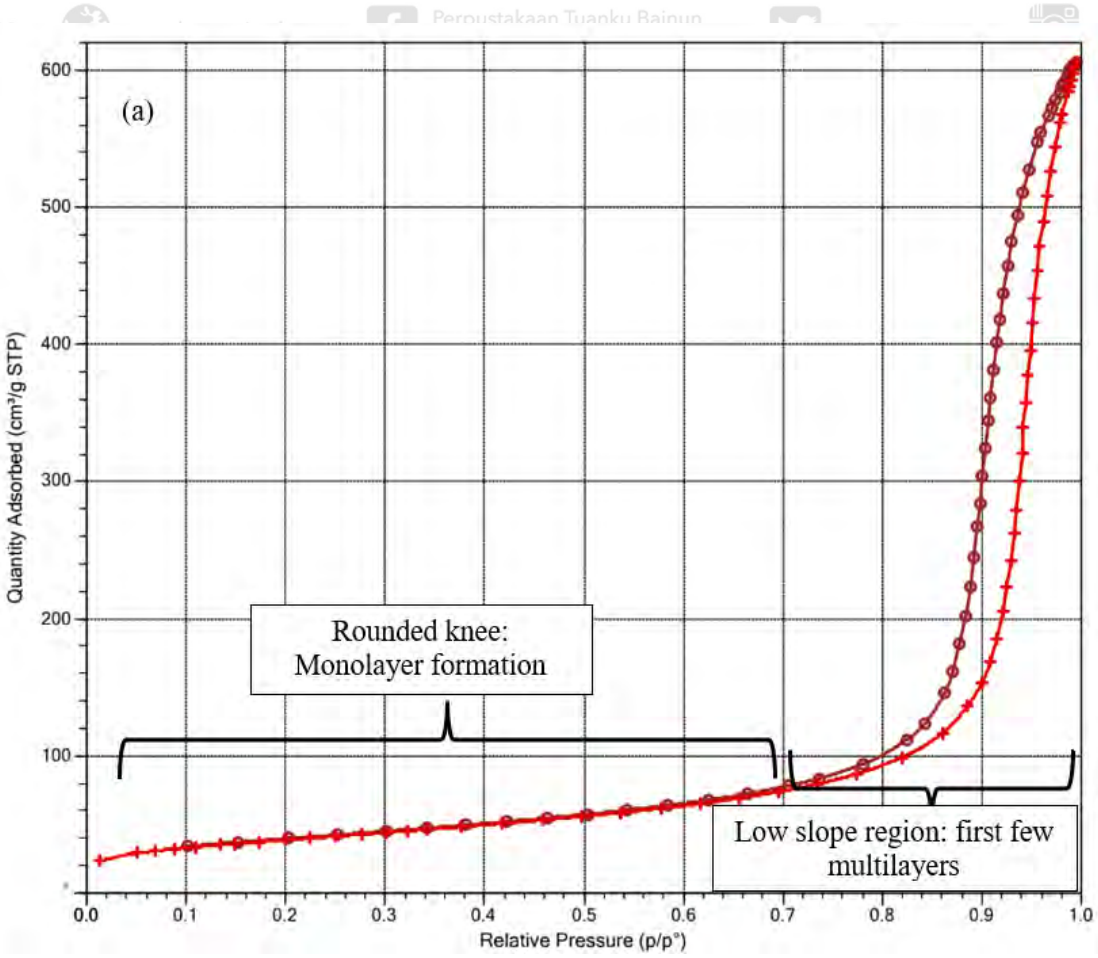

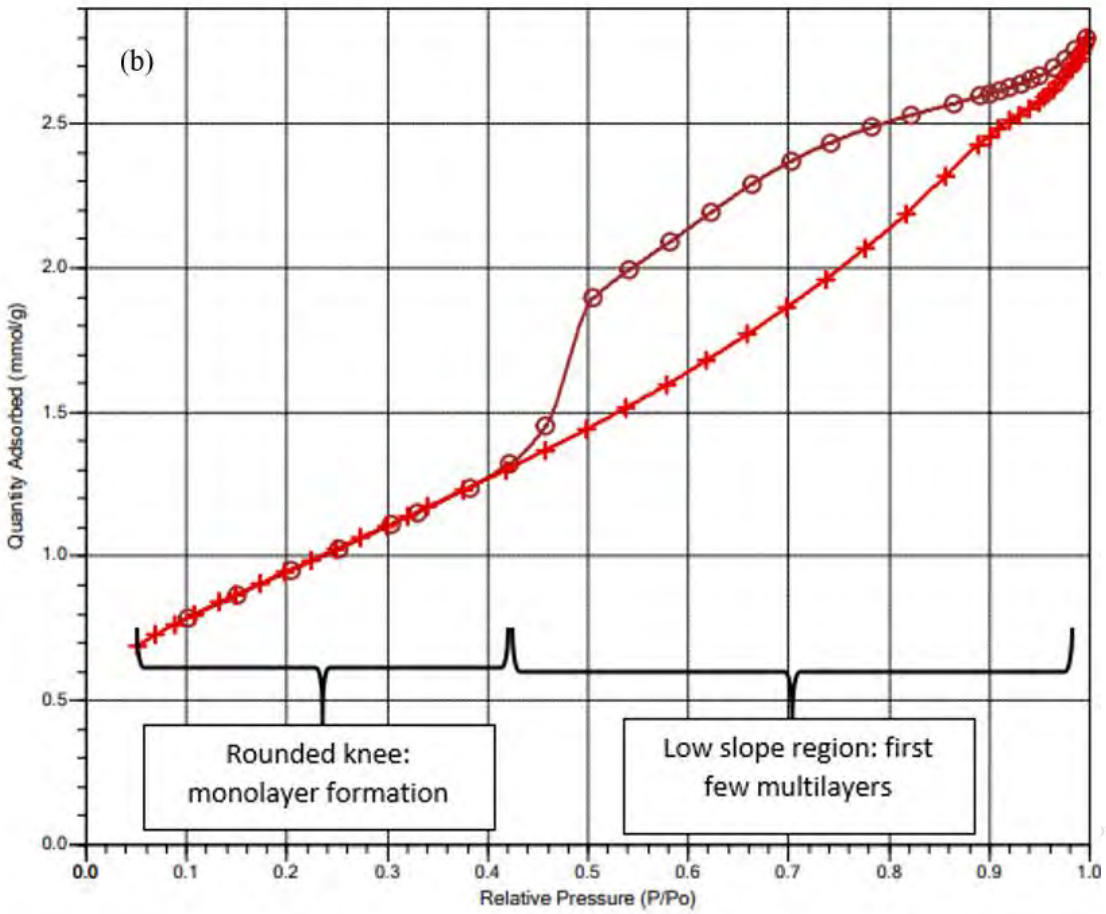

4.3.3 FESEM analysis

Figure 4.3 illustrates the surface morphology of γ-Al_2O_3(S), which closely resembles that reported by Thabet and Ismaiel (2016). Both this study and the aforementioned studies depict images of particles characterised by minimal aggregation, irregular and non-spherical shapes. From the figure, several pores were observed on the surface of the particles (indicated with red arrows). The particle sizes measured in this analysis ranged from 20-35 µm, which was considered small particle size according to How et al. (2017), who reported particle sizes ranging from 25-50 µm. How et al. (2017) indicated that small particle sizes and high surface areas enhance the effectiveness of

materials as catalysts and adsorbents within industrial applications. The previously discussed surface area of γ-Al_2O_3(S) indicated that this compound was smaller in size compared to γ-Al_2O_3(C). Therefore, γ-Al_2O_3(S) may also serve as an effective catalytic material and quality adsorbent due to its small particle size.

Figure 4.3

FESEM image of γ-Al_2O_3(S)

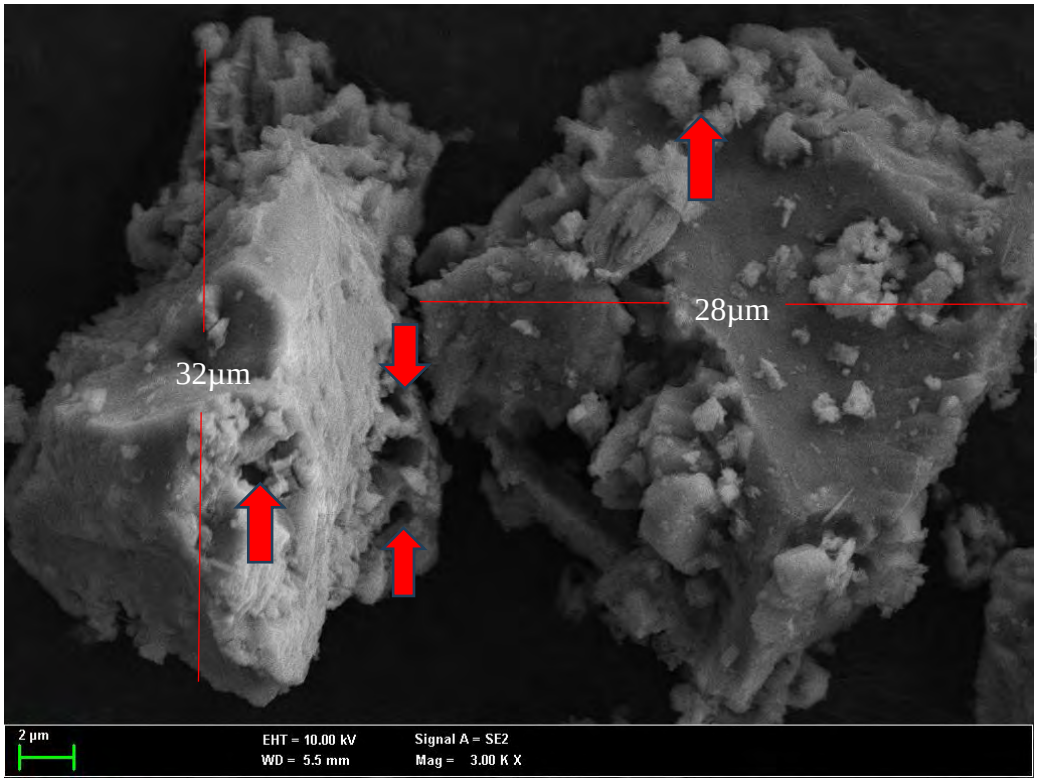

4.2.4 EDX analysis

Figure 4.4 displays the EDX analysis results of γ-Al_2O_3(S). The spectrum reveals that the composition was predominantly composed of Al and O elements, with percentages of 52.3% and 40.8% respectively. A small amount of carbon (6.9%) was also detected

and no sulphur was found (0%). The carbon may have originated from epoxy resins, which are used as coatings in food and beverage cans. These resins are composed of Bisphenol A (BPA) and Bisphenol A diglycidyl ether (BADGE), with the chemical formulas $C_{15}H_{16}O_2$ and $C_{21}H_{24}O_4$, respectively (Lestido-Cardama et al., 2022). Both compounds contain carbon elements. These findings align closely with the study conducted by Sheel et al. (2016), which reported an elemental composition of Al (52.81%) and O (44.28%) for aluminium oxide obtained from beverage cans. Based on these results, it can be concluded that γ-Al_2O_3(S) was primarily composed of Al and O.

Figure 4.4

EDX spectrum of γ-Al_2O_3 (S)

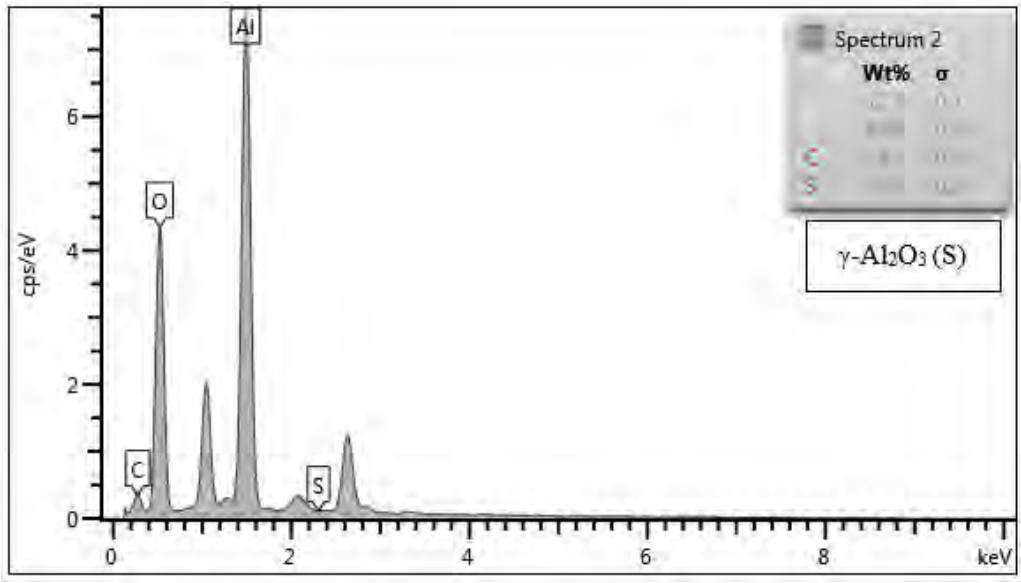

Characterisation using XRD, BET, FESEM and EDX showed that the synthesised γ-Al_2O_3 was in good condition and proceeded to Stage 2, Section 2 which was the characterisation of γ-Al_2O_3 -BDMT and γ-Al_2O_3-TgA.

4.4 Stage 2, Section 2: Characterisation of γ-Al_2O_3 -BDMT and γ-Al_2O_3-TgA

In this section, four adsorbents were synthesised; γ-Al_2O_3(C)-BDMT, γ-Al_2O_3(S)-BDMT, γ-Al_2O_3(C)-TgA and γ-Al_2O_3(S)-TgA. These four adsorbents were analysed using field emission scanning electron microscopy **(**FESEM) to determine surface methodology, energy-dispersive X-ray spectroscopy **(**EDX) for elemental composition analysis, X-ray photoelectron spectroscopy **(**XPS) to verify the intercalation between γ-Al_2O_3 and thiols, Fourier transform infrared spectroscopy **(**FTIR) to investigate functional groups and bonding characteristics, and thermogravimetric analysis (TGA) to evaluate thermal stability and decomposition behaviour.

4.4.1 XRD Analysis

γ-Al_2O_3(C)-BDMT, γ-Al_2O_3(S)-BDMT, γ-Al_2O_3(C)-TgA and γ-Al_2O_3(S)-TgA also provided the same pattern of diffraction peaks at 2 theta values and planes which the corresponding values can be appraised in Table 4.3. The XRD patterns of the adsorbents shown (Figure 4.5) which are the same as that of the γ-Al_2O_3(C) and γ-Al_2O_3(S) parent substrate indicating that the functionalisation did not affect the crystal structure of the substrate which is the adsorbents.

Table 4.3

2 theta values and planes of XRD analysis for γ-Al_2O_3(C)-BDMT, γ-Al_2O_3(S)-BDMT, γ-Al_2O_3(C)-TgA and γ-Al_2O_3(S)-TgA

Adsorbent	2 theta	Plane
γ-Al_2O_3(C)-BDMT	31.95, 37.66, 45.82 and 66.80	(2 2 0), (3 1 1), (4 0 0), and (4 4 0) respectively
γ-Al_2O_3(S)-BDMT	31.84, 37.52, 45.64 and 66.53	(2 2 0), (3 1 1), (4 0 0), and (4 4 0) respectively
γ-Al_2O_3(C)-TgA	32.01, 37.73, 45.90 and 66.93	(2 2 0), (3 1 1), (4 0 0), and (4 4 0) respectively
γ-Al_2O_3(S)-TgA	31.87, 37.56, 45.70 and 66.62	(2 2 0), (3 1 1), (4 0 0), and (4 4 0) respectively

Figure 4.5

XRD pattern of γ-Al₂O₃(C)-BDMT, γ-Al₂O₃(S)-BDMT, γ-Al₂O₃(C)-TgA and γ-Al₂O₃(S)-TgA

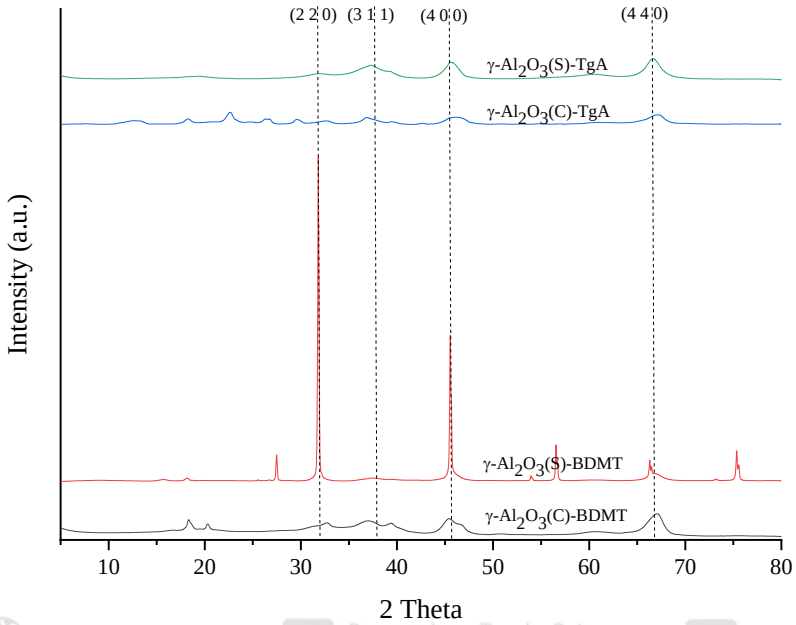

4.4.2 FESEM Analysis

Figure 4.6(b-e) shows the images for γ-Al₂O₃(C)-BDMT, γ-Al₂O₃(S)-BDMT, γ-Al₂O₃(C)-TgA and γ-Al₂O₃(S)-TgA. The images reveal that the adsorbents have rougher and more aggregated surfaces compared to γ-Al₂O₃(S), as depicted in Figure 4.6(a). This observation aligns with a study conducted by Hao et al. (2009), wherein blended activated alumina with pre-synthesized thiol-functionalised silica sol exhibited more congeries on the surface in SEM images compared to virgin activated alumina, indicating the attachment of mercaptopropyl silica onto the activated alumina. Moreover, Figure 4.6(b-e) also show that there were several pores (20-25 pores) were observed on the surfaces. The pores were present a lot more than the pores in γ-Al₂O₃(S)

which was ~ 10 pores. A large number of pores in γ-Al_2O_3(C)-BDMT, γ-Al_2O_3(S)-BDMT, γ-Al_2O_3(C)-TgA and γ-Al_2O_3(S)-TgA suggested that the adsorbents have more available adsorption sites than in γ-Al_2O_3(S). These findings demonstrate that the surfaces of γ-Al_2O_3(C)-BDMT, γ-Al_2O_3(S)-BDMT, γ-Al_2O_3(C)-TgA and γ-Al_2O_3(S)-TgA were covered by aggregated thiol particles and presented with plenty of available adsorption sites, confirming the successful intercalation of γ-Al_2O_3(C) and γ-Al_2O_3(S) with thiol compounds.

Figure 4.6

FESEM images of (a) γ-Al_2O_3(S), (b) γ-Al_2O_3(C)-BDMT, (c) γ-Al_2O_3(S)-BDMT, (d) γ-Al_2O_3(C)-TGA and (e) γ-Al_2O_3(S)-TGA. The red arrows show some pores found on the surfaces of these adsorbents

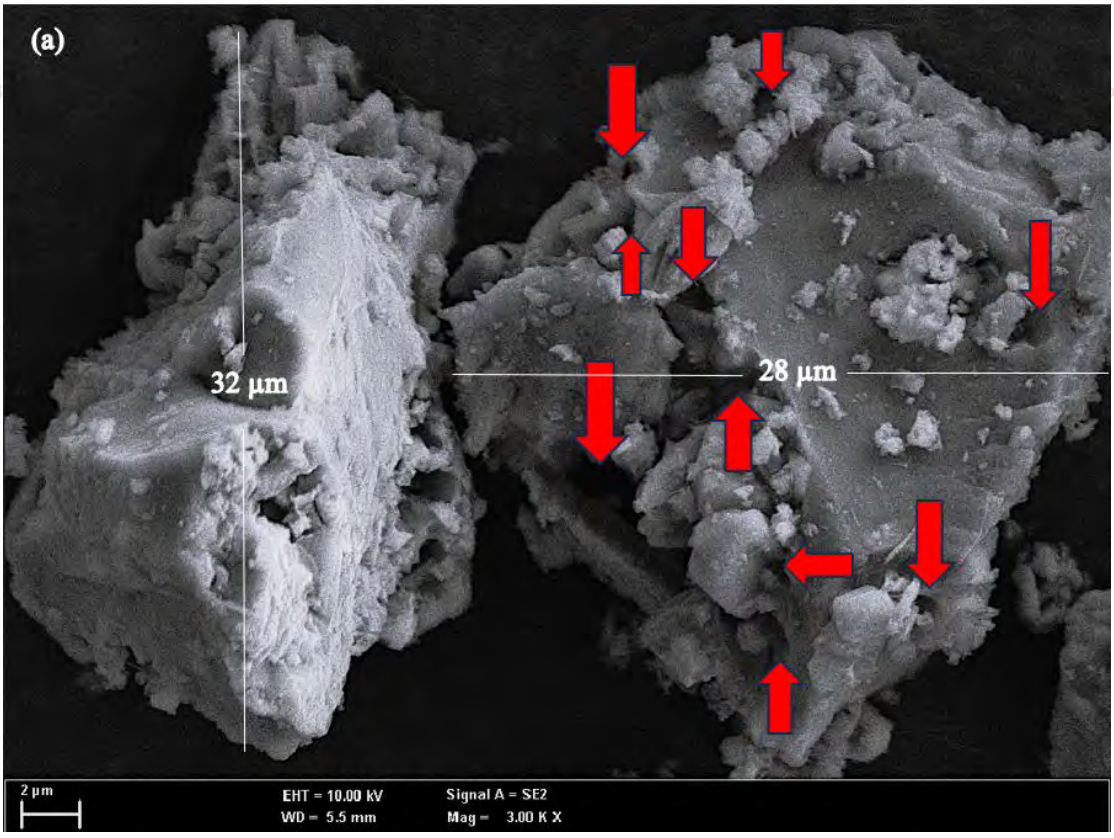

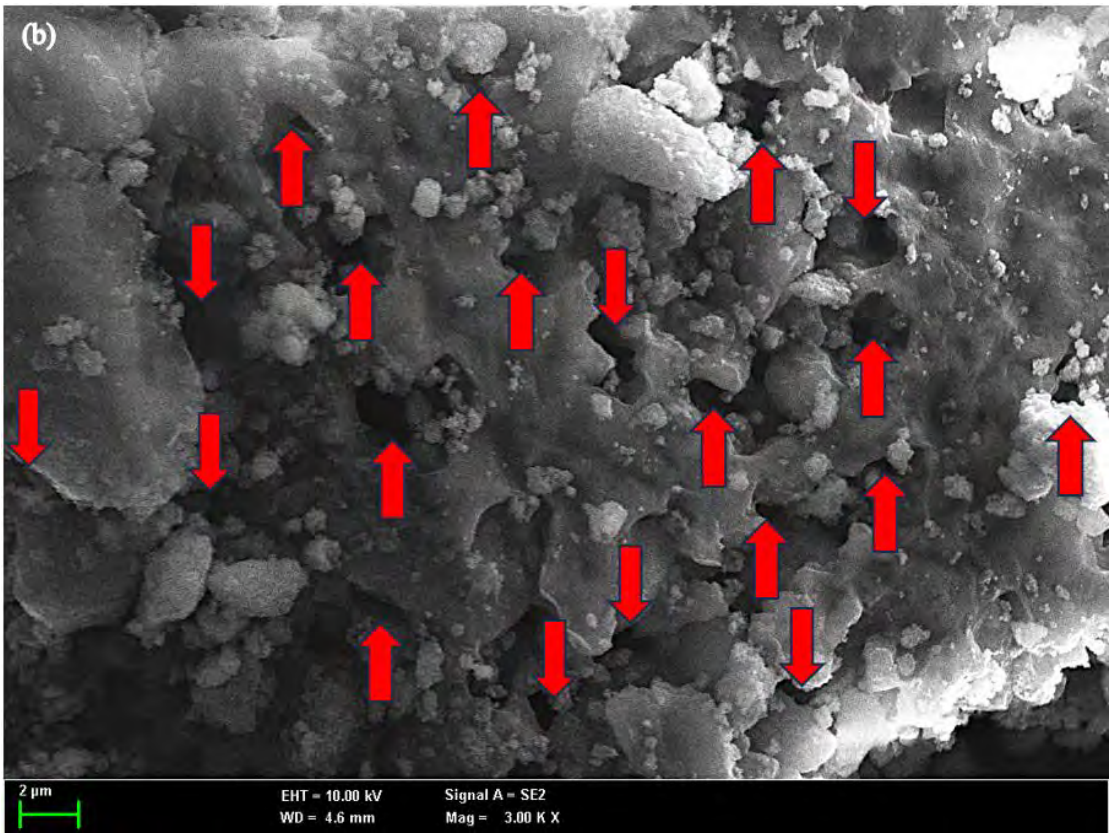

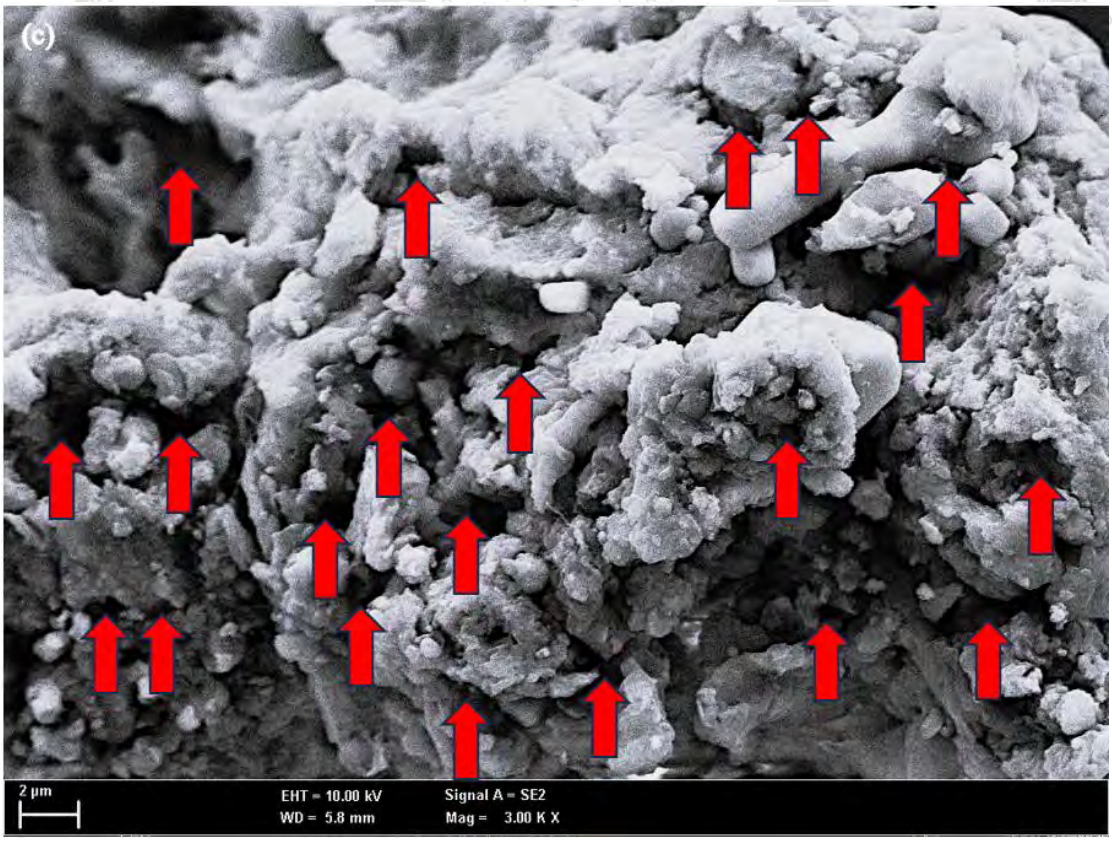

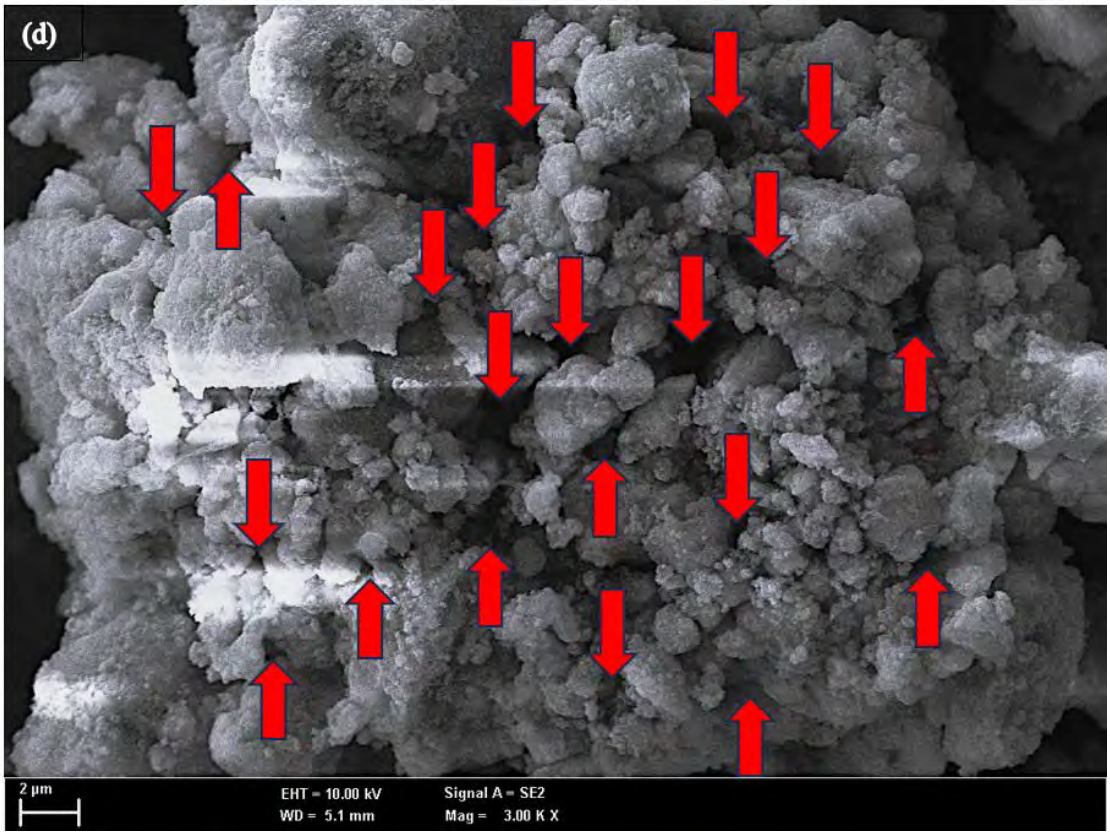

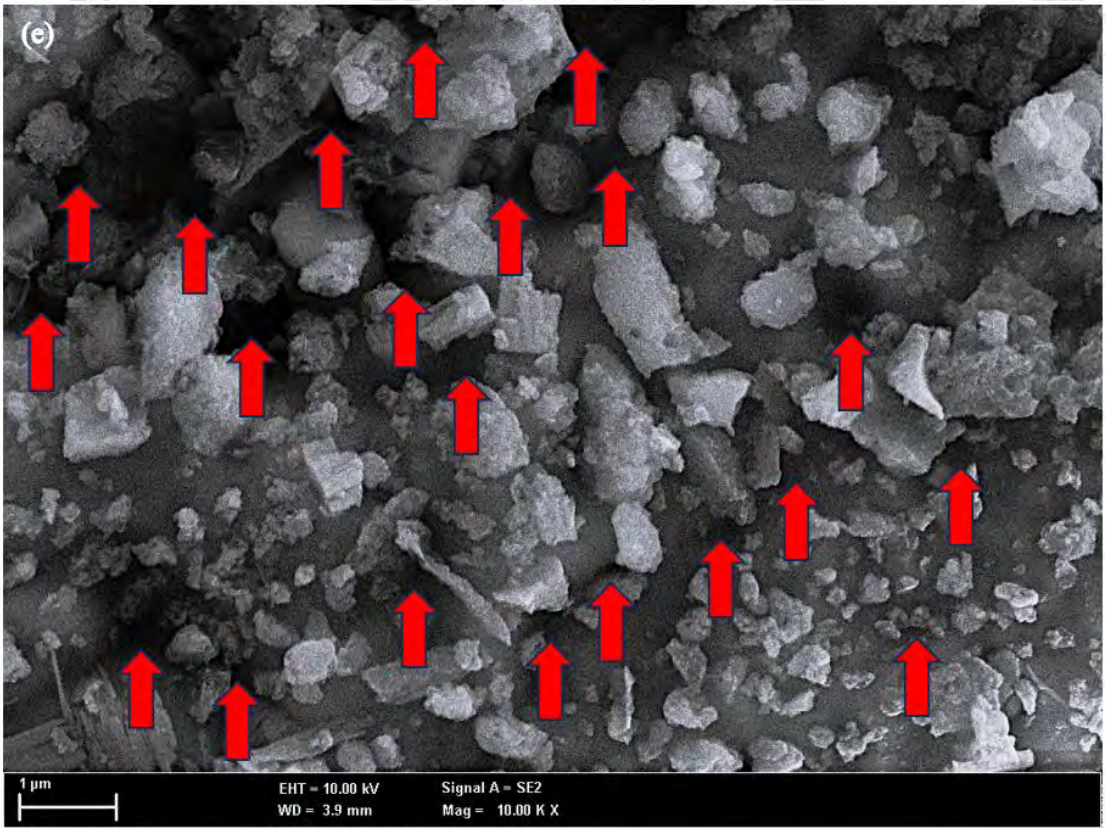

4.4.3 EDX Analysis

The EDX spectra of the γ-Al_2O_3(C)-BDMT, γ-Al_2O_3(S)-BDMT, γ-Al_2O_3(C)-TgA and γ-Al_2O_3(S)-TgA samples are shown in Figure 4.7.

Figure 4.7 depicts the combination of γ-Al_2O_3(C) and γ-Al_2O_3(S) with the 1,4-BDMT compound. Specifically, Figure 4.7 shows (a) γ-Al_2O_3(C)-BDMT and (b) γ-Al_2O_3(S)-BDMT which demonstrate the presence of the S element in the sample, with a weight percentage of 6.5% and 25.6%, respectively. This provides further evidence that the intercalation between γ-Al_2O_3 and 1,4-BDMT was successful. The interpretation aligns with the findings of Wang et al. (2021), who observed the appearance of sulphur in their EDX pattern after attaching thiol groups onto porous boron nitride. Their study focused on modifying porous boron nitride for mercury adsorption.

Figure 4.7

EDX spectra of (a) γ-Al_2O_3(C)-BDMT and (b) γ-Al_2O_3(S)-BDMT

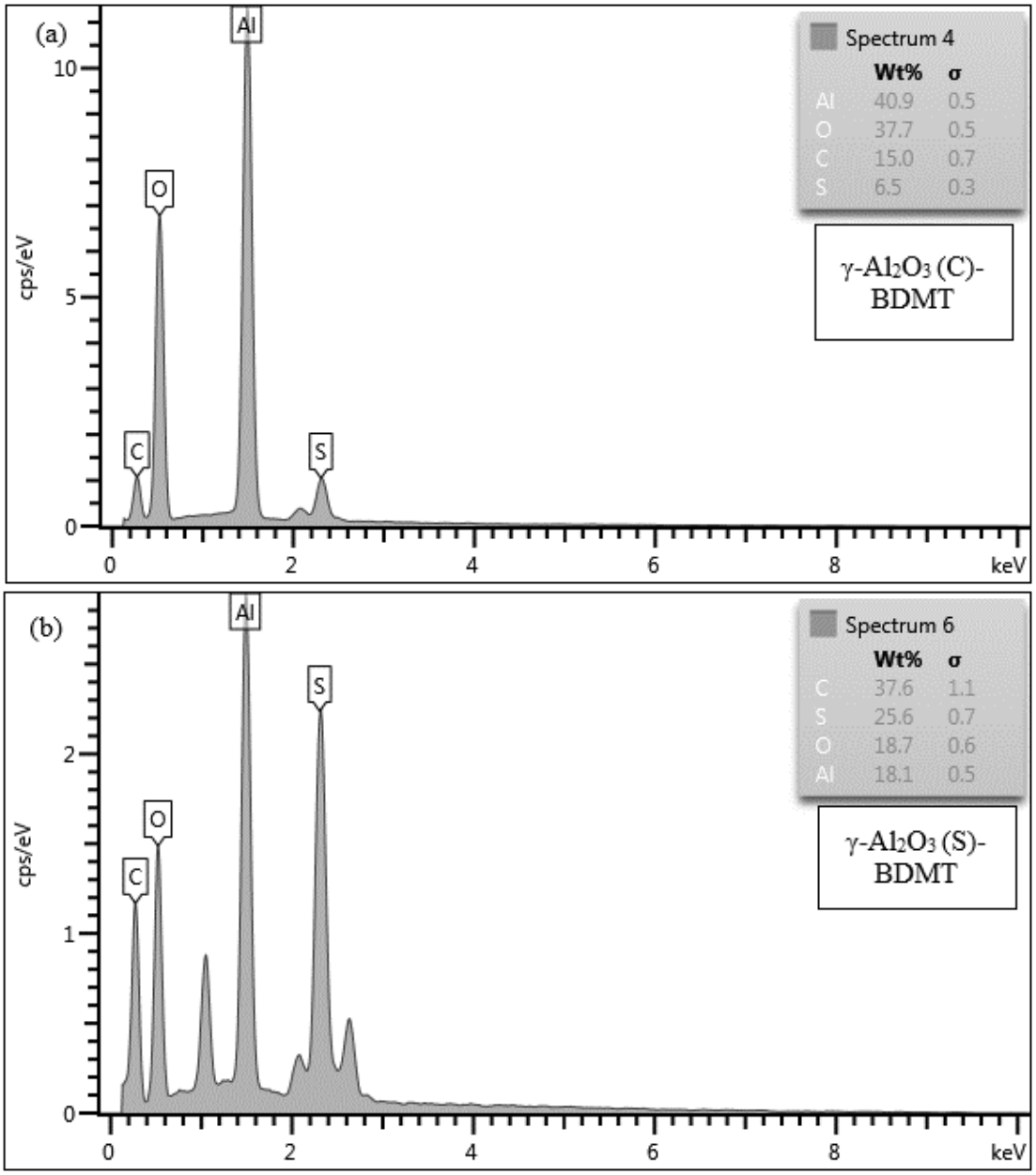

Figure 4.8 illustrates the combination of γ-Al_2O_3(C) and γ-Al_2O_3(S) with the TgA compound, specifically γ-Al_2O_3(C)-TgA in Figure 4.8(a) and γ-Al_2O_3(S)-TgA in Figure 4.8(b). In Figure 4.8(a) and Figure 4.8(b), the presence of the S element in the

sample is demonstrated, with weight percentages of 7.4% and 2.4% respectively. Thus, the finding confirms the successful intercalation of γ-Al_2O_3 and TgA. This aligns with the information presented in Figure 4.7(a) and Figure 4.7(b).

Figure 4.8

EDX spectra of (a) γ-Al_2O_3 (C)-TgA and (b) γ-Al_2O_3 (S)-TgA

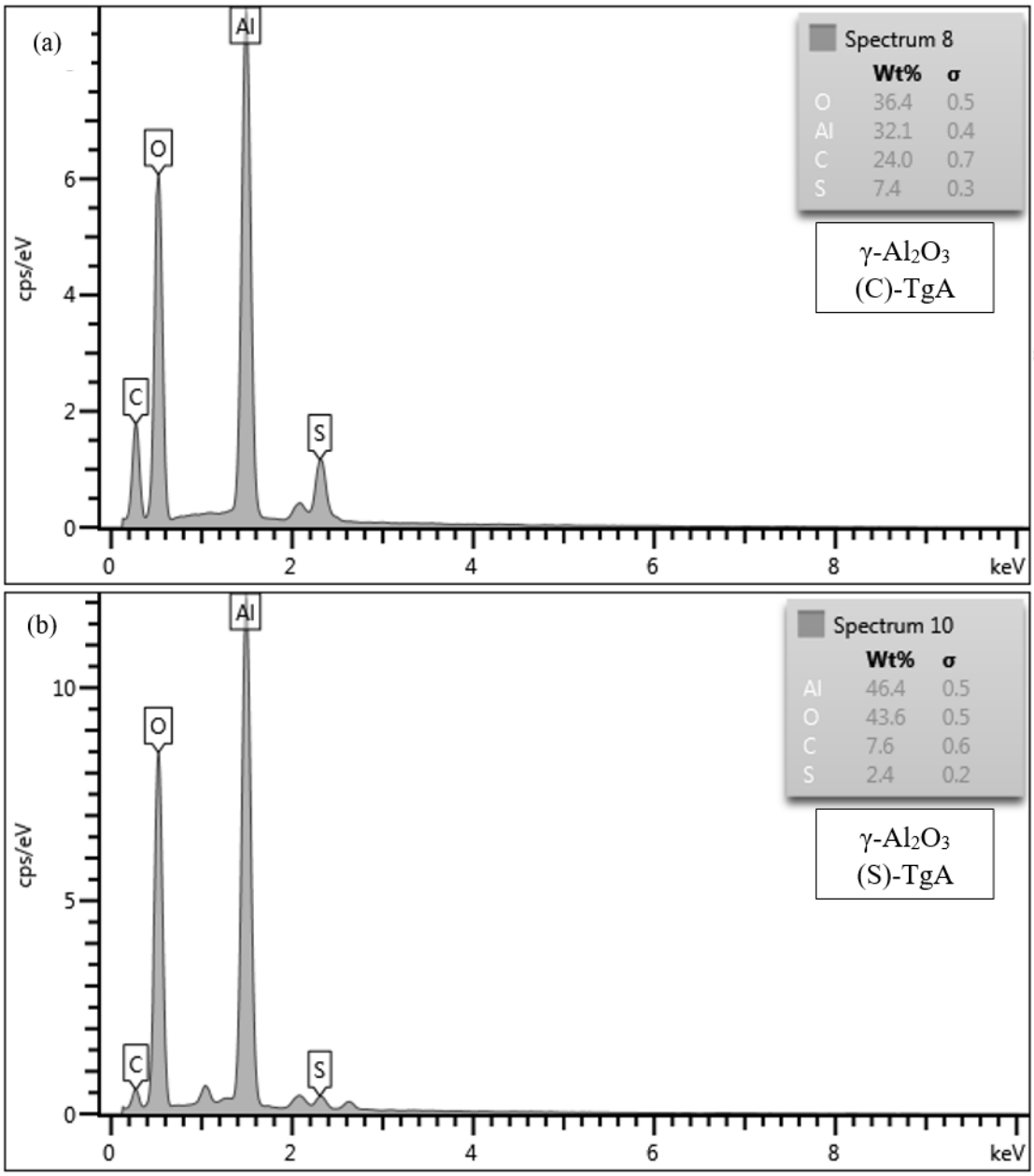

4.4.4 XPS analysis

Figure 4.9(a-b) shows the XPS wide scans of γ-Al_2O_3(C)-BDMT, γ-Al_2O_3(S)-BDMT, γ-Al_2O_3(C)-TgA and γ-Al_2O_3(S)-TgA for O 1s, C 1s, S 2p and Al 2p, which were observed at around 530, 282, 160 and 71 eV respectively. All major elements in the samples exhibited their respective peaks, indicating that the elements were present in the samples. Figures 4.10-4.13 show the bond and valence state of O 1s, C 1s, S 2p and Al 2p for γ-Al_2O_3(C)-BDMT, γ-Al_2O_3(S)-BDMT, γ-Al_2O_3(C)-TgA and γ-Al_2O_3(S)-TgA.

Figure 4.10 displays the XPS spectra of γ-Al_2O_3(C)-BDMT at the O 1s, C 1s, S 2p, and Al 2p regions. As shown in Figure 4.10(a), two peaks were observed at 530 eV and 533.64 eV, which corresponded to the Al-O and Al-OH respectively (Fang et al., 2013). Similarly, two peaks were observed in the C 1s region, as shown in Figure 4.10(b). The first peak appeared at 283.21 eV and was attributed to C=C (Baik et al., 2017) and the second peak at 286.73 eV corresponded to C-S (Das et al., 2017). These attributed to the 1,4-BDMT compound. Moving on to the S 2p region (Figure 4.10(c)), two peaks were observed at 162 eV, which were assigned to sulphide, S^{2-} (Raevskaya et al., 2018), and at 165.36 eV, which was assigned to -SH (Siril et al., 2009). This indicates that in the 1,4-BDMT compound, one -SH end terminal was bonded with γ-Al_2O_3(C) while the other -SH end terminal remained unbonded. Finally, the Al 2p region (Figure 4.10(d)) showed a peak at 73.36 eV, which corresponded to the Al^{3+} oxidation state (White et al., 2019).

Figure 4.11 shows the XPS spectra of γ-Al_2O_3(S)-BDMT at the O 1s, C 1s, S 2p, and Al 2p regions. In Figure 4.11(a), a peak at 529 eV can be observed in the O 1s region. This peak corresponds to the oxide species, O^{2-} (Gordovskaya et al., 2014), which was present in γ-Al_2O_3(S). Additionally, a peak was present in the C 1s region, as shown in Figure 4.11(b). This peak has an energy of 281.88 eV and was assigned to C-C or C=C in 1,4-BDMT (Park et al., 2011). Two peaks can be seen in the S 2p region in Figure 4.11(c), at 160.70 eV and 161.61 eV. Both of these peaks were assigned to S^{2-} (Shutthanandan et al., 2019), indicating that both -SH end terminals in 1,4-BDMT were bonded. Finally, Figure 4.11(d) displays a single peak in the Al 2p region at 72.08 eV, corresponding to Al^{3+} (Smajic et al., 2021). Both compounds exhibited obvious difference in peaks in S 2p region. This may be attributed to several factors. Both compounds are influenced by the chemical environment, oxidation states, and local electronic structure. Additionally, charge transfer and screening effects can modify peak positions. Surface charging, contamination, and sample preparation can also affect the spectral quality (Morgan, 2023). Those factors may have shifted the peaks in the S 2p region even though both compounds were prepared using the same method and materials.

Next are the XPS spectra for γ-Al_2O_3(C)-TgA in the O 1s, C 1s, S 2p, and Al 2p regions. Figure 4.12(a) displays the XPS spectrum for the O1s region, which exhibits a single peak. This peak at 529.31 eV is attributed to O^{2-} (Gordovskaya et al., 2014) from γ-Al_2O_3(C). The C 1s region (Figure 4.12(b)) shows two peaks at 282.77 eV and 286.65 eV, corresponding to C-C (Tuguhiro et al., 2017) and C-S (Das et al., 2017), respectively. In the same region, a peak belonged to C=O may exist around 288 eV (Baik et al., 2017) but it overlapped with the obvious peaks. In the S 2p region (Figure

4.12(c)), a single peak was observed at 161.83 eV, which was associated with S^{2-} (Raevskaya et al., 2018), showing that the -SH from TgA was bonded. The final region for γ-Al_2O_3(C)-TgA is presented in Figure 4.12(d), revealing a single peak at 72.31 eV assigned to Al^{3+} (Smajic et al., 2021).

The XPS spectra for γ-Al_2O_3(S)-TgA are presented in Figure 4.13, showing the regions of O 1s, C 1s, S 2p, and Al 2p. The first region examined was O 1s, which displayed a single peak (Figure 4.13(a)). The peak appeared at 528.74 eV and corresponded to O^{2-} (Tuguhiro et al., 2017) from γ-Al_2O_3(S). In the C 1s region, two peaks were observed (Figure 4.13(b)). The peaks were located at 282.15 eV and 286 eV, assigned to C-C (Tuguhiro et al., 2017) and C-S (Das et al., 2017) respectively. In the same region, a peak corresponding to C=O may be present around 288 eV (Baik et al., 2017), but it overlaps with more prominent peaks. The S 2p region, as shown in Figure 4.13(c), exhibited a single peak at 161.5 eV, representing S^{2-} (Shutthanandan et al., 2019). The peak confirmed that the -SH from TgA was bonded. Lastly, the Al 2p region of γ-Al_2O_3(S)-TgA in Figure 4.13(d) displayed a single peak at 72 eV, indicating the presence of Al^{3+} (Smajic et al., 2021). Both γ-Al_2O_3(C)-TgA and γ-Al_2O_3(S)-TgA have the same peaks in all regions; thus, the configurations for both compounds were the same.

Figure 4.9

XPS wide scan of (a) γ-Al_2O_3(C)-BDMT and γ-Al_2O_3(S)-BDMT and (b) γ-Al_2O_3(C)-TgA and γ-Al_2O_3(S)-TgA

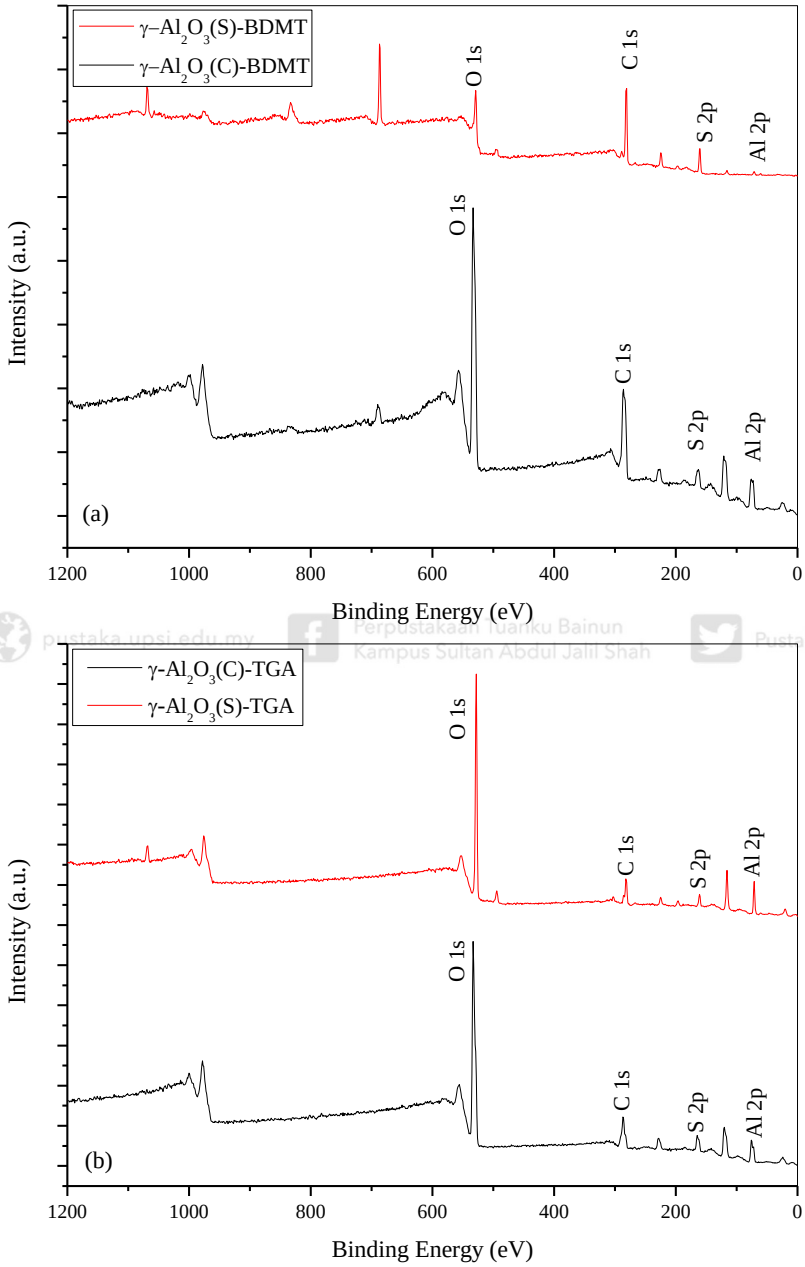

Figure 4.10

The XPS spectra of γ-Al_2O_3(C)-BDMT at regions (a) O 1s, (b) C 1s, (c) S 2p and (d) Al 2p

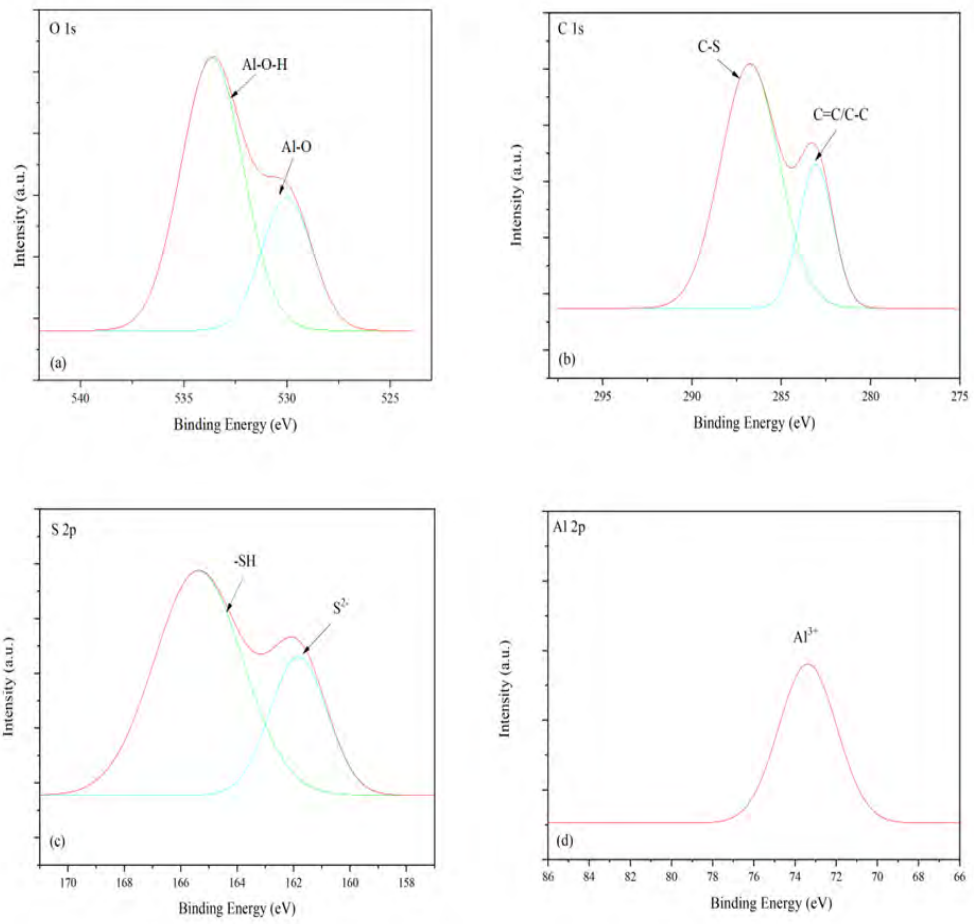

Figure 4.11

The XPS spectra of γ-Al_2O_3(S)-BDMT at regions (a) O 1s, (b) C 1s, (c) S 2p and (d) Al 2p

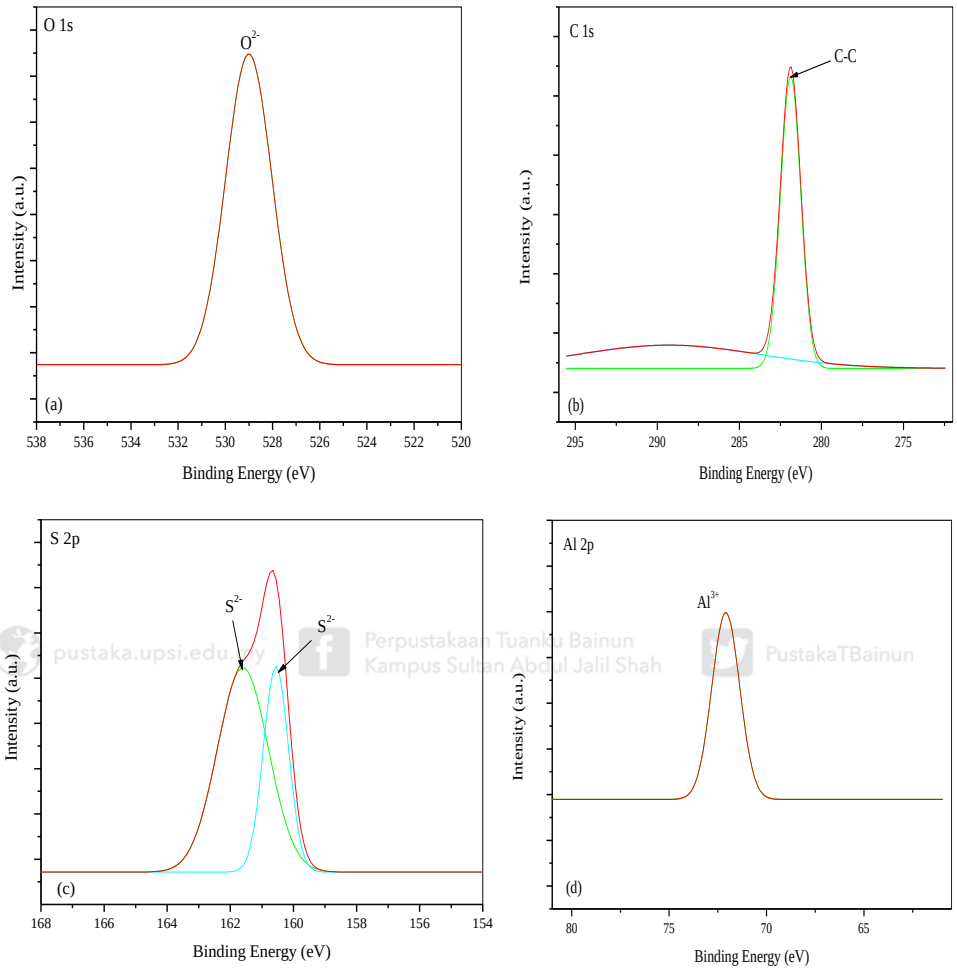

Figure 4.12

The XPS spectra of γ-Al_2O_3(C)-TgA at regions (a) O 1s, (b) C 1s, (c) S 2p and (d) Al 2p

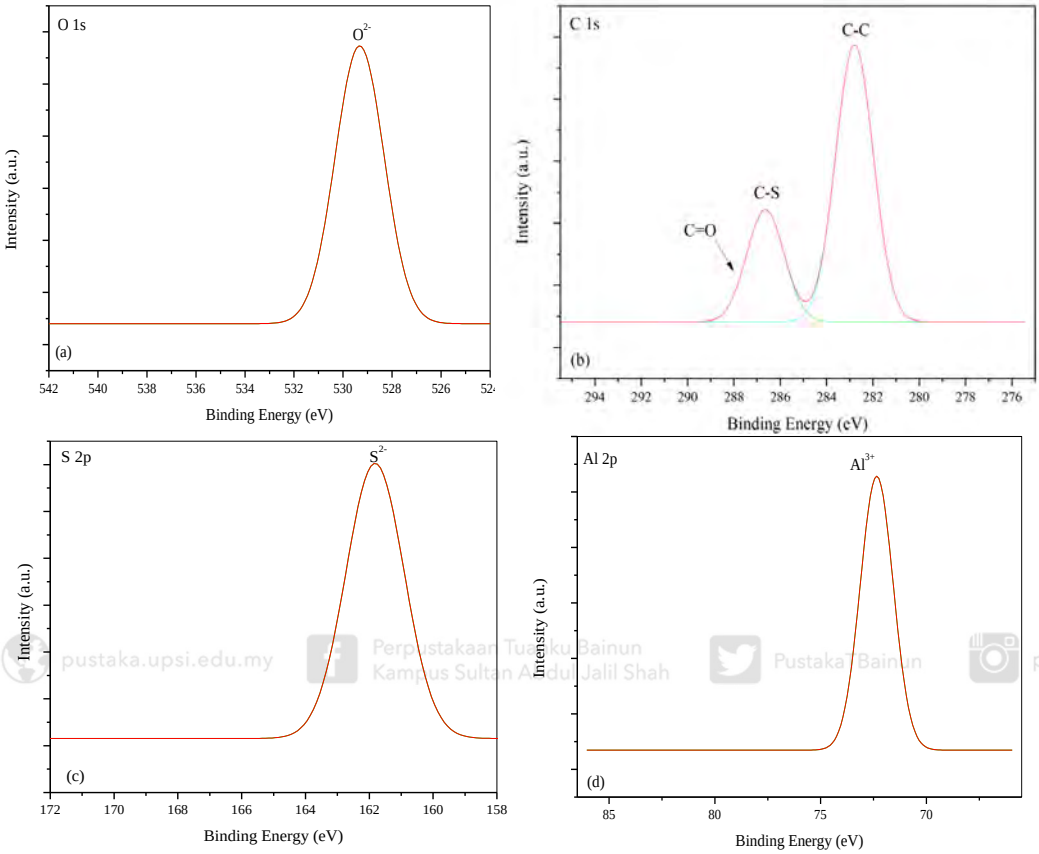

Figure 4.13

The XPS spectra of γ-Al_2O_3(S)-TgA at regions (a) O 1s, (b) C 1s, (c) S 2p and (d) Al 2p

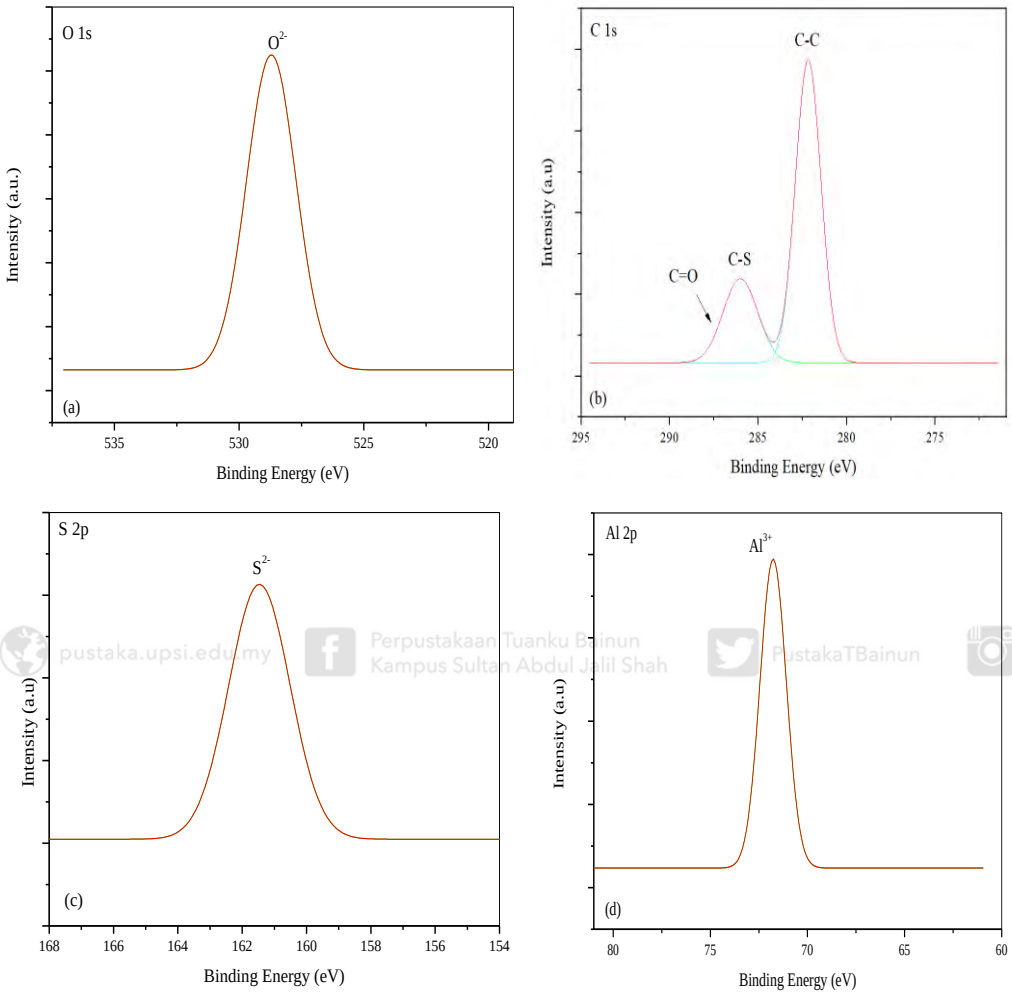

4.4.5 FTIR analysis

Figure 4.14 shows the spectra of γ-Al_2O_3(C) and γ-Al_2O_3(S). The bands in the range of 500-1000 cm^{-1} for both spectra corresponded to the vibrational frequencies of co-ordinate O-Al-O, which are the characteristic of nano amorphous γ-Al_2O_3. In this range, there was also a stretching vibration of the Al-O-Al bond due to chemisorbed and adsorbed species. The Al-O vibrations can be observed in peaks between 612-1070 cm^{-1} (Thabet & Ismaiel, 2016). Since γ-Al_2O_3(S) exhibited the same peaks as γ-Al_2O_3(C), γ-Al_2O_3(S) was indeed successfully synthesised and was in alignment with the XRD result.

Figure 4.14

FTIR spectra of γ-Al_2O_3(C) and γ-Al_2O_3(S)

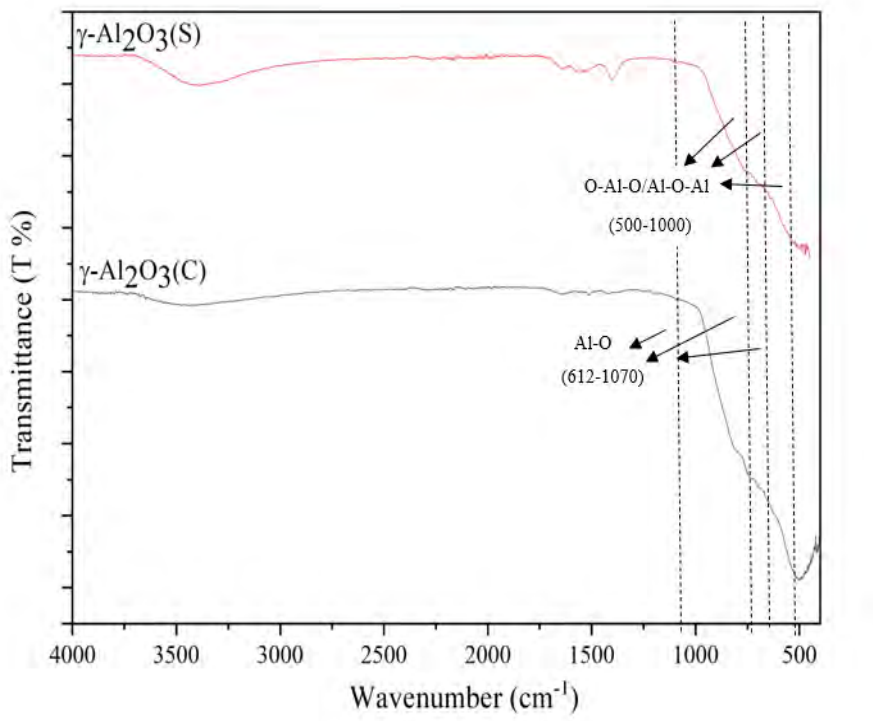

Figure 4.15(a) presents the FTIR spectra of 1,4-BDMT, γ-Al_2O_3(C) and the functionalized γ-Al_2O_3(C)-BDMT composite. In the spectrum of 1,4-BDMT, distinct vibrational bands are observed at approximately 2552 cm^{-1} and 669 cm^{-1}, corresponding to the –SH (thiol) stretching and C-S stretching, respectively (Venkataramanan & Pradeep, 2000). Upon functionalisation, the γ-Al_2O_3(C)-BDMT spectrum exhibits a shifted C–S stretching band at ~666 cm^{-1} and a thiol (–SH) stretching band at ~2556 cm^{-1}, the latter showing a noticeable decrease in intensity and a slight peak shift compared to pure 1,4-BDMT. The absence of an –SH peak in pristine γ-Al_2O_3(C) further confirms the successful intercalation of 1,4-BDMT into the γ-Al_2O_3(C). Additionally, the emergence of a new band at ~1158 cm^{-1} in the γ-Al_2O_3(C)-BDMT spectrum can be assigned to the Al–S bond formation (Liu et al., 2012), suggesting covalent interaction between the alumina surface and the thiol ligand. Given the bifunctional nature of 1,4-BDMT, which possesses two terminal –SH groups, this observation implies that one thiol group binds to Al^{3+} sites on the γ-Al_2O_3 surface, while the remaining –SH group stays free, potentially enhancing Cd^{2+} adsorption in aqueous media.

Figure 4.15(b) compares the FTIR spectra of 1,4-BDMT, γ-Al_2O_3(S), and the functionalised γ-Al_2O_3(S)-BDMT. The spectrum of γ-Al_2O_3(S) closely resembles that of γ-Al_2O_3(C), displaying similar characteristic peaks. However, while γ-Al_2O_3(C)-BDMT and γ-Al_2O_3(S)-BDMT share some spectral features, their functionalisation mechanisms differ significantly. Notably, γ-Al_2O_3(S)-BDMT lacks the distinct –SH stretching band (~2556 cm^{-1}) observed in γ-Al_2O_3(C)-BDMT, suggesting complete consumption of thiol groups during intercalation. Instead, the presence of a C–S stretching vibration at ~666 cm^{-1} (Venkataramanan & Pradeep, 2000), an Al–S bond at

~1158 cm^{-1} (Liu et al., 2012), and weak S–S stretching bands (510–560 cm^{-1}) (Sáiz et al., 2023), indicates that both terminal –SH groups of 1,4-BDMT have reacted with the γ-Al_2O_3(S) surface. This contrasts with γ-Al_2O_3(C)-BDMT, where only one –SH group binds to Al, leaving the second free. The absence of free –SH in γ-Al_2O_3(S)-BDMT implies a different coordination geometry, likely due to variations in surface reactivity or binding sites between the two γ-Al_2O_3 phases.

Meanwhile, Figure 4.15(c) shows the spectra of γ-Al_2O_3(C) and the functionalised γ-Al_2O_3(C)-TgA. For reference, the spectrum of TgA consisted of several typical peaks; 2562 cm^{-1} for -SH stretching, 1782 cm^{-1} for C=O, 1346 cm^{-1} for C-H, 1114 cm^{-1} for C-S and 3132 cm^{-1} for -COOH (Hassan, 2017). The TgA sample could not be run in FTIR because it was in a liquid state, while the instrument only accepted samples in solid state. Critically, γ-Al_2O_3(C)-TgA exhibits two diagnostically significant peaks: (i) a thiol -SH stretch at 2563 cm^{-1}, absent in pristine γ-Al_2O_3(C), confirming TgA incorporation, and (ii) an Al-S vibration at 1158 cm^{-1} (Liu et al., 2012), demonstrating covalent bonding between TgA's thiol group and alumina surface sites. The persistence of the ν-SH signal, coupled with the appearance of νC=O at 1705 cm^{-1} (Wahyono et al., 2019), suggests a coexistence of both bonded (Al-S) and non-bonded TgA species. This contrasts with 1,4-BDMT's dual-thiol functionality, where unambiguous coordination was observed. The simultaneous detection of Al-S and -SH vibrations imply partial thiolate coordination, potentially arising from steric constraints or surface site saturation. Definitive resolution of the bonding configuration awaits complementary XPS analysis of sulfur speciation and aluminum coordination environments.

The FTIR spectrum of γ-Al_2O_3(S)-TgA (Figure 4.15(d)) reveals critical differences from its γ-Al_2O_3(C)-TgA counterpart. Most notably, the absence of the characteristic thiol vibration at 2552 cm^{-1} suggests complete consumption of -SH groups during functionalisation. This observation, coupled with the presence of an Al-S stretching mode at 1158 cm^{-1} (Liu et al., 2012), provides compelling evidence for complete thiolate bond formation between TgA and the γ-Al_2O_3(S) surface. The detection of a carbonyl stretches at 1740 cm^{-1} (Singh et al., 2015) confirms the retention of TgA's carboxylic functionality post-intercalation. The spectral contrast with γ-Al_2O_3(C)-TgA (where residual -SH was observed) implies distinct surface reactivity between the two alumina phases, potentially attributable to differences in surface hydroxyl density or Lewis acidity. These findings demonstrate that γ-Al_2O_3(S) facilitates more efficient thiol coordination, likely creating a different interfacial architecture that may influence subsequent Cd^{2+} adsorption behavior.

Figure 4.15

FTIR spectra of (a) γ-Al_2O_3(C), 1,4-BDMT and γ-Al_2O_3(C)-BDMT; (b) γ-Al_2O_3(S), 1,4-BDMT and γ-Al_2O_3 (S)-BDMT; (c) γ-Al_2O_3(C) and γ-Al_2O_3(C)-TgA and (d) γ-Al_2O_3(S) and γ-Al_2O_3(S)-TgA

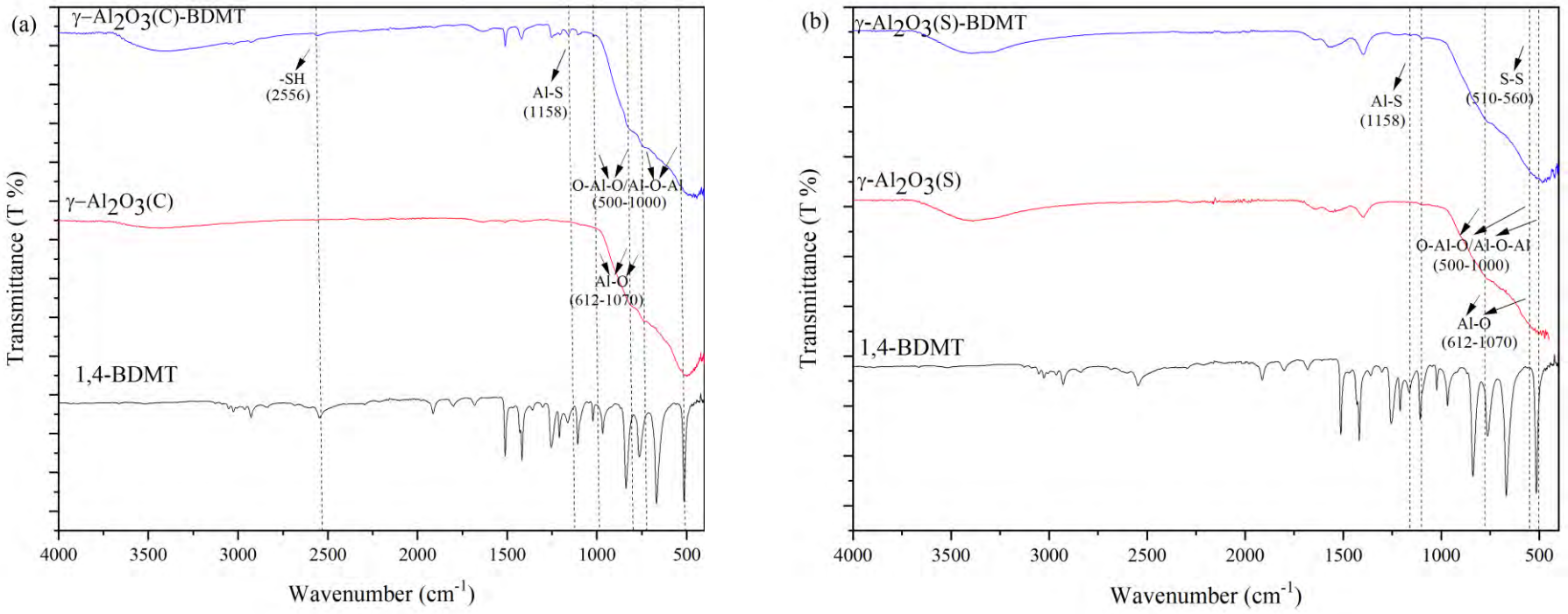

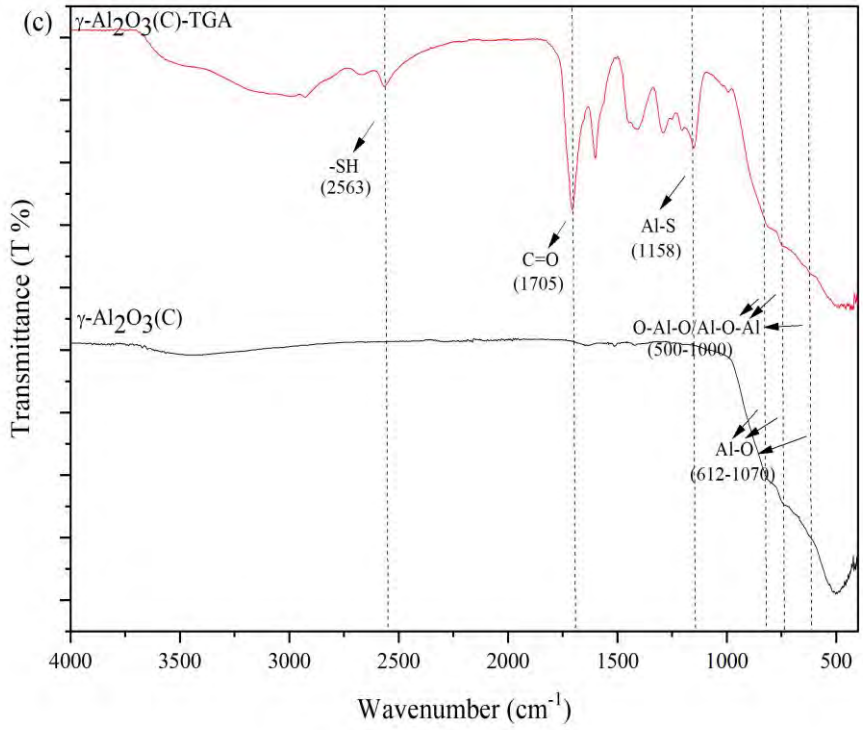

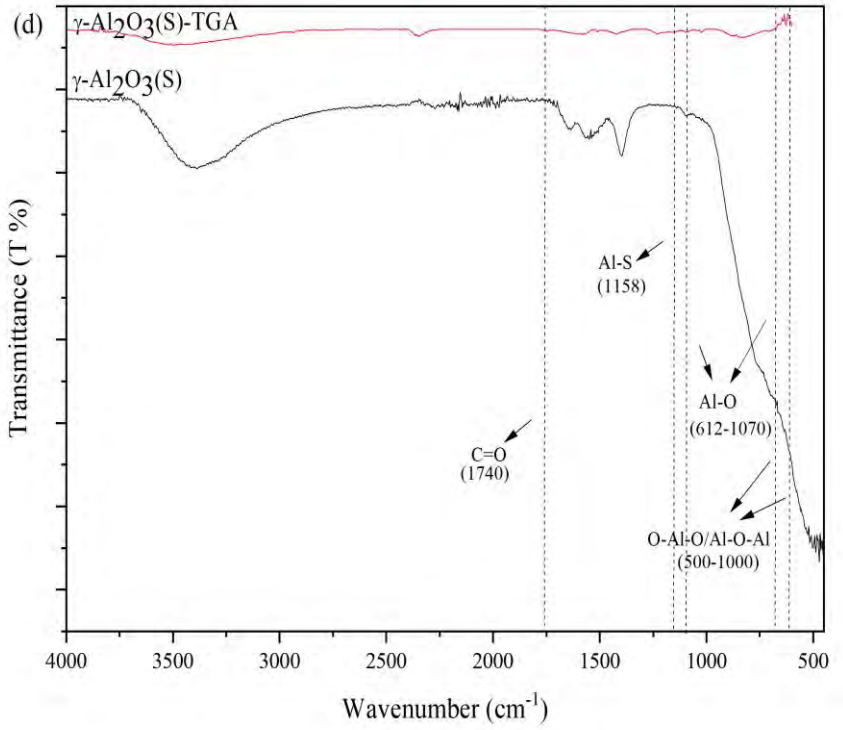

For predicting configurations of γ-Al_2O_3(C)-BDMT, γ-Al_2O_3(S)-BDMT, γ-Al_2O_3(C)-TgA, and γ-Al_2O_3(S)-TgA, it is important to consider XPS and FTIR analyses, as both techniques provide information regarding the bonds present in all compounds. Tables 4.4 and Table 4.5 compile the bonds assigned to each binding energy (BE) and band in the XPS and FTIR analyses, respectively.

Table 4.4

Compilation of compounds, important BE and assignments for XPS analysis

Compound	BE (eV)	Assignment
γ-Al_2O_3(C)-BDMT	530	Al-O
	533.64	Al-OH
	283.21	C=C
	286.73	C-S
	162	S^{2-}
	165.36	-SH
	73.36	Al^{3+}
γ-Al_2O_3(S)-BDMT	529	O^{2-}
	281.88	C-C/C=C
	160.70 and 161.61	S^{2-}
	72.02	Al^{3+}
γ-Al_2O_3(C)-TgA	529.31	O^{2-}
	282.77	C-C
	286.65	C-S

Compound	BE (eV)	Assignment
	288	C=O
	161.83	S^{2-}
γ-Al_2O_3(S)-TgA	528.74	O^{2-}
	282.15	C-C
	286	C-S
	288	C=O
	161.5	S^{2-}
	72	Al^{3+}

Table 4.5

Compilation of compounds, important bands and assignments for FTIR analysis

Compound	Band (cm^{-1})	Assignment
γ-Al_2O_3(C) and γ-Al_2O_3(S)	500-1000	O-Al-O Al-O-Al
	612-1070	Al-O
1,4-BDMT	2552	-SH
	669	C-S
TgA	2562	-SH
	1782	C=O
	1346	C-H
	1114	C-S
	3132	-COOH

Compound	Band (cm^{-1})	Assignment
γ-Al_2O_3(C)-BDMT	500-1000	O-Al-O Al-O-Al
	612-1070	Al-O
	2556	-SH
	1158	Al-S
γ-Al_2O_3(S)-BDMT	500-1000	O-Al-O Al-O-Al
	612-1070	Al-O
	1158	Al-S
	510-560	S-S
γ-Al_2O_3(C)-TgA	500-1000	O-Al-O Al-O-Al
	612-1070	Al-O
	1705	C=O
	2563	-SH
	1158	Al-S
γ-Al_2O_3(S)-TgA	500-1000	O-Al-O Al-O-Al
	612-1070	Al-O
	1740	C=O
	1158	Al-S

4.4.6 TGA analysis

This analysis was conducted to investigate the thermal behaviour of 1,4-BDMT, γ-Al_2O_3(C), γ-Al_2O_3(S), γ-Al_2O_3(C)-BDMT, γ-Al_2O_3(S)-BDMT, γ-Al_2O_3(C)-TgA and γ-Al_2O_3(S)-TgA. The mass change over time was observed as the temperature increased up to 1000 ^oC, as shown in Figure 4.16(a-g). Figure 4.16(a) exhibits 1,4-BDMT, which decomposed at around 200 ^oC, leaving a residue mass of 1.76% and experiencing a mass loss of approximately 98.35%. This demonstrates that the thiol group decomposed within the expected temperature range of 180-320 ^oC for organic compounds, as referenced by Fecher et al. (2014).

Figure 4.16(b) and (c) show the TGA analysis results for γ-Al_2O_3(C) and γ-Al_2O_3(S) respectively. Both samples began to decompose at a lower temperature (about 100 ^oC) due to the removal of moisture, which also occurred in all samples (Maldonado et al., 2017). γ-Al_2O_3(S) exhibited a higher mass loss compared to γ-Al_2O_3(C). At the final temperature, γ-Al_2O_3(S) lost 55.86% of its mass, while γ-Al_2O_3(C) lost 89.89% of its mass. For γ-Al_2O_3(S), the peak of degradation was observed at 854 ^oC, similar to the study by Ishaq et al. (2018). This indicates that γ-Al_2O_3(S) had high thermal stability. γ-Al_2O_3(C), on the other hand, did not show an obvious peak of degradation like γ-Al_2O_3(S), but it can also be said that γ-Al_2O_3(C) exhibited high thermal stability. This is consistent with the γ phase, which is known to resist high temperatures while maintaining its purity, as mentioned in Table 2.4. The difference in mass loss between them was 34.03%. Even though γ-Al_2O_3(C) and γ-Al_2O_3(S) have the same chemical composition, there is a significant difference in mass loss between the two compounds.

This may be due to the composition and particle size of the biomass samples, which can influence TGA curves and affect mass loss readings (Velázquez Martí et al., 2023).

Figure 4.16(d) and (e) show TGA analysis results for γ-Al_2O_3(C)-BDMT and γ-Al_2O_3(S)-BDMT, respectively. Both samples began to decompose at a lower temperature due to the removal of moisture in the first mass loss region (around 100 ^oC). In the second mass loss region, γ-Al_2O_3(S)-BDMT exhibited a higher mass loss (23.11%) in the range of 169-418 ^oC compared to γ-Al_2O_3(C)-BDMT which had a mass loss of 5.72% in the range of 139-405 ^oC. This mass loss region was attributed to the decomposition of the thiol group in both γ-Al_2O_3(C)-BDMT and γ-Al_2O_3(S)-BDMT, as the temperature range was almost the similar as that reported in the study by Maldonado et al. (2017). The decomposition temperature observed was higher than that of 1,4-BDMT, which degraded in the range of 100-200 ^oC (Figure 4.16(a)). This is because a higher dissociation energy was required to break the strong bond between γ-Al_2O_3 and the thiol compound (Ouellette & Rawn, 2015). Therefore, this indicates that the chemical bonding between these compounds is strong and stable for the adsorbents γ-Al_2O_3(C)-BDMT and γ-Al_2O_3(S)-BDMT. The third mass loss region is related to the degradation of γ-Al_2O_3, which can be seen in the profile in Figure 4.16(b) and Figure 4.16(c) mentioned earlier. The residual mass for both γ-Al_2O_3(C)-BDMT and γ-Al_2O_3(S)-BDMT after being heated to 1000 ^oC was 85.07% and 51.86%, respectively. These values were similar to the residual mass of γ-Al_2O_3(C) and γ-Al_2O_3(S) (89.9% and 55.86%, respectively). This indicates that the third mass loss region corresponds to the decomposition of γ-Al_2O_3 after the earlier decomposition of the thiol group in the second mass loss region. Although γ-Al_2O_3(C)-BDMT and γ-Al_2O_3(S)-BDMT share the same chemical composition, a significant difference in mass loss is observed

between the two compounds. This discrepancy may be attributed to the composition and particle size of the biomass samples, which can influence TGA curves and affect mass loss measurements (Velázquez Martí et al., 2023).

Figure 4.16(f) and (g) display the TGA analysis results for γ-Al_2O_3(C)-TgA and γ-Al_2O_3(S)-TgA, respectively. In the first mass loss region, which occurs at lower temperatures (around 100 ^oC), the loss was attributed to moisture from the samples. The second mass loss region occurs at different temperature ranges: 50-248 ^oC for γ-Al_2O_3(C)-TgA and 176-471 ^oC for γ-Al_2O_3(S)-TgA, and was related to thiol loss from the samples. These temperature ranges align with those studied by Dang-Bao et al. (2023), who observed thiol group loss from the surface of their thiol-functionalised cellulose nanocrystals sample in the range of 175-275 ^oC using TgA. The chemical bonding between γ-Al_2O_3(S) and TgA was strong and stable for γ-Al_2O_3(S)-TgA, as evidenced by the higher dissociation energy required to break the bond, up to 471 ^oC. In this region, γ-Al_2O_3(C)-TgA experienced a mass loss of 24.87%, while γ-Al_2O_3(S)-TgA experienced a loss of 10.40%. Comparing the two, the chemical bond in γ-Al_2O_3(S)-TgA was stronger, requiring a higher temperature of 471 ^oC to break the thiol group, compared to the bond in γ-Al_2O_3(C)-TgA, which breaks at 248 ^oC. The third mass loss region was attributed to the decomposition of γ-Al_2O_3, which was similar to what occurs in γ-Al_2O_3(C)-BDMT and γ-Al_2O_3(S)-BDMT. In this region, γ-Al_2O_3(C)-TgA experienced a mass loss of 19.83%, while γ-Al_2O_3(S)-TgA experienced a loss of 18.91%. The residual mass for γ-Al_2O_3(C)-TgA and γ-Al_2O_3(S)-TgA is 52.52% and 67.13%, respectively.

Figure 4.16

TGA analysis of (a) 1,4-BDMT, (b) γ-Al_2O_3(C), (c) γ-Al_2O_3(S), (d) γ-Al_2O_3(C)-BDMT, (e) γ-Al_2O_3(S)-BDMT, (f) γ-Al_2O_3(C)-TgA and (g) γ-Al_2O_3(S)-TgA

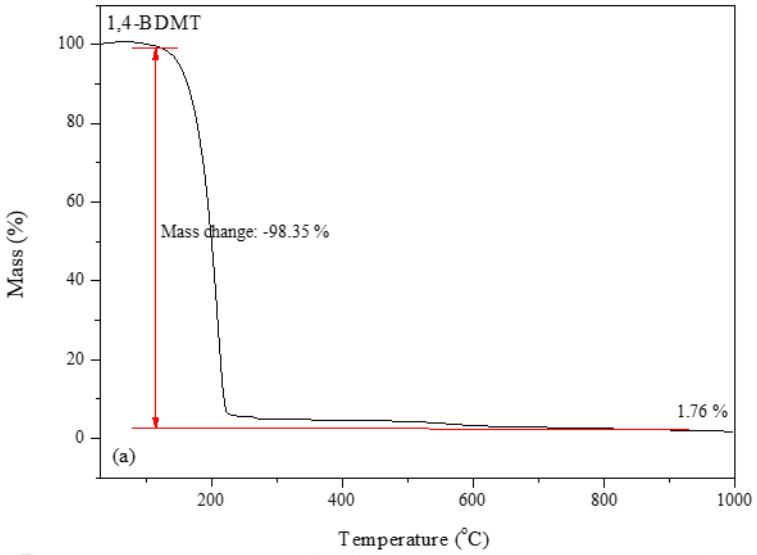

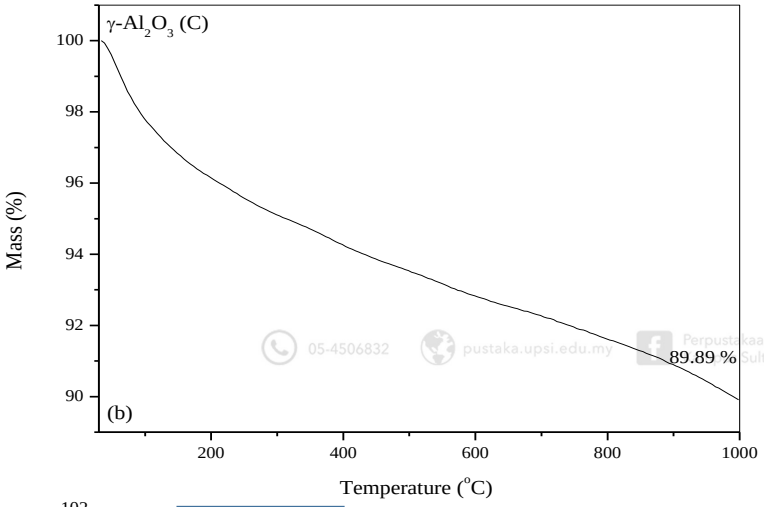

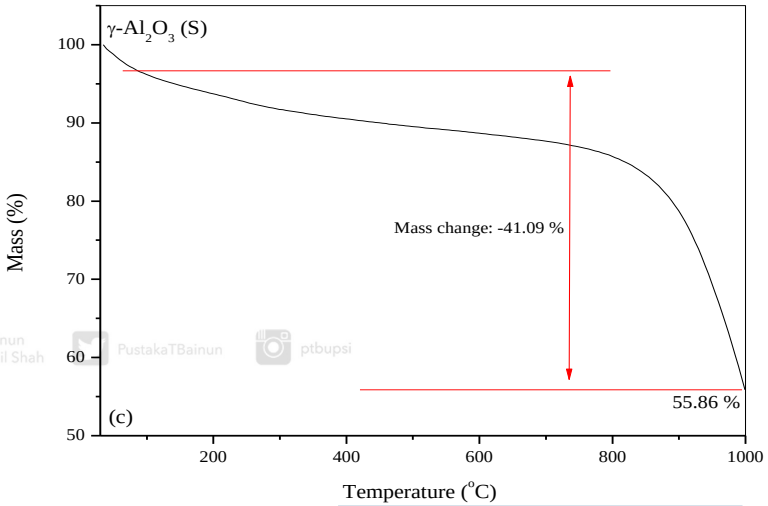

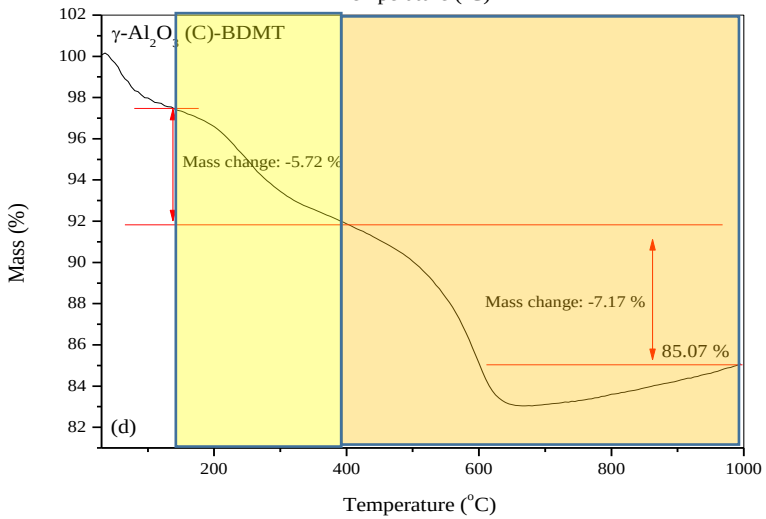

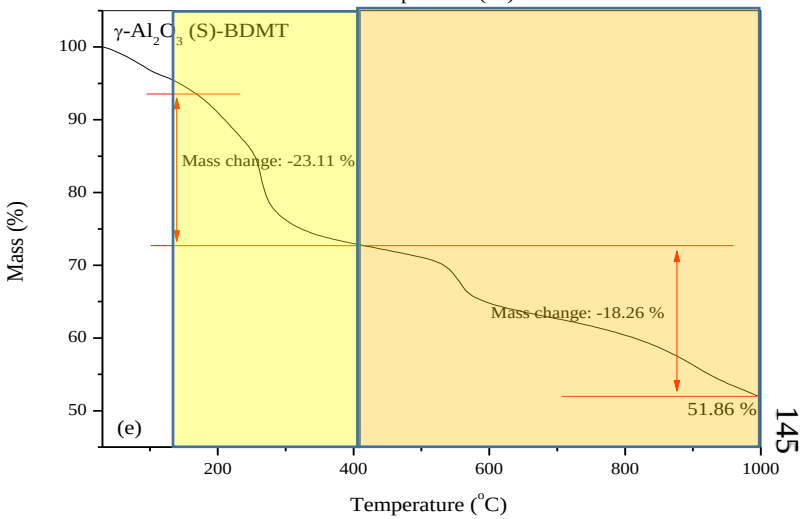

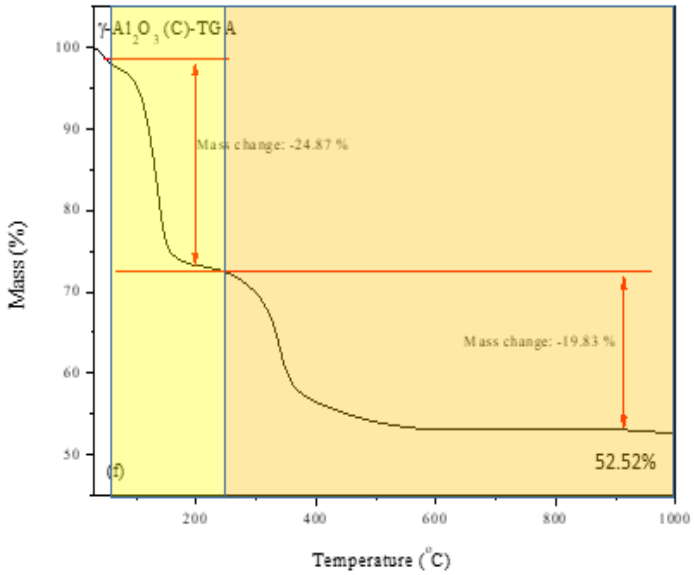

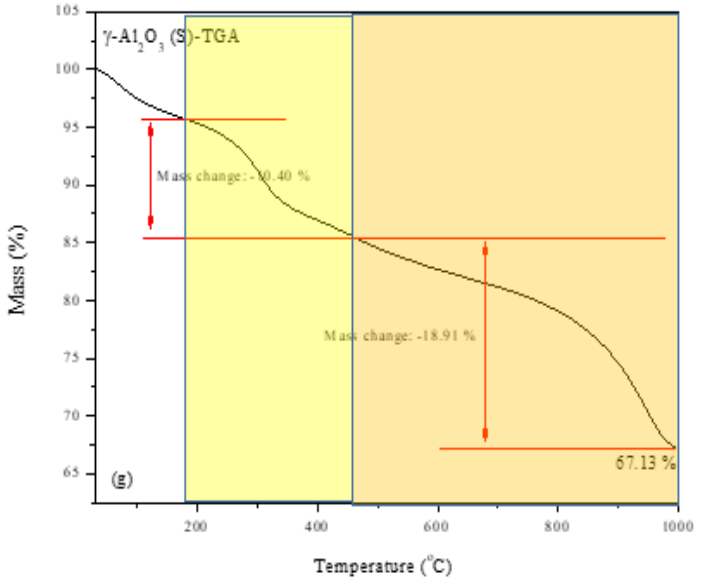

All the analyses conducted, especially XPS and FTIR analyses were able to predict the nature and structure γ-Al_2O_3(C)-BDMT, γ-Al_2O_3(S)-BDMT, γ-Al_2O_3(C)-TgA and γ-Al_2O_3(S)-TgA as depicted in Figure 4.17. TGA, EDX, XPS and FTIR were the important analysis that showed how the structures were predicted. TGA showed enhanced thermal stability over pure 1,4-BDMT, with decomposition shifts to higher temperatures (139–471°C) due to strong Al–S bonding (Ouellette & Rawn, 2015), where γ-Al_2O_3(S)-BDMT and γ-Al_2O_3(S)-TgA required higher energy (up to 471°C) than their (C) counterparts, indicating phase-dependent bond strength. EDX analysis for all the adsorbents showed the existence of S element after the intercalation of γ-Al_2O_3(C) and γ-Al_2O_3(S) with thiol group from 1,4-BDMT and TgA.

Meanwhile, XPS analysis showed that in γ-Al_2O_3(C)-BDMT, one -SH end terminal was bounded while the other -SH end terminal was unbounded. The Al^{3+} oxidation state that existed in Al 2p region confirmed that the one -SH end terminal was bounded with Al. The existence of Al-S bond in FTIR supported the claimed made from XPS analysis.

γ-Al_2O_3(S)-BDMT exhibited two peaks in S 2p region of XPS analysis which belonged to S^{2-}. Both -SH end terminals were bounded unlike in γ-Al_2O_3(C)-BDMT. Moreover, in Al 2p region of XPS analysis, there existed a peak belonged to Al^{3+}. Thus, both the -SH end terminals bounded with Al. FTIR analysis also showed similar results with XPS analysis. In FTIR analysis, there was no peak for -SH while there was a peak belonged to Al-S and S-S. Thus, the predicted configuration of γ-Al_2O_3(C)-BDMT and γ-Al_2O_3(S)-BDMT have different configuration from each other as seen in Figure 4.17(a) and (b).

γ-Al_2O_3(C)-TgA and γ-Al_2O_3(S)-TgA exhibited similar results for XPS and FTIR analysis. Both adsorbents displayed peak for S^{2-} and Al^{3+} in S 2p and Al 2p region of XPS analysis respectively. In FTIR, a peak attributed to Al-S bond also can be seen. Thus, from the XPS and FTIR analysis, the predicted final configuration of both adsorbents was the same and can be seen in Figure 4.17(c).

Figure 4.17

Prediction of configurations for (a) γ-Al_2O_3 (C)-BDMT, (b) γ-Al_2O_3 (S)-BDMT, (c) γ-Al_2O_3 (C)-TgA and γ-Al_2O_3 (S)-TgA

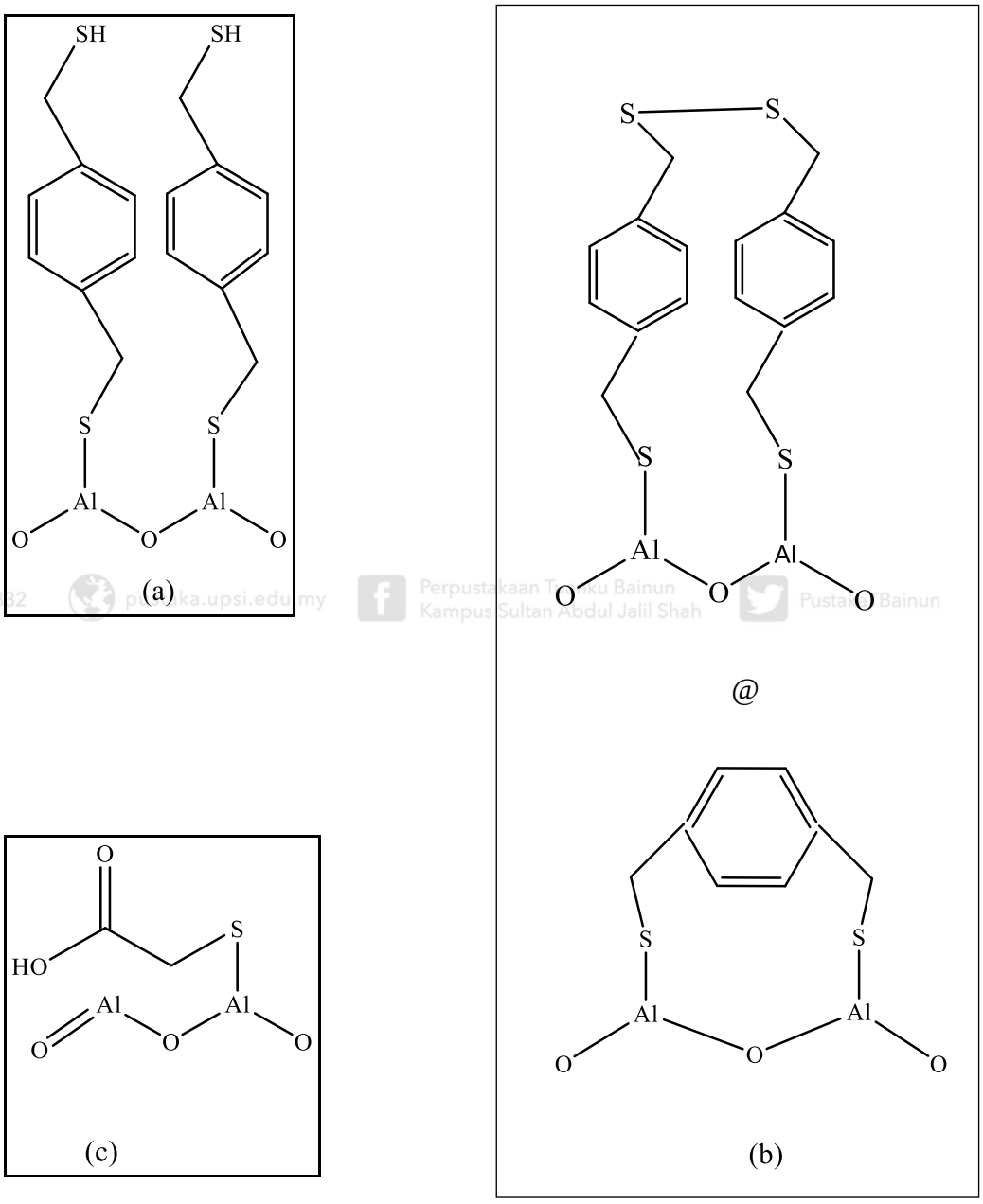

4.5 Adsorption Study

4.5.1 Overview

The adsorption behaviour of Cd^{2+} was evaluated through batch experiments using γ-Al_2O_3(C)-BDMT, γ-Al_2O_3(S)-BDMT, γ-Al_2O_3(C)-TgA and γ-Al_2O_3(S)-TgA. The pH of the solution, initial concentration of the Cd^{2+} solution and contact time effect between γ-Al_2O_3(C)-BDMT, γ-Al_2O_3(S)-BDMT, γ-Al_2O_3(C)-TgA and γ-Al_2O_3(S)-TgA and Cd^{2+} solution were assessed.

4.5.2 Adsorption of Cd^{2+}

4.5.2.1 pH of Cd^{2+} Solution Effect

The pH of the heavy metal ion solution greatly affects the stability and adsorption capacity of the adsorbent (Ryu et al., 2020). It also has a significant impact on the speciation of metal ions and the surface charge of the adsorbent (Zhang et al., 2023). This section examines the influence of Cd^{2+} solution pH on the adsorption of Cd^{2+} by γ-Al_2O_3(C)-BDMT, γ-Al_2O_3(S)-BDMT, γ-Al_2O_3(C)-TgA and γ-Al_2O_3(S)-TsA after 1 minute. This time point was chosen because there was no noticeable difference in the uptake of Cd^{2+} between contact times of 0.5 minutes and 40 minutes in preliminary studies.

In this study, the effect of pH on Cd^{2+} solution was investigated over a range of 2 to 8. A pH of 1 was not included in the study due to its highly acidic conditions which

are not conducive to the adsorption process (Shamsudin, 2016). The upper limit of pH studied was set at 8 based on previous research that demonstrated levels above 8 results in hydrated cadmium complexes dominating the system, leading to a decrease in sorption percentage (Sun et al., 2018; Memon et al., 2008). To ensure safety, a maximum pH of 8.0 was selected, aligning with the findings of Memon et al. (2008). Figure 4.18(a-d) presents the impact of Cd^{2+} solution pH on the uptake of Cd^{2+} by γ-Al_2O_3(C)-BDMT, γ-Al_2O_3(S)-BDMT, γ-Al_2O_3(C)-TgA and γ-Al_2O_3(S)-TgA.

In Figure 4.18(a), the uptake trend of γ-Al_2O_3(C)-BDMT started with a relatively high value of 158.46 mg/g at pH 2. However, there was a drop in value at pH 3 (140.8 mg/g). Subsequently, there was a significant increase in value from pH 4 (159.08 mg/g) to pH 6 (199.38 mg/g). At pH 7, the uptake slightly decreased (194.96 mg/g) before reaching the highest uptake of γ-Al_2O_3(C)-BDMT at pH 8 (199.58 mg/g). The value remained relatively stable between pH 5 and 8.

On the other hand, the uptake trend for γ-Al_2O_3(S)-BDMT started at 88.48 mg/g at pH 2, which is significantly lower compared to γ-Al_2O_3(C)-BDMT, which was 158.46 mg/g. The trend continued to rise from pH 3 (162.08 mg/g) until pH 5 (197.3 mg/g). At pH 6, the value slightly decreased (196.54 mg/g) before increasing to 198.58 mg/g at pH 7. There was a significant drop in value at pH 8 (128.76 mg/g). Similarly to γ-Al_2O_3(C)-BDMT, this trend showed relatively constant values from pH 5-7 before a significant drop in value at pH 8, after experiencing higher values at pH 2-4. At these pH levels, the uptake values of γ-Al_2O_3(S)-BDMT were notably different compared to pH 5-7. The trends for both γ-Al_2O_3(C)-BDMT and γ-Al_2O_3(S)-BDMT were quite similar to the trend studied by Zhao et al. (2021). The study mentioned that the

maximum uptake of Cd^{2+} occurred at pH 7 and decreased under acidic conditions. A study by Khan et al. (2020) also mentioned that Cd^{2+} uptake increased between pH 6-8, with the lowest uptake occurring at pH 3 (the lowest pH studied in that research).

Singh et al. (2022) also reported that the maximum removal of Cd^{2+} occurred within the pH range of 5-7. Therefore, for the subsequent study on the effects of γ-Al_2O_3(C)-BDMT and γ-Al_2O_3(S)-BDMT, pH 6 was chosen and utilised. This is because both adsorbents experienced almost similar uptake at pH 6, with 199.38 mg/g for γ-Al_2O_3(C)-BDMT and 196.54 mg/g for γ-Al_2O_3(S)-BDMT.

Figure 4.18(b) illustrates the uptake trend for γ-Al_2O_3(C)-TgA, which reached its maximum value of 180.2 mg/g at pH 5. The adsorption capacity increased from pH 2 (150.62 mg/g) to pH 3 (158.52 mg/g), before decreasing at pH 4 (150.2 mg/g). The trend then reached its highest point at pH 5, dropping significantly at pH 6 (161 mg/g), pH 7 (154.68 mg/g), and pH 8 (154.24 mg/g). This trend demonstrates a clear pattern of ups and downs, with a prominent peak.

The uptake of γ-Al_2O_3(S)-TgA, as shown in Figure 4.18(b), appeared to be consistent at pH 2 (154.06 mg/g), pH 3 (152.4 mg/g) and pH 4 (155.94 mg/g). There was then a slight increase in values, which remained relatively constant at pH 5 (191.4 mg/g), pH 6 (199.24 mg/g), pH 7 (199.1 mg/g), and pH 8 (199.44 mg/g). The highest value was observed at pH 8, although the values at pH 5-8 did not show a significant difference. Therefore, pH 6 was selected as the optimal pH for Cd^{2+} adsorption for both γ-Al_2O_3(C)-TgA and γ-Al_2O_3(S)-TgA since γ-Al_2O_3(C)-TgA reached plateau at that pH and γ-Al_2O_3(S)-TgA experienced plateau after dropping in uptake after pH 5.

The pH of a Cd^{2+} solution effect can be discussed from two perspectives: the surface charge of an adsorbent and the speciation of metal ions (Zhang et al., 2023). The low efficiency of adsorption at low pH may be due to an excess of H^+ or H_3O^+ ions, which compete with Cd^{2+} for the available adsorption sites on γ-Al_2O_3(C)-BDMT, γ-Al_2O_3(S)-BDMT, γ-Al_2O_3(C)-TgA, and γ-Al_2O_3(S)-TgA. An increase in pH improves the adsorption capacity by increasing the negative charges on the adsorbent surface through the deprotonation process. This reduces the competition between Cd^{2+} and protons, making it easier for Cd^{2+} to occupy the available sorption sites. When the pH exceeds 9, Cd^{2+} in the solution may combine with OH^- ions to form $Cd(OH)_2$ complexes, which can disrupt the adsorption process (Zhao et al., 2021). In a study by Mustapha et al. (2019), pH 6 to 8 was identified as the optimum pH range for their studied metal ions, while this study concludes that pH 6 is the optimum pH for Cd, even though the removal rate remains nearly constant for pH values higher than 5. In conclusion, the pH of the solution significantly affects the adsorption capacity of Cd.

Figure 4.18

pH of Cd^{2+} solution effect on (a) γ-Al_2O_3(C)-BDMT and γ- Al_2O_3(S)-BDMT and (b) γ-Al_2O_3 (C)-TgA and γ-Al_2O_3(S)-TgA (Constant variables: contact time = 1 minute, dosage of adsorbent = 5 mg, initial Cd^{2+} concentration = 10 mg/L)

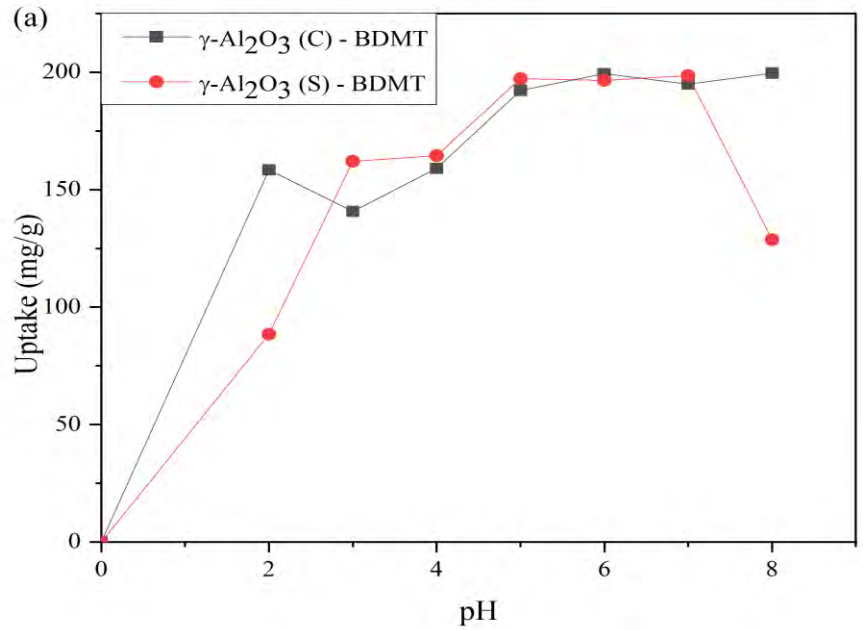

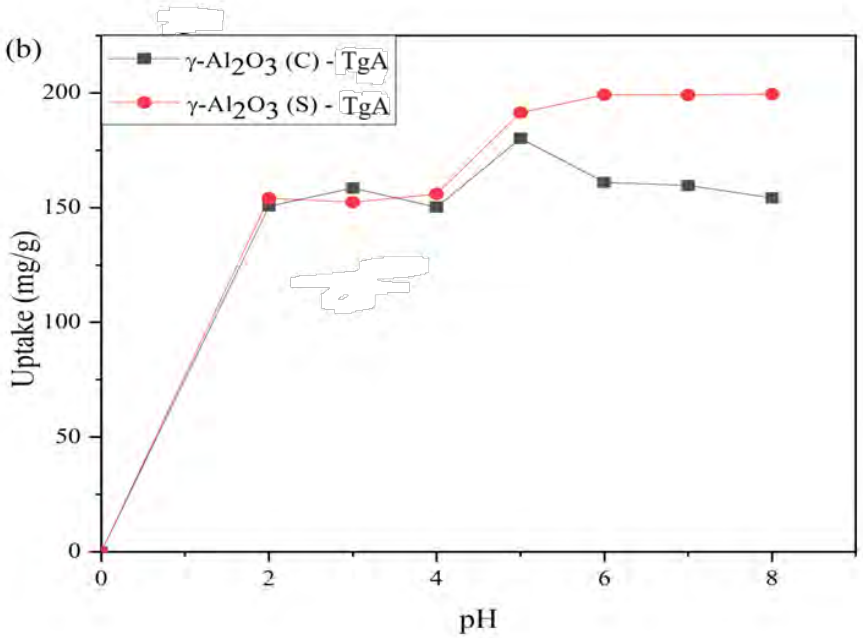

4.5.2.2 Initial Concentration of Cd^{2+} Solution Effect

In Cd^{2+} remediation research, it is important to select materials with a high affinity for the metal, especially at low equilibrium concentrations (Lopez et al., 2020). This ensures that the adsorption process proceeds smoothly and efficiently. To determine the suitability of the chosen materials for metal ions adsorption, a study at different concentrations is necessary. This section discusses the effect of the initial concentration of the Cd^{2+} solution on the adsorption of Cd^{2+} by γ-Al_2O_3(C)-BDMT, γ-Al_2O_3(S)-BDMT, γ-Al_2O_3(C)-TgA and γ-Al_2O_3(S)-TgA.

γ-Al_2O_3(C)-BDMT exhibited almost similar pattern of uptake at 5 mg/L and 10mg/L of initial Cd^{2+} concentration which is almost constant until 40 minutes as shown in Figure 4.19(a). The figure also shows that the Cd^{2+} uptake for γ-Al_2O_3(C)-BDMT continued to rise until at 50 mg/L. This may due to enough available adsorption sites (Pang et al., 2022) of γ-Al_2O_3(C)-BDMT for Cd^{2+} to occupy. At concentration 20-50 mg/L, the uptake started to decrease at 2 minutes. This is due to excess Cd^{2+} cannot be retained to occupy γ-Al_2O_3(C)-BDMT (Zhao et al., 2021).

Meanwhile, γ-Al_2O_3(S)-BDMT showed almost similar pattern of uptake at 5-20 mg/L which is almost constant until 40 minutes as seen in Figure 4.19(b). The figure also shows that the Cd^{2+} uptake for γ-Al_2O_3(S)-BDMT continued to rise until at 50 mg/L. At concentration 30-50 mg/L, the uptake started to decrease at 10 minutes. Compared to γ-Al_2O_3(C)-BDMT which had constant pattern until 40 minutes at 5-10 mg/L, γ-Al_2O_3(S)-BDMT had constant pattern until 40 minutes at 5-20 mg/L as well as

had decreasing uptake in 10 minutes at 30-50 mg/L unlike its (C) counterpart which was in 2 minutes at 20-50 mg/L. Thus, it can be concluded that γ-Al_2O_3(S)-BDMT had a better adsorption uptake compared to γ-Al_2O_3(C)-BDMT.

Figure 4.19(c) displays the uptake for γ-Al_2O_3(C)-TgA. γ-Al_2O_3(C)-TgA demonstrated a similar pattern for all concentrations and had decreasing pattern at 2-5 minutes. The reason for the decrease in uptake at 2-5 minutes was that the adsorption of γ-Al_2O_3(C)-TgA was limited, resulting in the excess Cd^{2+} not being retained by γ-Al_2O_3(C)-TgA (Zhao et al., 2021).

In contrast, γ-Al_2O_3(S)-TgA has sufficient adsorption sites, which is why the uptake continues to increase in 40 minutes at 30-50 mg/L. At 5-20 mg/L, the pattern was remained almost constant until 40 minutes as displayed in Figure 4.19(d). Since γ-Al_2O_3(S)-TgA had a sudden increase when reached 40 minutes at 30-50 mg/L, the adsorbent was chosen as the better adsorbent compared to γ-Al_2O_3(C)-TgA.

Overall, γ-Al_2O_3(C)-BDMT, γ-Al_2O_3(S)-BDMT, γ-Al_2O_3(C)-TgA and γ-Al_2O_3(S)-TgA possessed extraordinary ability in adsorption of Cd^{2+}. This is because they had desired behaviour for environmental remediation, which is to have an impact even at low Cd^{2+} concentrations (Lopez et al., 2020). γ-Al_2O_3(C)-BDMT, γ-Al_2O_3(S)-BDMT, γ-Al_2O_3(C)-TgA and γ-Al_2O_3(S)-TgA can adsorb Cd^{2+} at low concentrations thus proving that they had potentials in environmental remediation.

4.5.2.3 Contact Time Effect

Contact time can determine operational time and cost for water remediation. The shorter time required to operate, the lower operating cost involved (Naihi et al., 2022). This study aimed to see at what contact time the adsorption process reached equilibrium.

The effect of time on the adsorption capacity or the uptake of Cd^{2+} can be seen in Figure 4.19(a-b) for γ-Al_2O_3(C)-BDMT and γ-Al_2O_3(S)-BDMT. It can be seen that even during 0.5 minute the uptake rose rapidly for all the initial concentrations. The rapid increase at first was due to unoccupied large surface area (Mustapha et al., 2019) of γ-Al_2O_3(C)-BDMT and γ-Al_2O_3(S)-BDMT. According to Wahyuhadi et al. (2023), adsorption capacity increase with the time but will decline when it reached at some point due to possibility of desorption process triggered by longer than the ideal times.

Meanwhile for γ-Al_2O_3(C)-TgA and γ-Al_2O_3(S)-TgA, their uptake of Cd^{2+} is shown in Figure 4.19(c-d). Same as for γ-Al_2O_3(C)-BDMT and γ-Al_2O_3(S)-BDMT previously that even during 0.5 minute the uptake rose and remained constant. Tan et al. (2020) mentioned that equilibrium achieved when there is no much improvement in percentage removal despite longer contact time. In conclusion, for γ-Al_2O_3(C)-BDMT, the ideal contact time was at 30 minutes while for γ-Al_2O_3(S)-BDMT it was at 20 minutes. For γ-Al_2O_3(C)-TgA, the ideal contact time was at 30 minutes and γ-Al_2O_3(S)-TgA it was 20 minutes.

Figure 4.19

Effect of initial concentration of Cd^{2+} and effect of contact time on the (a) γ-Al_2O_3(C)-BDMT, (b) γ-Al_2O_3(S)-BDMT, (c) γ-Al_2O_3(C)-TgA and (d) γ-Al_2O_3(S)-TgA at 5-50 mg/L (Constant variables: dosage of adsorbent = 5 mg and pH = 6)

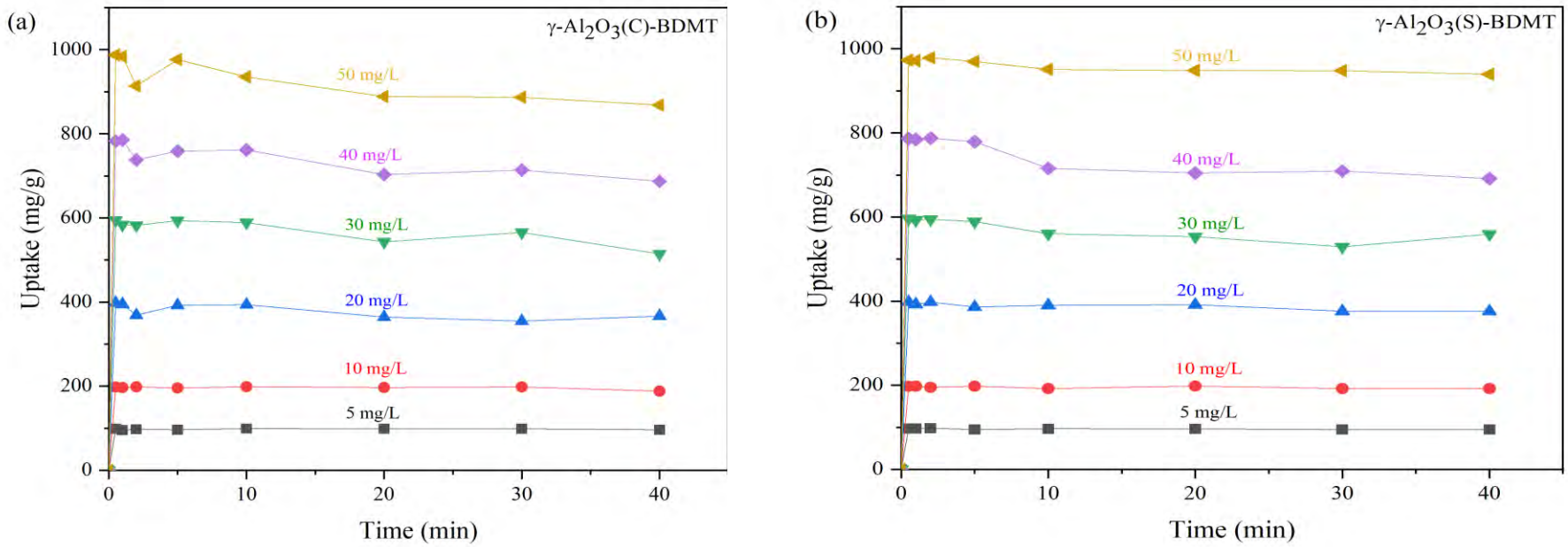

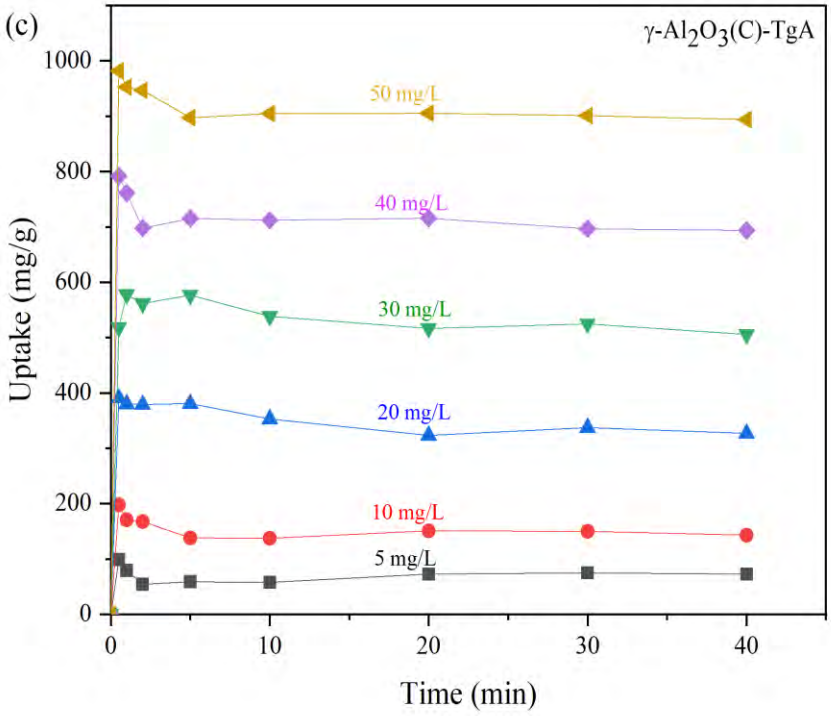

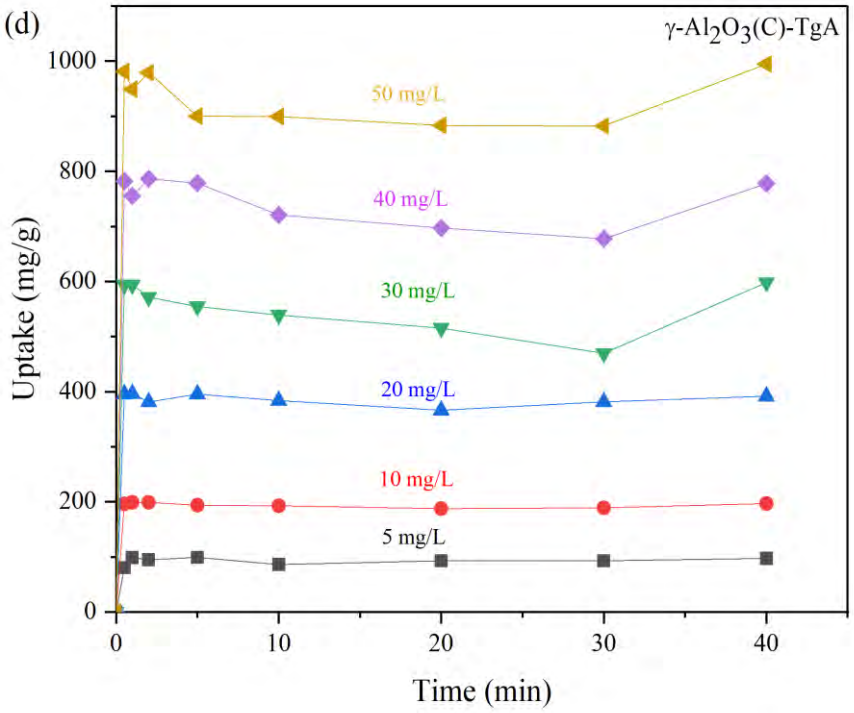

4.6 Adsorption Isotherms

The role of adsorption isotherm is very important to investigate the mechanism between an absorbent and adsorbate (Zhao et al., 2021). For this study, the adsorption isotherms used were the Freundlich and Langmuir isotherm models.

Figure 4.20 shows Langmuir adsorption isotherm for γ-Al_2O_3(C)-BDMT, γ-Al_2O_3(S)-BDMT, γ-Al_2O_3(C)-TgA and γ-Al_2O_3(S)-TgA. All the adsorbents exhibited positive slope except for γ-Al_2O_3(C)-TgA which had a negative slope. Figure 4.21 shows Freundlich adsorption isotherm for γ-Al_2O_3(C)-BDMT, γ-Al_2O_3(S)-BDMT, γ-Al_2O_3(C)-TgA and γ-Al_2O_3(S)-TgA. All the adsorbents exhibited positive slope, contrasted to their counterpart in Langmuir isotherm. Moreover, their linear fit of line did come out as best fit linear line compared to their Langmuir isotherm counterpart. For more details, the calculated data from Langmuir and Freundlich isotherm models can be seen in Table 4.6 for γ-Al_2O_3(C)-BDMT, γ-Al_2O_3(S)-BDMT, γ-Al_2O_3(C)-TgA and γ-Al_2O_3(S)-TgA.

For γ-Al_2O_3(C)-TgA, the Langmuir isotherm is already out of question since it had a negative slope. Based on the Table 4.6, each adsorbent has to be compared with their correlation coefficient values (R^2) among Langmuir isotherm and Freundlich isotherm and choose which one of them is the highest. Each adsorbent; γ-Al_2O_3(C)-BDMT (R^2 = 0.994), γ-Al_2O_3(S)-BDMT (R^2 = 0.999), γ-Al_2O_3(C)-TgA (R^2 = 0.996) and γ-Al_2O_3(S)-TgA (R^2 = 0.991) exhibited highest R^2 from Freundlich isotherm instead from Langmuir isotherm which were γ-Al_2O_3(C)-BDMT (R^2 = 0.993), γ-

Al_2O_3(S)-BDMT (R^2 = 0.986), γ-Al_2O_3(C)-TgA (R^2 = 0.954) and γ-Al_2O_3(S)-TgA (R^2 = 0.974). From the information, all the adsorbents were best fitted to Freundlich isotherm model. The linearised Freundlich isotherm indicates that adsorption takes place in multiple layers on the surface of the adsorbents. As the concentration increases, so does the level of adsorption (Wahyuhadi et al., 2023). Typically, it suggests that the adsorbents possess a heterogeneous surface (Mahmoud et al., 2021).

Based on the maximum adsorption capacities, K_F for γ-Al_2O_3(C)-BDMT, γ-Al_2O_3(S)-BDMT, γ-Al_2O_3(C)-TgA and γ-Al_2O_3(S)-TgA, the order of Cd^{2+} uptake by the adsorbents is as following; γ-Al_2O_3(C)-BDMT (463.767 mg/g) > γ-Al_2O_3(S)-BDMT (428.410 mg/g) > γ-Al_2O_3(S)-TgA (217.871 mg/g) > γ-Al_2O_3(C)-TgA (48.228 mg/g). The result showed that γ-Al_2O_3(C)-BDMT can occupy the most Cd^{2+} based on the K_F value.

From Freundlich model, the values of 1/n for γ-Al_2O_3(C)-BDMT, γ-Al_2O_3(S)-BDMT, γ-Al_2O_3(C)-TgA and γ-Al_2O_3(S)-TgA can be accessed. According to Das et al. (2016), the value of 1/n acts as an indicator to see whether the adsorption is favourable or not. The value of 1/n < 1 indicates a favourable adsorption. From the Table 4.6, all the adsorbents showed 1/n values less than 1 except for γ-Al_2O_3(C)-TgA (γ-Al_2O_3(C)-BDMT = 0.342, γ-Al_2O_3(S)-BDMT = 0.314, γ-Al_2O_3(C)-TgA = 1.795 and γ-Al_2O_3(S)-TgA = 0.774). This concludes that all the adsorbents were favourable except for γ-Al_2O_3(C)-TgA.

Figure 4.20

Langmuir adsorption isotherm for (a) γ-Al_2O_3(C)-BDMT and (b) γ-Al_2O_3(S)-BDMT, (c) γ-Al_2O_3(C)-TgA and (d) γ-Al_2O_3(S)-TgA

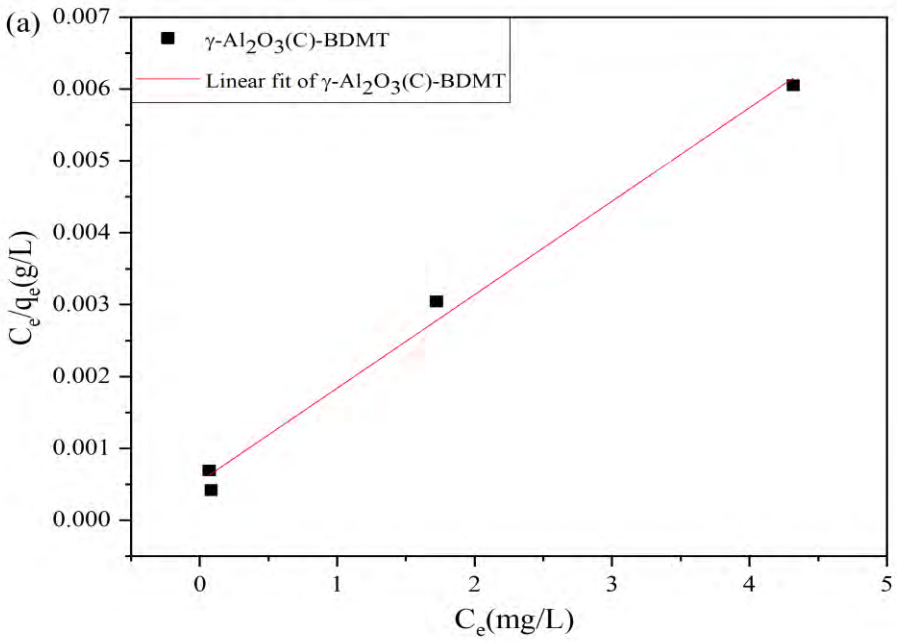

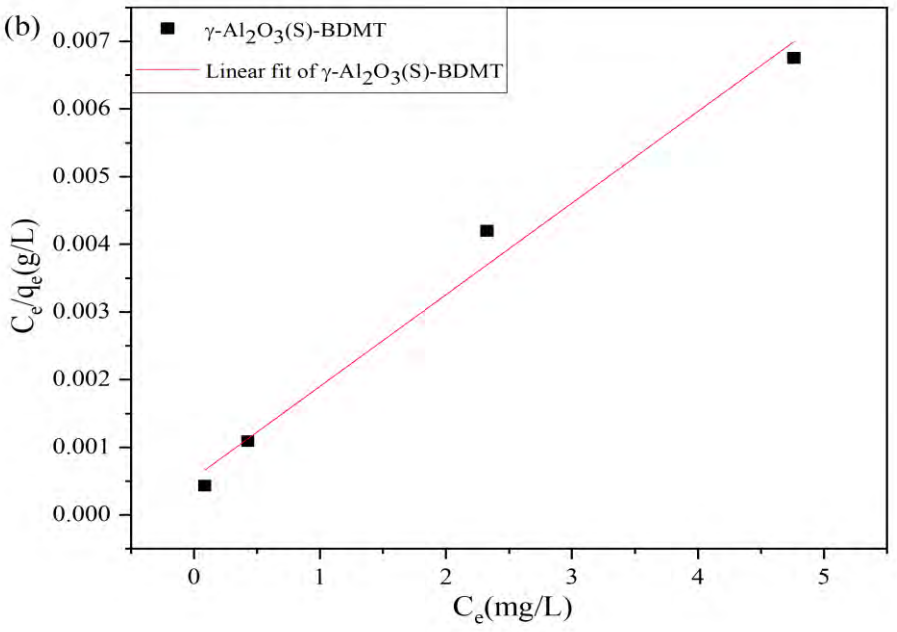

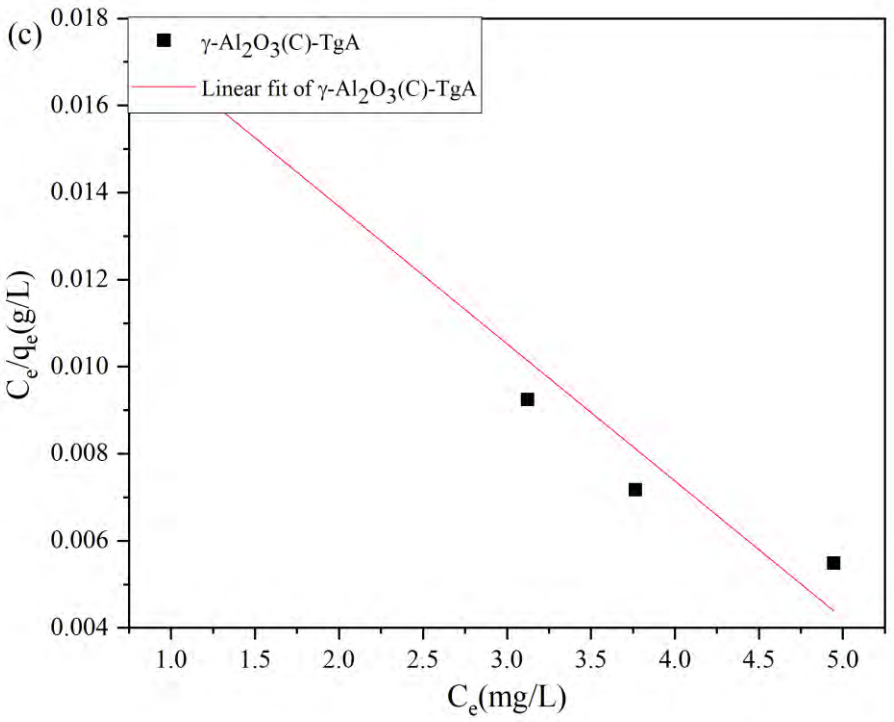

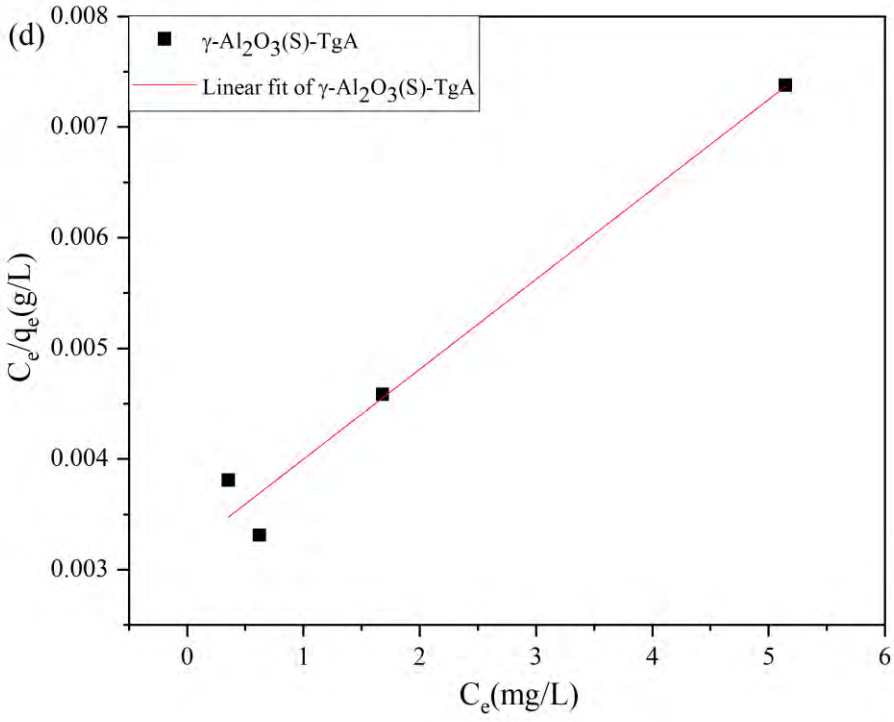

Figure 4.21

Freundlich adsorption isotherm for (a) γ-Al_2O_3(C)-BDMT and (b) γ-Al_2O_3(S)-BDMT, (c) γ-Al_2O_3(C)-TgA and (d) γ-Al_2O_3(S)-TgA

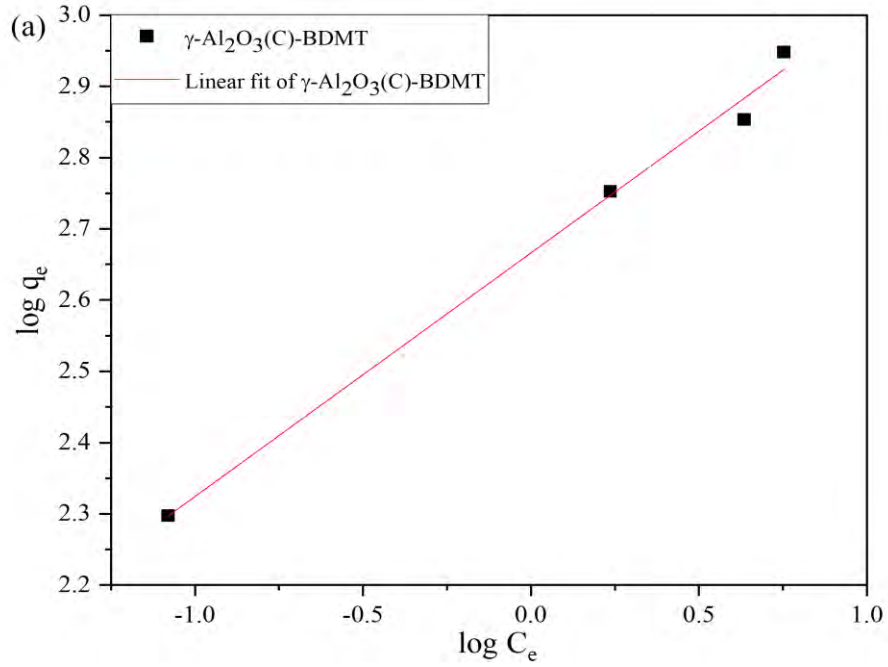

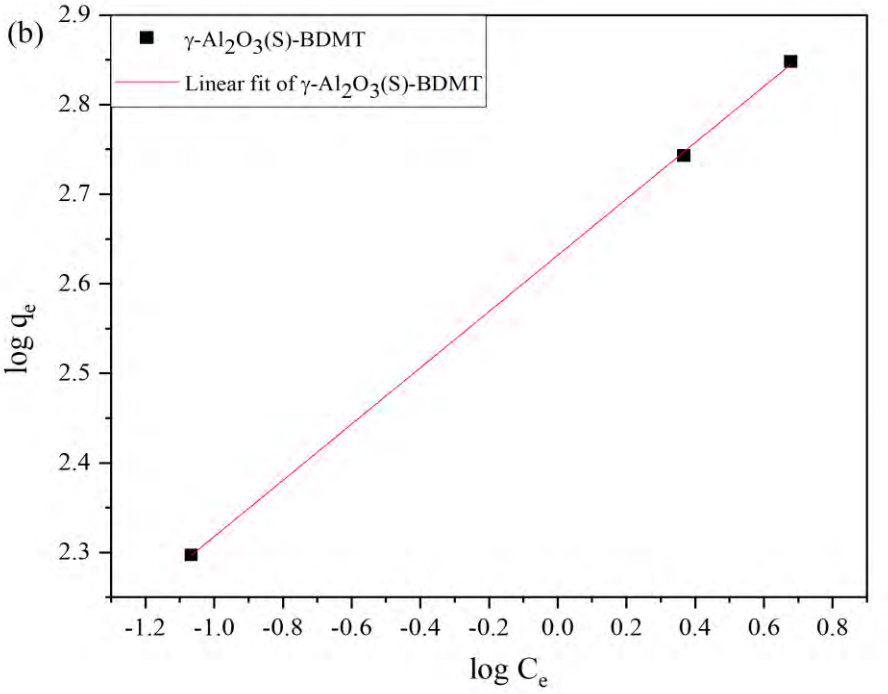

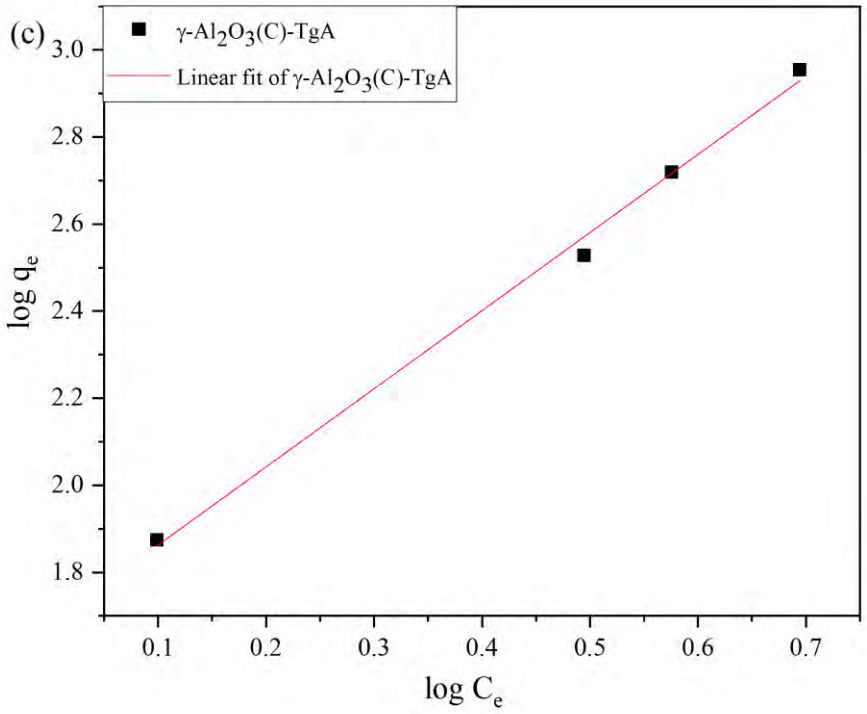

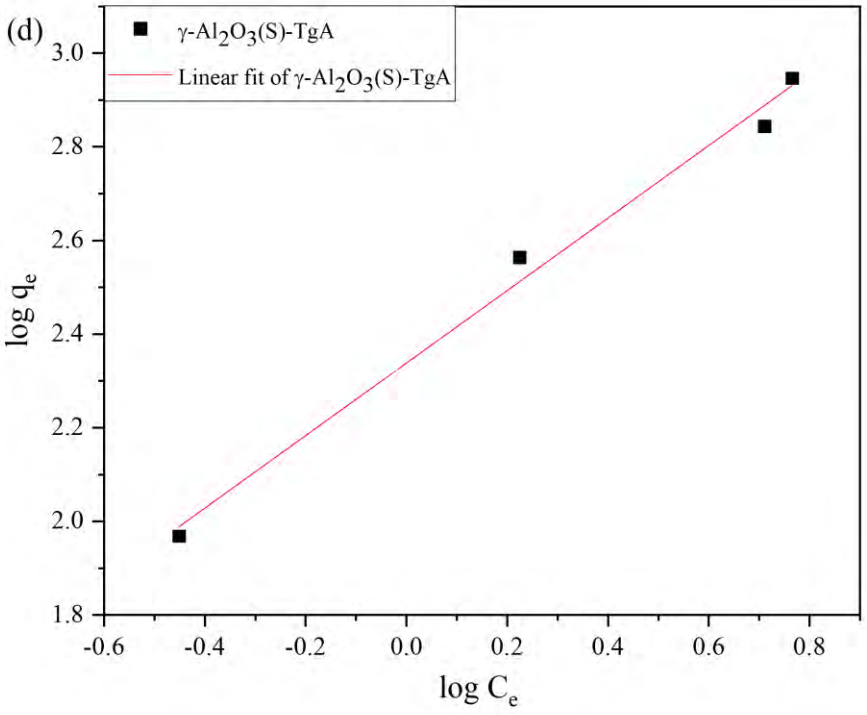

Table 4.6

Parameters of the Langmuir and Freundlich Isotherm for the adsorption of γ-Al_2O_3(C)-BDMT, γ-Al_2O_3(S)-BDMT, γ-Al_2O_3(C)-TgA and γ-Al_2O_3(S)-TgA

	Langmuir			Freundlich		
Adsorbent	q_{max} (mg/g)	K_L	R^2	1/n	K_F (mg/g)	R^2
γ-Al_2O_3(C)-BDMT	769.231	2.600	0.993	0.342	463.767	0.994
γ-Al_2O_3(S)-BDMT	714.286	2.800	0.986	0.314	428.410	0.999
γ-Al_2O_3(C)-TgA	-312.500	-0.160	0.954	1.795	48.228	0.996
γ-Al_2O_3(S)-TgA	1250.000	0.250	0.974	0.774	217.871	0.991

4.7.1 Adsorption Kinetics

Figure 4.22(a) shows first order adsorption kinetics for γ-Al_2O_3(C)-BDMT, γ-Al_2O_3(S)-BDMT, γ-Al_2O_3(C)-TgA and γ-Al_2O_3(S)-TgA. From the figure, γ-Al_2O_3(C)-TgA exhibited straight line with negative slope while γ-Al_2O_3(S)-TgA did not have a line at all. For γ-Al_2O_3(C)-BDMT and γ-Al_2O_3(S)-BDMT, the line possessed positive slope but all the points were not in right order, which were the reason why the first order adsorption kinetics were rejected for all adsorbents. Meanwhile, Figure 4.22(b) shows the second order adsorption kinetics for γ-Al_2O_3(C)-BDMT, γ-Al_2O_3(S)-BDMT, γ-Al_2O_3(C)-TgA and γ-Al_2O_3(S)-TgA. All the adsorbents exhibited straight line with positive slope, making the second order adsorption kinetic more favourable compared to the first order kinetic adsorption. In addition, the coefficient of determination, R^2 for all adsorbents in both orders of adsorption kinetics were observed to clarify which order fit the best for all adsorbents. The R^2 for all the adsorbents at all initial concentration

showed high values for second order adsorption kinetics as seen in Table 4.7 compared to the first order adsorption kinetics. This shows that the second order adsorption kinetics is indeed more fit and suitable for all adsorbents than the first order adsorption kinetics. It is best to describe that all the adsorbents undergo adsorption processes that take longer to fully occupy the adsorption sites which assumes that the adsorption rate is influenced by the interactions between the adsorbent and the adsorption sites on the adsorbent surface throughout the process (Wang et al., 2022). This also indicates that the process was mainly controlled by chemical action as in study by Zhang et al (2023).

Figure 4.22

Adsorption kinetic (a) pseudo-first order and (b) pseudo-second order of γ-Al_2O_3(C)-BDMT, γ-Al_2O_3(S)-BDMT, γ-Al_2O_3(C)-TgA and γ-Al_2O_3(S)-TgA for 10 mg/L at pH 6

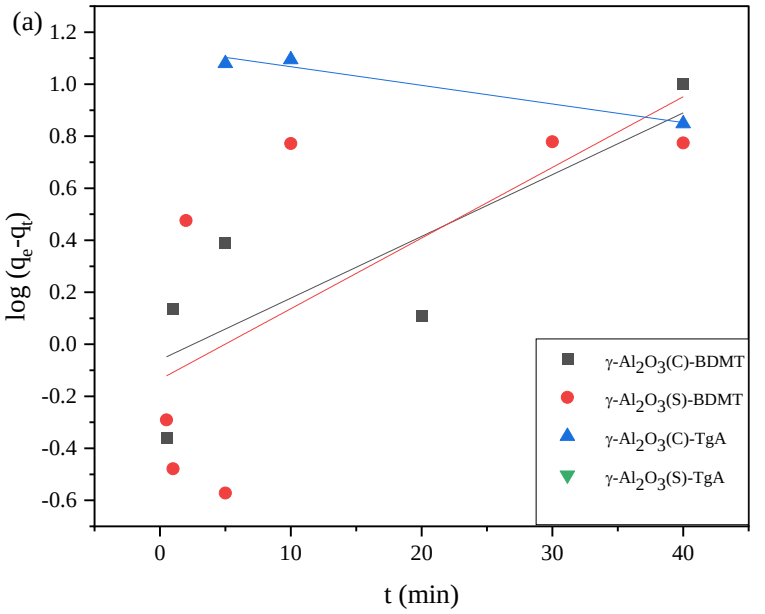

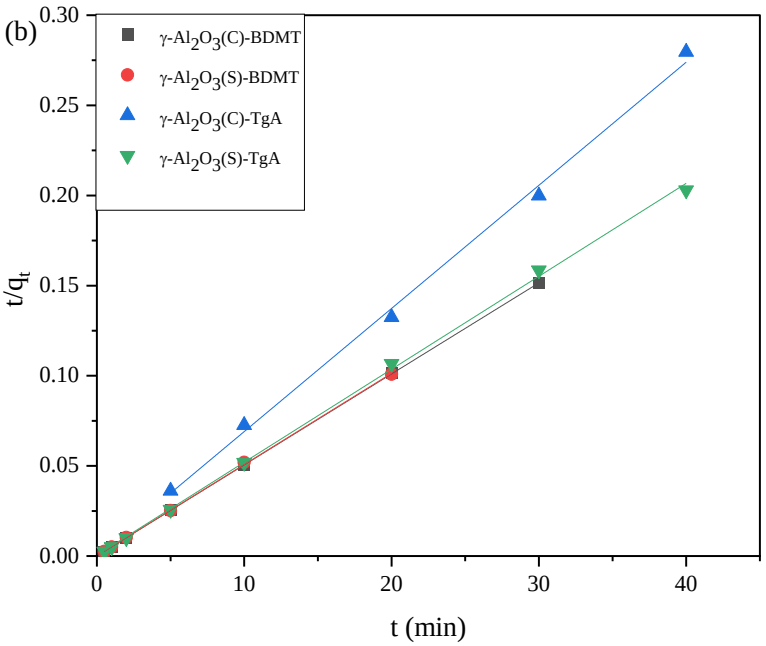

Table 4.7

Parameters of the pseudo-first order and pseudo-second order kinetic for the adsorption of γ-Al_2O_3(C)-BDMT, γ-Al_2O_3(S)-BDMT, γ-Al_2O_3(C)-TgA and γ-Al_2O_3(S)-TgA

	Pseudo-first order			Pseudo-second order		
Adsorbent	q_e (mg/g)	K_1	R^2	q_e (mg/g)	K_2	R^2
γ-Al_2O_3(C)-BDMT	0.871	-0.055	0.537	198.019	0.398	0.999
γ-Al_2O_3(S)-BDMT	0.733	-0.063	0.366	197.628	0.138	0.999
γ-Al_2O_3(C)-TgA	13.770	0.017	0.931	146.412	0.064	0.996
γ-Al_2O_3(S)-TgA	-	-	-	193.80	0.0582	0.999

Cd^{2+} is expected to bond with S from 1,4-BDMT, forming the S-Cd thiolate complex. The presence of two S-H groups in 1,4-BDMT increases the likelihood that one end will bind to γ-Al_2O_3 while the other binds to Cd^{2+}, resulting in the loss of only one thiol proton (Murty et al., 1998). Therefore, the expected complex containing Cd^{2+} after adsorption can be illustrated in Figure 4.23(a) and Figure 4.23(b).

As illustrated by Figure 2.8, there are various ways the carboxyl group is expected to bind to Cd^{2+}, as referenced by Azócar et al. (2014). The carboxylate ion (RCO2-) can act as a monodentate ligand, a bridging bidentate ligand, a symmetric bidentate ligand (isobidentate), or an unsymmetric bidentate ligand (anisobidentate). Additionally, studies by Chung & Lee (2004) and Kayranli (2022) suggest that TgA may facilitate the removal of Cd^{2+} from water through intercalation with γ- Al_2O_3. Thus, the expected complex when binding Cd^{2+} can be appraised in Figure 4.23(c)-4.23(f).

As mentioned before, the linearised Freundlich isotherm indicates that adsorption occurs in multiple layers on the surface of the adsorbents. As concentration increases, the level of adsorption also rises (Wahyuhadi et al., 2023). This typically suggests that the adsorbents have a heterogeneous surface (Mahmoud et al., 2021). The statement can be clarified as follows: during the adsorption study, the uptake of Cd increases with higher initial concentrations. Additionally, since all the adsorbents have heterogeneous surfaces, the adsorption occurs in a multilayer manner, involving multiple binding affinities. This supports the presence of various types of Cd binding interactions with the adsorbents as seen in Figure 4.23. All the adsorbents align better with pseudo-second order kinetics, indicating that a chemical process is involved in the adsorption. In other words, the binding of Cd to the adsorbents forms chemical bonds (either ionic or covalent), which is also consistent with Figure 4.23.

Figure 4.23

Prediction of configurations for (a)-(b) γ-Al_2O_3 (C)-BDMT and) γ-Al_2O_3 (S)-BDMT when binding Cd^{2+} and for (c)-(f) γ-Al_2O_3 (C)-TgA and γ-Al_2O_3 (S)-TgA

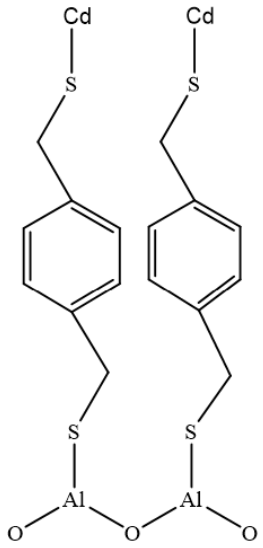

(a)

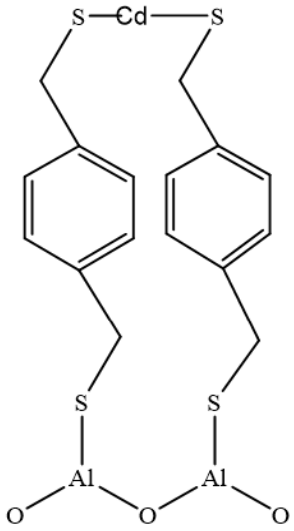

(b)

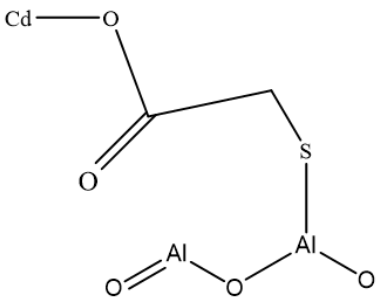

(c)

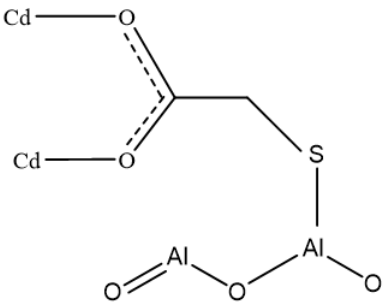

(d)

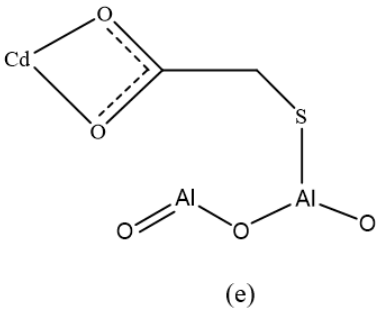

(e)

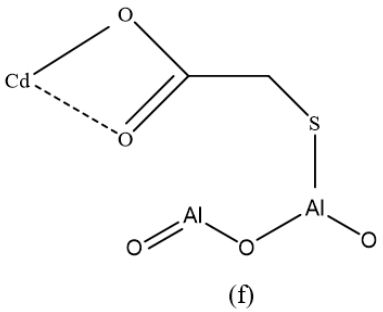

(f)

CHAPTER 5

CONCLUSIONS AND RECOMMENDATIONS

5.1 Conclusions

This research set out to create and investigate new Cd^{2+} adsorbents by intercalating between γ-Al_2O_3 and TgA and 1,4-BDMT respectively. The adsorbents; γ-Al_2O_3(C)-BDMT, γ-Al_2O_3(S)-BDMT, γ-Al_2O_3(C)-TgA and γ-Al_2O_3(S)-TgA, are expected to be simple, convenient to use and cost effective as outlined in the introductory chapter. The research was guided by the objectives of; to synthesise and characterise γ-Al_2O_3, γ-Al_2O_3-BDMT and γ-Al_2O_3-TgA adsorbents, to elucidate the adsorption studies of adsorbents γ-Al_2O_3-BDMT and γ-Al_2O_3-TgA as Cd^{2+} absorbent and to investigate the kinetic of adsorption reactions using pseudo first order and second order models.

Through the application of recycled Al beverage cans to produce γ-Al_2O_3, functionalisation of thiol to γ-Al_2O_3, performance of all adsorbents studied via batch adsorption studies and the analysis of various types of data through XRD, surface and pore diameter, FESEM, EDX, XPS, FTIR and TGA, the research has successfully met its primary objectives. The findings presented in Chapter 4 demonstrate that all adsorbents showed high potential to be utilised in water treatment from Cd^{2+}, which align with and expand upon the assumptions and gaps identified in Chapter 1. Notably, the results provide new insight into being adsorbents that are simple, convenient to use and cost effective coupled with high performance during adsorption studies. The study contributes to the broader understanding of water remediation from Cd^{2+} by validating Pearson's hard soft acid-base for thiol. Furthermore, it reinforces the relevance of the problem highlighted in Chapter 1 and offers evidence-based conclusions that support future research and practical applications. In the subsequent sections of this chapter, the implications of these findings, limitations of the research, and recommendations for further study will be discussed.

The γ-Al_2O_3(S) was successfully synthesised in Stage 1 after validated it with XRD in Stage 2. The analysis showed peaks at 2 theta and respective planes which align with JCPDS-ICDD file No. 00-050-074. The file number belonged to γ-Al_2O_3. The XRD analysis showed that γ-Al_2O_3(S) has a crystallite size of 16.3 nm, a surface area of 78.08 m^2/g, and a pore diameter of 4.47 nm. In Stage 1, The First Procedure: Synthesis of γ-Al_2O_3 was analysed using XRD, surface area and pore diameter analysis, FESEM and EDX. In Stage 1 (The Second Procedure: Synthesis of γ-Al_2O_3-BDMT and γ-Al_2O_3–TgA), the intercalation of γ-Al_2O_3(C) and γ-Al_2O_3(S) with thiol compounds (1,4-BDMT and TgA) were also successful. This was confirmed by the results of XRD

analysis which showed the crystal structure of γ-Al_2O_3 did not affect. FESEM analysis, which showed the agglomeration and the number of pores on the surface of the adsorbents. EDX analysis displayed the existence of S element after intercalation with thiol. XPS analysis exhibited the intercalation through an Al-S bond, while FTIR analysis presented the intercalation through an Al-S bond. TGA analysis was also conducted, which required high temperature to break the thiol group from the adsorbents. It is important to note that the intercalation did not use a complex route. Thus, Stage 1 and Stage 2 were successfully completed, and at the same time, the first objective of this research was achieved.

The effect of pH on the Cd^{2+} solution, the effect of initial Cd^{2+} concentration, and the effect of contact time were studied in the adsorption studies which was in Stage 3. The pH of the Cd^{2+} solution ranged from 2 to 8, the initial Cd^{2+} concentration ranged from 5 to 50 mg/L and the contact time ranged from 0.5 to 40 minutes. The dosage of adsorbents and the shaking speed remained constant at 5 mg and 220 rpm, respectively, at room temperature.

The optimum conditions for each adsorbent were determined through adsorption studies consisting of three parameters. For γ-Al_2O_3(C)-BDMT, the optimal conditions were as follows: pH = 6, initial concentration of Cd^{2+} solution = 10 mg/L and contact time = 30 minutes. For γ-Al_2O_3(S)-BDMT, the optimal conditions were pH = 6, initial concentration of Cd^{2+} solution = 10 mg/L and contact time = 20 minutes. For γ-Al_2O_3(C)-TgA, the optimal conditions were pH = 6, initial concentration of Cd^{2+} solution = 10 mg/L and contact time = 30 minutes. Lastly, for γ-Al_2O_3(S)-TgA, the

optimal conditions were pH = 6, initial concentration of Cd^{2+} solution = 10 mg/L and contact time = 20 minutes.

The research utilised the Langmuir and Freundlich isotherm models to study the interaction between an adsorbent and adsorbate. In all cases, the adsorbents showed a better linear fit when plotted on the linearised Freundlich isotherm model. This indicates that all the adsorbents preferred the linearised Freundlich isotherm model, suggesting that they primarily underwent adsorption in multiple layers on the surface of the adsorbents. In general, it indicates that all the adsorbents possess a heterogeneous surface.

The research utilised pseudo-first and pseudo-second order adsorption kinetics. All the adsorbents leaning towards pseudo-second order adsorption kinetics. Additionally, the value of R^2 for all the adsorbents in the second order adsorption kinetic indicated a better fit compared to the first order adsorption kinetic. This suggests that the second order adsorption kinetic is more favourable for all the adsorbents. Among γ-Al_2O_3(C)-BDMT and γ-Al_2O_3(S)-BDMT adsorbent, γ-Al_2O_3(C)-BDMT showed a bit superior than γ-Al_2O_3(S)-BDMT when comparing K_F values in Freundlich isotherm (K_F = 463.767 mg/g for γ-Al_2O_3(C)-BDMT and K_F = 428.410 mg/g for γ-Al_2O_3(S)-BDMT). For γ-Al_2O_3(S)-BDMT which comprised of γ-Al_2O_3(S) (synthesised in Stage 1), it was almost on par with γ-Al_2O_3(C)-BDMT which comprised of γ-Al_2O_3(C) (commercial γ-Al_2O_3). Meanwhile for γ-Al_2O_3(C)-TgA and γ-Al_2O_3(S)-TgA, there was a large difference in performance when also comparing K_F values in Freundlich isotherm (K_F = 48.228 mg/g for γ-Al_2O_3(C)-TgA and K_F = 217.871 mg/g for γ-Al_2O_3(S)-TgA). This showed that γ-Al_2O_3(S) capable to perform as support when

functionalised with thiol. Among the four adsorbents, γ-Al_2O_3(C)-BDMT achieved the highest K_F value, indicating it had the best performance when adsorb Cd^{2+} in solution. Thus, Stage 3 of this research concluded successfully and at the same time, the second and third objectives of this research was achieved.

The selection of Cd as the studied heavy metal was to address some Cd-related pollution in Malaysia (in Chapter 1) after also considering the affinity between Cd and thiols as the studied functional group. Based on Pearson's hard-soft acid-base theory, which discusses the affinity between Cd and thiols, the expected union between γ-Al_2O_3 and thiols will be able to adsorb Cd^{2+} in solution. After going through batch adsorption studies in Stage 3, all the adsorbents were able to perform well when adsorbing Cd^{2+}. Thus, the selection of the studied heavy metal, which was Cd, was the right call for this research.

5.2 Recommendations

Future researchers can enhance the adsorption studies by adding additional parameters such as temperature, dosage of the adsorbents and shaking speed. These parameters were kept constant in the current research. By including more parameters, the optimal conditions for each adsorbent can be more accurately determined. Furthermore, the other parameters investigated in this research, including the pH of the

solution, initial concentration of the solution and contact time, can be further explored in future studies.

The current research focused on Cd as the particular heavy metal under study. In future research, other heavy metals such as Hg, Cr, Cu, Zn, Co, Fe, As, and Pb can be considered for a selectivity study. This study would help determine which heavy metal exhibits a higher affinity towards the adsorbents. Consequently, the adsorbents can be modified to effectively remove multiple heavy metals simultaneously.

The adsorbents in this research can also be studied for applications other than the removal of heavy metals, such as the removal of dyes from aqueous solutions. The removal of heavy metals and dyes from aqueous solutions is widely investigated in the field of water treatment. Therefore, for further research on these adsorbents, it is recommended to consider the removal of common dyes in this field, such as methylene blue, methyl red, eosin yellow and malachite green.

For γ-Al_2O_3 (S)-BDMT, the prediction of configuration displayed a bond of S-S. For future research, Raman Spectroscopy can be utilised to confirm the bond since the current research only used FTIR as the instrument to validate the existence of the bond.

REFERENCES

Abdulhadi, B., Kot, P., Hashim, K., Shaw, A., Muradov, M., & Al-Khaddar, R. (2021). Continuous-flow electrocoagulation (EC) process for iron removal from water: Experimental, statistical and economic study. *Science of The Total Environment*, *760*(1), 143417. https://doi.org/10.1016/j.scitotenv.2020.143417

Abd Mutalib, M., Rahman, M. A., Othman, M. H. D., Ismail, A. F., & Jaafar, J. (2017). Scanning Electron Microscopy (SEM) and Energy-Dispersive X-Ray (EDX) Spectroscopy. In *Membrane Characterization* (pp. 161–179). Elsevier. https://doi.org/10.1016/B978-0-444-63776-5.00009-7

Abd Wahab, M. H., Kadir, A. A., Tomari, M. R., & Jabbar, M. H. (2014). Smart recycle bin: A conceptual approach of smart waste management with integrated web based system. *2014 international conference on IT convergence and security (ICITCS)*, *1*(1), 1-4. https://doi.org/10.1109/ICITCS.2014.7021812

Ab Razak, N. H., Praveenaa, S. M., Aris, A. Z., & Hashim, Z. (2015). Drinking water studies: A review on heavy metal, application of biomarker and health risk assessment (a special focus in Malaysia). *Journal of Epidemiology and Global Health*, *5*(4), 297-310. https://doi.org/10.1016/j.jegh.2015.04.003

Abu-El-Halawa, R., & Zabin, S. (2017). Removal efficiency of Pb, Cd, Cu and Zn from polluted water using dithiocarbamate ligands. Journal of Taibah University for Science, 11(1), 57–65. https://doi.org/10.1016/j.jtusci.2015.07.002

Acharya, S. (2013). Lead between the lines. *Nature Chemistry*, *5*(12), 894. https://doi.org/10.1038/nchem.1761

Adans, Y. F., Martins, A. R., Coelho, R. E., Virgens, C. F. D., Ballarini, A. D., & Carvalho, L. S. (2016). A simple way to produce γ-alumina from aluminum cans by precipitation reactions. *Materials Research*, *19*(5), 977-982. https://doi.org/10.1590/1980-5373-MR-2016-0310

Aguirre-Terrazas, K. A., Medellín-Castillo, N., Ruíz-Baltazar, Á. de J., Torres-Pérez, J., & Reyes-López, S. Y. (2021). Review of alumina in adsorption processes for emerging pollutants. *International Journal of Research -GRANTHAALAYAH*, 9(4), 435–453. https://doi.org/10.29121/granthaalayah.v9.i4.2021.3846

Ahmed, M. F., & Mokhtar, M. B. (2020). Assessing cadmium and chromium concentrations in drinking water to predict health risk in Malaysia. *International Journal of Environmental Research and Public Health*, *17*(8), 2966. https://doi.org/10.3390/ijerph17082966

Ahmed, M. F., Mokhtar, M. B., Alam, L., Mohamed, C. A. R., & Ta, G. C. (2020). Investigating the status of cadmium, chromium and lead in the drinking water supply chain to ensure drinking water quality in Malaysia. *Water*, *12*(10), 2653. https://doi.org/10.3390/w12102653

Ahmedzeki, N. S., Hussein, S., & Abdulnabi, W. A. (2017). Recycling waste cans to nano gamma alumina: Effect of the calcination temperature and pH. *Int. J. Curr. Eng. Technol*, *7*(1), 82-88. https://inpressco.com/wp-content/uploads/2017/01/Paper1482-88.pdf

Ahmedzeki, N. S., Hussein, S. J., & Abdulnabi, W. A. (2018). Synthesis of nano crystalline gamma alumina from waste cans. *Iraqi J. Chem. Pet. Eng*, *19*(1), 45-49. https://doi.org/10.31699/IJCPE.2018.1.5

Aini, N. (2015). *Cadmium concentration in water supply from Telibong Water Treatment 2 to its receivers* (Student Project). Universiti Teknologi MARA. Retrieved from https://ir.uitm.edu.my/id/eprint/108007

Alamouti, A. F., Nadafan, M., Dehghani, Z., Ara, M. M., & Noghreiyan, A. V. (2021). Structural and optical coefficients investigation of γ-Al_2O_3 nanoparticles using Kramers-Kronig relations and Z–scan technique. *Journal of Asian ceramic societies*, *9*(1), 366-373. https://doi.org/10.1080/21870764.2020.1869881

Alexander, S., Gomez, V., & Barron, A. R. (2016). Carboxylation and decarboxylation of aluminum oxide nanoparticles using bifunctional carboxylic acids and octylamine. *Journal of Nanomaterials*, *2016*(1), 2-2. https://doi.org/10.1155/2016/7950876

Al-Ghouti, M. A., Da'ana, D., Abu-Dieyeh, M., & Khraisheh, M. (2019). Adsorptive removal of mercury from water by adsorbents derived from date pits. *Scientific reports*, *9*(1), 15327. https://doi.org/10.1038/s41598-019-51594-y

Al Haiqi, O., Bin Mokaizh, A. A., & Shariffuddin, J. H. B. (2021). Low-calcination temperature to synthesize alumina from aluminium waste can using sol-gel method. *IOP Conference Series: Earth and Environmental Science*, *641*(1), 012023. https://doi.org/10.1088/1755-1315/641/1/012023

Ali, A., Chiang, Y. W., & Santos, R. M. (2022). X-ray diffraction techniques for mineral characterization: A review for engineers of the fundamentals, applications, and research directions. *Minerals*, *12*(2), 205. https://doi.org/10.3390/min12020205

Ali, M. E., Hoque, M. E., Safdar Hossain, S. K., & Biswas, M. C. (2020). Nanoadsorbents for wastewater treatment: next generation biotechnological solution. *International Journal of Environmental Science and Technology*, *17*(1), 4095-4132. https://doi.org/10.1007/s13762-020-02755-4

Ali, S., Abbas, Y., Zuhra, Z., & Butler, I. S. (2019). Synthesis of γ-alumina (Al_2O_3) nanoparticles and their potential for use as an adsorbent in the removal of methylene blue dye from industrial wastewater. *Nanoscale Advances*, *1*(1), 213-218. https://doi.org/10.1039/C8NA00014J

Aljamali, N., Alfatlawi, I., Sahib Mohammed, N., Abdulhssein, A., & Almosawy, M. (2020). Review on effect of chemical waste on environment. *International Journal of Green Chemistry, 6*(1), 1-9. https://chemical.journalspub.info/index.php?journal=IJGC&page=article&op=view&path%5B%5D=940

ALOthman, Z. A. (2012). A review: fundamental aspects of silicate mesoporous materials. *Materials*, *5*(12), 2874-2902. https://doi.org/10.3390%2Fma5122874

Al-Saydeh, S. A., El-Naas, M. H., & Zaidi, S. J. (2017). Copper removal from industrial wastewater: A comprehensive review. *Journal of industrial and engineering chemistry*, *56*(1), 35-44. https://doi.org/10.1016/j.jiec.2017.07.026

Aweng, E. R., Karimah, M., & Suhaimi, O. (2011). Heavy metal concentration in irrigation water, soils and fruit vegetables in coastal area, Kota Bharu, Kelantan, Malaysia. In *Proceedings of the 7th ACSA Conference, 1*(1) (407-411). https://repository.ipb.ac.id/bitstream/handle/123456789/62169/ACSAC-ISBN-82.pdf?isAllowed=y&sequence=66

Awual, M. R., Hasan, M. M., Islam, A., Asiri, A. M., & Rahman, M. M. (2020). Optimization of an innovative composited material for effective monitoring and removal of cobalt (II) from wastewater. *Journal of Molecular Liquids*, *298*(1), 112035. https://doi.org/10.1016/j.molliq.2019.112035

Azócar, M. I., Gómez, G., Levín, P., Paez, M., Muñoz, H., & Dinamarca, N. (2014). Antibacterial behavior of carboxylate silver (I) complexes. *Journal of Coordination Chemistry*, *67*(23-24), 3840-3853.

Babel, S., & Kurniawan, T. A. (2003). Low-cost adsorbents for heavy metals uptake from contaminated water: a review. *Journal of hazardous materials*, *97*(1-3), 219-243.

Bagheri, S., Amini, M. M., Behbahani, M., & Rabiee, G. (2019). Low cost thiol-functionalized mesoporous silica, KIT-6-SH, as a useful adsorbent for cadmium ions removal: a study on the adsorption isotherms and kinetics of KIT-6-SH. *Microchemical Journal*, *145*(1), 460-469. https://doi.org/10.1016/j.microc.2018.11.006

Baik, S., Zhang, H., Kim, Y. K., Harbottle, D., & Lee, J. W. (2017). Enhanced adsorption capacity and selectivity towards strontium ions in aqueous systems by sulfonation of CO_2 derived porous carbon. *RSC advances*, *7*(86), 54546-54553. http://dx.doi.org/10.1039/C7RA09541D

Banza Lubaba Nkulu, C., Casas, L., Haufroid, V., De Putter, T., Saenen, N. D., Kayembe-Kitenge, T., Obadia, P.M., Mukoma, D.K.W., Iluga, J.L., Nawrot, T.S., Numbi, O.L, Smolders, E., & Nemery, B. (2018). Sustainability of artisanal mining of cobalt in DR Congo. *Nature sustainability*, *1*(9), 495-504. https://doi.org/10.1038/s41893-018-0139-4

Bardestani, R., Patience, G. S., & Kaliaguine, S. (2019). Experimental methods in chemical engineering: specific surface area and pore size distribution measurements—BET, BJH, and DFT. *The Canadian Journal of Chemical Engineering*, *97*(11), 2781-2791. https://doi.org/10.1002/cjce.23632

Bednarska & Koniorczyk. (2019). Comparison of various methods applied in porous materials microstructure analysis in regard to hardened cement paste. MATEC Web Conf., 282 (2019) 02043 https://doi.org/10.1051/matecconf/201928202043

Benu, D. P., Hardian, A., Mukti, R. R., Yuliarto, B., Fukumitsu, N., Ide, Y., Yamauchi, Y., Kaneti, Y.V., & Suendo, V. (2021). Reverse micelle-mediated synthesis of plate-assembled hierarchical three-dimensional flower-like gamma-alumina particles. *Microporous and Mesoporous Materials*, *321*(1), 111055. https://doi.org/10.1016/j.micromeso.2021.111055

Bernama. (2019, April 9). Makanan laut bercengkerang di Selat Melaka dicemari logam berat-Pakar. *Astro awani*. https://www.astroawani.com/berita-malaysia/makanan-laut-bercengkerang-di-selat-melaka-dicemari-logam-berat-pakar-203853

Beyene, H. D., Hailegebrial, T. D., & Direrse, W. B. (2016). Investigation of coagulation activity of cactus powder in water treatment. *Journal of Applied Chemistry*, *2016*(1), 7815903. http://dx.doi.org/10.1155/2016/7815903

Beyene, H. D., & Berhe, G. B. (2015). The level of heavy metals in potable water in Dowhan, Erop Wereda, Tigray, Ethiopia. *Journal of Natural Sciences Research*, *5*(3), 190-194.

Bhaskar, M., Anand, G., Nalluswamy, T., & Suresh, P. (2022). Die Life in Aluminium High-Pressure Die Casting Industries. *Journal of The Institution of Engineers (India): Series D*, *103*(1), 117-123. https://doi.org/10.1007/s40033-021-00317-7

Bijelic, A., & Rompel, A. (2018). Polyoxometalates: more than a phasing tool in protein crystallography. *ChemTexts*, *4*(3), 10. https://doi.org/10.1007/s40828-018-0064-1

Branca, J. J., Fiorillo, C., Carrino, D., Paternostro, F., Taddei, N., Gulisano, M., Pacini, A., & Becatti, M. (2020). Cadmium-induced oxidative stress: focus on the central nervous system. *Antioxidants*, *9*(6), 492. https://doi.org/10.3390/antiox9060492

Brough, D. & Jouhara, H. (2020). The aluminium industry: A Review On State-Of-The-Art Technologies, Environmental Impacts and Possibilities For Waste Heat Recovery. *International Journal of Thermofluids, 1-2*, 1-38. https://doi.org/10.1016/j.ijft.2019.100007

Capuzzi, S., & Timelli, G. (2018). Preparation and melting of scrap in aluminum recycling: A review. *Metals*, *8*(4), 249. https://doi.org/10.3390/met8040249

Carter, C. B., & Norton, M. G. (2007). Sols, gels, and organic chemistry. In *Ceramic materials: Science and engineering* (pp. 400–411). Springer New York. https://doi.org/10.1007/978-0-387-46271-4_22

Carter, P. (2023, November 6). Thioglycolic Acid Market Size Challenges 2023, Scopes, Share, Revenue and Forecasts 2031. *Taiwan News.* https://www.taiwannews.com.tw/en/news/5034314

Chargui, F., Hamidouche, M., Belhouchet, H., Jorand, Y., Doufnoune, R., & Fantozzi, G. (2018). Mullite fabrication from natural kaolin and aluminium slag. *Boletín de la Sociedad Española de Cerámica y Vidrio*, *57*(4), 169-177. https://doi.org/10.1016/j.bsecv.2018.01.001

Charvát, P., Klimeš, L., Pospíšil, J., Klemeš, J. J., & Varbanov, P. S. (2020). An overview of mercury emissions in the energy industry-A step to mercury footprint assessment. *Journal of cleaner production*, *267*(1), 122087. https://doi.org/10.1016/j.jclepro.2020.122087

Cheku, N. H., Mamat, I., & Ibrahim, M. Y. (2017). Faktor penentu amalan kitar semula generasi Y di Terengganu. *Sains Humanika*, *9*(3), 9-15. https://doi.org/10.11113/sh.v9n3.1045

Chen, X., Hossain, M. F., Duan, C., Lu, J., Tsang, Y. F., Islam, M.S., & Zhou, Y. (2022). Isotherm models for adsorption of heavy metals from water-A review. *Chemosphere*, 135545. https://doi.org/10.1016/j.chemosphere.2022.135545

Chen, Y., Zou, C., Mastalerz, M., Hu, S., Gasaway, C., & Tao, X. (2015). Applications of micro-fourier transform infrared spectroscopy (FTIR) in the geological sciences—a review. *International journal of molecular sciences*, *16*(12), 30223-30250. https://doi.org/10.3390/ijms161226227

Chung & Lee (2004). Self-Assembled Monolayers of Mercaptoacetic Acid on Ag Powder: Characterization by FT-IR Diffuse Reflection Spectroscopy. *Bulletin of the Korean Chemical Society*. *25*(1). 10.5012/bkcs.2004.25.10.1461. http://dx.doi.org/10.5012/bkcs.2004.25.10.1461

Dang-Bao, T., Nguyen, T. M. C., Hoang, G. H., Lam, H. H., Phan, H. P. & Tran, T. K. A. (2023). Thiol-Surface-Engineered Cellulose Nanocrystals in Favor of Copper Ion Uptake. *Polymers*, *15*(11), 2562. https://doi.org/10.3390/polym15112562

Das, R., Giri, S., Muliwa, A. M., & Maity, A. (2017). High-performance Hg (II) removal using thiol-functionalized polypyrrole (PPy/MAA) composite and effective catalytic activity of Hg (II)-adsorbed waste material. *ACS Sustainable*

Chemistry & Engineering, *5*(9), 7524-7536. https://doi.org/10.1021/acssuschemeng.7b00477

Das, P., Goswami, S., & Maity, S. (2016). Removal of naphthalene present in synthetic waste water using novel G/GO nano sheet synthesized from rice straw: comparative analysis, isotherm and kinetics. *Front. Nanosci Nanotech*, *2,* 38-42. http://dx.doi.org/10.15761/FNN.1000107

David, E. & Kopac, J. (2015). Use of Separation and Impurity Removal Methods to ImproveAluminium Waste Recycling Process. *Materials Today: Proceedings, 2*(2015), 5071 – 5079. https://doi.org/10.1016/j.matpr.2015.10.098

Deng, S., Yu, C., Liu, X., Wu, F., Lin, H., Liao, J., & Liu, F. (2020). Efficient and enhanced Hg^{2+} removal from water using a thio functionalized fibrous adsorbent prepared with microwave irradiation: Batch and fixed-bed column study. *Journal of cleaner production*, *267*(1), 122163. https://doi.org/10.1016/j.jclepro.2020.122163

De Paoli, F., Bishara, R. H., & van Asselt, E. J. (2021). How to define the right ambient temperature range for storage and distribution of pharmaceutical raw materials. *Biologicals, 69(1),* 66–69. https://doi.org/10.1016/j.biologicals.2020.12.001

Department of Environment, Ministry of Natural Resources and Environmental Sustainability. (2024). *Standard untuk kegunaan rawatan air mentah secara-konvensional air minuman*. Retrieved from https://www.doe.gov.my/standard-dan-indeks-kualiti/standard-untuk-kegunaan-rawatan-air-mentah-secara-konvensional-air-minuman-3/

Derakhshani, M., Hashemzadeh, A., & Amini, M. (2018). Novel synthesis of mesoporous crystalline γ-alumina by replication of MOF-5-derived nanoporous carbon template. *Ceramics International*, *44*(14), 10.1016/j.ceramint.2018.06.161

Dey, S. (2014). *Synthesis and application of γ-alumina nanopowders* (Master's thesis, National Institute of Technology, Rourkela). http://ethesis.nitrkl.ac.in/5862/1/E-62.pdf

Dey, S., Sreenivasulu, A., Veerendra, G. T. N., Manoj, A. P., & Haripavan, N. (2022). Synthesis and characterization of mango leaves biosorbents for removal of iron and phosphorous from contaminated water. *Applied Surface Science Advances*, *11*(1), 100292. https://doi.org/10.1016/j.apsadv.2022.100292

Dynys, F. W., & Halloran, J. W. (1982). Alpha alumina formation in alum-derived gamma alumina. *Journal of the American Ceramic Society, 65*(9), 442-448. https://doi.org/10.1111/j.1151-2916.1982.tb10460.x

Elfeghe, S., Anwar, S., & Zhang, Y. (2022). Adsorption and removal studies of cadmium ion onto sulphonic/phosphonic acid functionalization resins. *The*

Canadian Journal of Chemical Engineering, *100*(10), 3006–3014. https://doi.org/10.1002/cjce.24400

Elias, E. M., Othman, Z., Mahidin, N., Nawi, M. N. M., & Nadarajan, S. S. (2016). Program Kitar Semula: Persepsi Masyarakat Terhadap ReDMac. *Sains Humanika*, *8*(4-2), 1-7. https://doi.org/10.11113/sh.v8n4-2.1051

El-Saadani, Z., Mingqi, W., He, Z., Hamukwaya, S. L., Abdel Wahed, M. S., & Abu Khatita, A. (2022). Environmental geochemistry and fractionation of cadmium metal in surficial bottom sediments and water of the Nile River, Egypt. *Toxics*, *10*(5), 221.

Fan, J., Cai, C., Chi, H., Reid, B. J., Coulon, F., Zhang, Y., et al. (2020). Remediation of cadmium and lead polluted soil using thiol-modified biochar. *Journal of hazardous materials*, *388*(1), 122037. https://doi.org/10.1016/j.jhazmat.2020.122037

Fang, R. C., Sun, Q. Q., Zhou, P., Yang, W., Wang, P. F., & Zhang, D. W. (2013). High-performance bilayer flexible resistive random access memory based on low-temperature thermal atomic layer deposition. *Nanoscale research letters*, *8*(1), 1-7. http://dx.doi.org/10.1186/1556-276X-8-92

Fatimah, T. S., Wahyudi, T., Khaerunisa, H., & Saleh, N. (2021). Characterization of the γ, α-alumina and its adsorption capability to adsorb nickel (ii) and magnesium (ii) from nickel sulfate as a result of solvent differences. In *IOP Conference Series: Materials Science and Engineering* (Vol. 1034, No. 1, p. 012151). IOP Publishing. 10.1088/1757-899X/1034/1/012151

Fecher, P. A., Schlemmer, G. C., & Schoeberl, K. S. (2014). Safety aspects, quality control, and quality assurance using microwave-assisted sample preparation systems. In *Microwave-Assisted Sample Preparation for Trace Element Analysis* (pp. 345-384). Elsevier. https://doi.org/10.1016/B978-0-444-59420-4.00012-X

Frisbie, S. H., & Mitchell, E. J. (2022). Arsenic in drinking water: An analysis of global drinking water regulations and recommendations for updates to protect public health. *PLoS One*, *17*(4), e0263505. https://doi.org/10.1371/journal.pone.0263505

Gan, W., Gao, L., Zhan, X., & Li, J. (2016). Preparation of thiol-functionalized magnetic sawdust composites as an adsorbent to remove heavy metal ions. *RSC advances*, *6*(44), 37600-37609.

García-Martínez, J.-M., & Collar, E. P. (2021). Organic–inorganic hybrid materials. *Polymers*, *13*(1), 86. https://doi.org/10.3390/polym13010086

Genchi, G., Sinicropi, M. S., Lauria, G., Carocci, A., & Catalano, A. (2020). The effects of cadmium toxicity. *International journal of environmental research and public health*, *17*(11), 3782. https://doi.org/10.3390/ijerph17113782

Gholizadeh, Z., Aliannezhadi, M., Ghominejad, M., & Tehrani, F. S. (2023). High specific surface area γ-Al_2O_3 nanoparticles synthesized by facile and low-cost co-precipitation method. *Scientific Reports*, *13*(1), 6131. https://doi.org/10.1038/s41598-023-33266-0

Ghosh, D., Devi, P., & Kumar, P. (2022). Intercalation in two-dimensional transition metal chalcogenides: interlayer engineering and applications. *Progress in Energy*, *4*(2), 022001. 10.1088/2516-1083/ac3c3d

González, C. M. O., Morales, E. M. C., Tellez, A. M. N., Quezada, T. E. S., Kharissova, O. V., & Méndez-Rojas, M. A. (2021). CO2 capture by MOFs. In C. M. O. González & O. V. Kharissova (Eds.), *Handbook of Greener Synthesis of Nanomaterials and Compounds: Volume 2: Synthesis at the Macroscale and Nanoscale* (pp. 407–448). Elsevier. https://doi.org/10.1016/B978-0-12-822446-5.00018-6

Gordovskaya, I. V., Hashimoto, T., Walton, J., Curioni, M., Thompson, G. E., & Skeldon, P. (2014). Development of cerium-rich layers on anodic films formed on pure aluminium and AA7075 T6 alloy. *Journal of The Electrochemical Society*, *161*(14), C601. 10.1149/2.0091501jes

Grimm, O. C., Somaratne, R. D. S., Wang, Y., Kim, S., & Whitten, J. E. (2021). Thiol adsorption on metal oxide nanoparticles. *Physical Chemistry Chemical Physics*, *23*(14), 8309-8317. https://doi.org/10.1039/D1CP00506E

Haldar, D., Duarah, P., & Purkait, M. K. (2020). MOFs for the treatment of arsenic, fluoride and iron contaminated drinking water: A review. *Chemosphere*, *251*(1), 126388. https://doi.org/10.1016/j.chemosphere.2020.126388

Halit, A. L., Azman, S., Said, M. I. M., Alias, N., & Ali, N. (2018). Cadmium and chromium accumulation in cockles along the estuary of Sungai Tampok and Sungai Sanglang. In *Journal of Physics: Conference Series* (Vol. 1049, No. 1, p. 012043). IOP Publishing. 10.1088/1742-6596/1049/1/012043

Hao, J., Han, M.-J., & Meng, X. (2009). Preparation and evaluation of thiol-functionalized activated alumina for arsenite removal from water. *Journal of Hazardous Materials*, *167*(1–3), 1215–1221. https://doi.org/10.1016/j.jhazmat.2009.01.124

Hashimoto, H., Shigehara, Y., Ono, S., & Asoh, H. (2018). Heat-induced structural transformations of anodic porous alumina formed in phosphoric acid. *Microporous and Mesoporous Materials*, *265*(1), 77-83. https://doi.org/10.1016/j.micromeso.2018.01.008

Hassan, M. M. (2017). Antibacterial and Antifungal Thioglycolic Acid-Capped Silver Nanoparticles and Their Application on Wool Fabric as a Durable

Antimicrobial Treatment. *ChemistrySelect*, *2*(1), 504-512. https://doi.org/10.1002/slct.201601508

Herath, I., Vithanage, M., Bundschuh, J., Maity, J. P., & Bhattacharya, P. (2016). Natural arsenic in global groundwaters: distribution and geochemical triggers for mobilization. *Current Pollution Reports*, *2*(1), 68-89. https://doi.org/10.1007/s40726-016-0028-2

Hong, J. Y., Chang, S. H., Ou Yang, K. H., Yeh, P. C., Shiu, H. W., Chen, C. H., ... & Lin, M. T. (2019). A multifunctional molecular spintronic platform with magnetoresistive and memristive responses via a self-assembled monolayer. *Journal of Applied Physics*, *125*(14). https://doi.org/10.1063/1.5057893

Hosseini, S. A., Niaei, A., & Salari, D. (2011). Production of γ-Al_2O_3 from Kaolin. *Open Journal of Physical Chemistry*, *1*(02), 23-27. http://dx.doi.org/10.4236/ojpc.2011.12004

How, L. F., Islam, A., Jaafar, M. S., & Taufiq-Yap, Y. H. (2017). Extraction and characterization of γ-alumina from waste aluminium dross. *Waste and biomass valorization*, *8*(2), 321-327. https://doi.org/10.1007/s12649-016-9591-4

Ibrahim, T. N. B. T., Othman, F., & Mahmood, N. Z. (2020). Baseline study of heavy metal pollution in a tropical river in a developing country. *Sains Malaysiana*, *49*(4), 729-742. http://dx.doi.org/10.17576/jsm-2020-4904-02

Igiri, B. E., Okoduwa, S. I., Idoko, G. O., Akabuogu, E. P., Adeyi, A. O., & Ejiogu, I. K. (2018). Toxicity and bioremediation of heavy metals contaminated ecosystem from tannery wastewater: a review. *Journal of toxicology*, *2018*(1). https://doi.org/10.1155/2018/2568038

Ishaq, K., Saka, A. A., Kamardeen, A. O., Abdulrahman, A., Adekunle, I. K., & Afolabi, A. S. (2018). Application of γ-alumina as catalyst support for the synthesis of CNTs in a CVD reactor. *Advances in Natural Sciences: Nanoscience and Nanotechnology*, *9*(3), 035012. 10.1088/2043-6254/aad5bb

Ismail, S. N. S., Salleh, F. H., Abidin, E. Z., Mahiddin, N. A. K., & Rangga, J. U. (2018). Cadmium (Cd) Exposure among Waste Collector in Urban Area, Malaysia. *Malaysian Journal of Medicine & Health Sciences*, *14*(SP1). 72-80. http://psasir.upm.edu.my/id/eprint/66146/1/2018080309050509_MJMHS_Aug_2018.pdf

Jia, J., Kara, A., Pasquali, L., Bendounan, A., Sirotti, F., & Esaulov, V. A. (2015). On sulfur core level binding energies in thiol self-assembly and alternative adsorption sites: An experimental and theoretical study. *The Journal of Chemical Physics*, *143*(10).

Jundam, N. E. F., Ahmad, N., & Puasa, S. W. (2020). Removal of cadmium ion from aqueous solution using plant-based anionic surfactant impregnated activated

carbon. *Malaysian Journal of Chemical Engineering and Technology (MJCET)*, *3*(2), 60-66. https://doi.org/10.24191/mjcet.v3i2.11228

Karim, M. R., Aijaz, M. O., Alharth, N. H., Alharbi, H. F., Al-Mubaddel, F. S., & Awual, M. R. (2019). Composite nanofibers membranes of poly(vinyl alcohol)/chitosan for selective lead(II) and cadmium(II) ions removal from wastewater. *Ecotoxicology and Environmental Safety*, 169(1), 479–486. https://doi.org/10.1016/j.ecoenv.2018.11.049

Kaunisto, K., Lagerbom, J., Honkanen, M., Varis, T., Lambai, A., Mohanty, G., Levänen, E., Kivikytö-Reponen, P., & Frankberg, E. (2023). Evolution of alumina phase structure in thermal plasma processing. *Ceramics International*, *49*(13), 21346-21354. https://doi.org/10.1016/j.ceramint.2023.03.263

Kaur, N., Singh, M., Moumen, A., Duina, G., & Comini, E. (2020). 1D titanium dioxide: Achievements in chemical sensing. *Materials, 13*(13), 2974. https://doi.org/10.3390/ma13132974

Kaya, M., Hussaini, S., & Kursunoglu, S. (2020). Critical review on secondary zinc resources and their recycling technologies. *Hydrometallurgy*, *195*(1), 105362. https://doi.org/10.1016/j.hydromet.2020.105362

Kayan, A. (2019). Inorganic-organic hybrid materials and their adsorbent properties. *Advanced Composites and Hybrid Materials*, *2*(1), 34-45. https://doi.org/10.1007/s42114-018-0073-y

Kayranli, B. (2022). Cadmium removal mechanisms from aqueous solution by using recycled lignocelluloses. *Alexandria Engineering Journal, 61*(1), 443-457. https://doi.org/10.1016/j.aej.2021.06.036

Kenawy, I. M. M., Abou El-Reash, Y. G., Hassanien, M. M., Alnagar, N. R., & Mortada, W. I. (2018). Use of microwave irradiation for modification of mesoporous silica nanoparticles by thioglycolic acid for removal of cadmium and mercury. *Microporous and Mesoporous Materials*, *258*(1), 217-227. https://doi.org/10.1016/j.micromeso.2017.09.021

Kennedy, K. K., Maseka, K. J., & Mbulo, M. (2018). Selected adsorbents for removal of contaminants from wastewater: towards engineering clay minerals. *Open Journal of Applied Sciences*, *8*(8), 355-369.

Kiyohara, P.K., Santos, H.D., Coelho, A.C., & Santos, S. (2000). Structure, surface area and morphology of aluminas from thermal decomposition of $Al(OH)(CH_3COO)_2$ crystals. *Anais Da Academia Brasileira De Ciencias, 72*(4), 471-495. http://dx.doi.org/10.1590/S0001-37652000000400003

Khan, Z. H., Gao, M., Qiu, W., Islam, M. S., & Song, Z. (2020). Mechanisms for cadmium adsorption by magnetic biochar composites in an aqueous solution. *Chemosphere*, *246*(1), 125701. https://doi.org/10.1016/j.chemosphere.2019.125701

Khatri, N., Tyagi, S., & Rawtani, D. (2017). Recent strategies for the removal of iron from water: A review. *Journal of Water Process Engineering*, *19*(1), 291-304. https://doi.org/10.1016/j.jwpe.2017.08.015

Kim, Y.S., Ko, H.S., Suh, J.K., Lee, J.M. & Ha, B.H. (2001). Characteristics of γ-Alumina Prepared From Rehydrated Amorphous Alumina. *Korean Journal of Materials Research, 11*(11), 978-985.

Krishna, D. N. G., & Philip, J. (2022). Review on surface-characterization applications of X-ray photoelectron spectroscopy (XPS): Recent developments and challenges. *Applied Surface Science Advances*, *12*, 100332. https://doi.org/10.1016/j.apsadv.2022.100332

Kristanti, R. A., Bunrith, S., Kumar, R., & Mohamed, A. O. (2023). Municipal wastewater treatment technologies in Malaysia: A short review. *Industrial and Domestic Waste Management*, *3*(1), 38-46. https://doi.org/10.53623/idwm.v3i1.243

Kumar, P. S., Korving, L., Keesman, K. J., van Loosdrecht, M. C., & Witkamp, G. J. (2019). Effect of pore size distribution and particle size of porous metal oxides on phosphate adsorption capacity and kinetics. *Chemical Engineering Journal*, *358*(1), 160-169. http://dx.doi.org/10.1016/j.cej.2018.09.202

Kumari, R., Kumar, A., Ghosh, T. K., & Basu, S. (2024). Facile synthesis of Aluminium fumarate metal–organic framework and hydroxyapatite composite with improved adsorption characteristics for efficient fluoride removal from water. *Chemical Engineering Science*, *283*(1), 119440. https://doi.org/10.1016/j.ces.2023.119440

Lavado-Meza, C., De la Cruz-Cerrón, L., Lavado-Puente, C., Gamarra-Gómez, F., Sacari-Sacari, E., & Dávalos-Prado, J. Z. (2023). Effective Removal of Cd (II) from Aqueous Solutions Using Theobroma cacao Agro-Industrial Waste. *Molecules*, *28*(14), 5491. https://doi.org/10.3390/molecules28145491

Lestido-Cardama, A., Barros-Velázquez, J., & Miranda, J. M. (2022). Polymeric coatings in food and beverage metal packaging: A review on types, interactions, migration, and safety. *Comprehensive Reviews in Food Science and Food Safety, 21*(6), 5039–5072. https://doi.org/10.1111/1541-4337.12976

Li, X., Ma, W., Li, H., Zhang, Q., & Liu, H. (2020). Sulfur-functionalized metal-organic frameworks: Synthesis and applications as advanced adsorbents. *Coordination Chemistry Reviews*, *408*(1), 213191. https://doi.org/10.1016/j.ccr.2020.213191

Li, Z., Sun, Y., Ge, S., Zhu, F., Yin, F., Gu, L., ... & Volinsky, A. A. (2023). An overview of synthesis and structural regulation of magnetic nanomaterials prepared by chemical coprecipitation. *Metals*, *13*(1), 152

Liang, R., & Zou, H. (2020). Removal of aqueous Hg (II) by thiol-functionalized nonporous silica microspheres prepared by one-step sol–gel method. *RSC advances*, *10*(31), 18534-18542. https://doi.org/10.1039/D0RA02759F

Liao, Y., Loures, E. R., Deschamps, F., Brezinski, G., & Venâncio, A. (2018). The impact of the fourth industrial revolution: a cross-country/region comparison. *Production*, *28*(1), e20180061. https://doi.org/10.1590/0103-6513.20180061

Liu, H., & Xie, X. (2021). Thiol-methyl-modified magnetic microspheres for effective cadmium (II) removal from polluted water. *Environmental Science and Pollution Research*, *28*(1), 42750-42762. https://doi.org/10.1007/s11356-021-13773-1

Liu, C., Shih, K., Gao, Y., Li, F., & Wei, L. (2012). Dechlorinating transformation of propachlor through nucleophilic substitution by dithionite on the surface of alumina. *Journal of soils and sediments*, *12*(5), 724-733. https://doi.org/10.1007/s11368-012-0506-0

Liu, W., Niu, T., Yang, J., Wang, Y., Hu, S., Dong, Y., & Xu, H. (2011). Preparation of micron-sized alumina powders from aluminium beverage can by means of sol–gel process. *Micro & Nano Letters*, *6*(10), 852-854. https://doi.org/10.1049/mnl.2011.0491

Liu, W., Zhang, Y., Wang, S., Bai, L., Deng, Y., & Tao, J. (2021). Effect of pore size distribution and amination on adsorption capacities of polymeric adsorbents. *Molecules*, *26*(17), 5267. https://doi.org/10.3390/molecules26175267

Loganathan, S., Valapa, R. B., Mishra, R. K., Pugazhenthi, G., & Thomas, S. (2017). Thermogravimetric analysis for characterization of nanomaterials. In *Thermal and rheological measurement techniques for nanomaterials characterization* (pp. 67-108). Elsevier. https://doi.org/10.1016/B978-0-323-46139-9.00004-9

López-Juárez, R., Razo-Perez, N., Pérez-Juache, T., Hernandez, O., & Reyes-López, S. (2018). Synthesis of α-Al_2O_3 from aluminum cans by wet-chemical methods. *Results in Physics*, *11*(2018), 1075-1079. https://doi.org/10.1016/j.rinp.2018.11.037

López, J. E., Builes, S., Heredia Salgado, M. A., Tarelho, L. A., Arroyave, C., Aristizábal, A., & Chavez, E. (2020). Adsorption of cadmium using biochars produced from agro-residues. *The Journal of Physical Chemistry C*, *124*(27), 14592-14602. https://doi.org/10.1021/acs.jpcc.0c02216

Loughlaımı, I., Bakher, Z., & Zouhri, A. (2024). Enhanced heavy metal removal from wastewater produced by chemical analysis laboratory using calcium oxide precipitation: pH improvement and characterization of precipitated phases.

Journal of the Turkish Chemical Society Section A: Chemistry, *11*(1), 83–92. https://doi.org/10.18596/jotcsa.1321183

Luque de Castro, M. D., & Luque García, J. L. (2002). Analytical freeze-drying. In *Techniques and Instrumentation in Analytical Chemistry* (Vol. 24, pp. 11-41). Elsevier. https://doi.org/10.1016/S0167-9244(02)80004-X

Mahinroosta, M., & Allahverdi, A. (2018). Enhanced alumina recovery from secondary aluminum dross for high purity nanostructured γ-alumina powder production: Kinetic study. *Journal of environmental management*, *212*(1), 278-291. https://doi.org/10.1016/j.jenvman.2018.02.009

Mahmoud, A. E. D., Al-Qahtani, K. M., Alflaij, S. O., Al-Qahtani, S. F., & Alsamhan, F. A. (2021). Green copper oxide nanoparticles for lead, nickel, and cadmium removal from contaminated water. *Scientific Reports*, *11*(1), 12547. https://doi.org/10.1038/s41598-021-91093-7

Mahmoud, M. E., Amira, M. F., Seleim, S. M., & Mohamed, A. K. (2017). Adsorption isotherm models, kinetics study, and thermodynamic parameters of Ni (II) and Zn (II) removal from water using the LbL technique. *Journal of Chemical & Engineering Data*, *62*(2), 839-850. https://doi.org/10.1021/acs.jced.6b00865

Malakootian, M., Yazdanpanah, G., & Poorjahanshahi, M. (2017). A comparison of the effectiveness of electrocoagulation to coagulation processes using ferric chloride for the removal of cadmium from aqueous solution. *Desalination and Water Treatment*, 78(1), 215–220. https://doi.org/10.5004/dwt.2017.20763

Malathi, S., Sudha, R., Anitha, P., Maheswari, P., Gomathi, M., & Poornima, K. (2020). Removal efficiency of cadmium (II) from electroplating wastewater by chemically modified cottonseed cake carbon. *Desalination and Water Treatment*, *196*(1), 377-387. http://dx.doi.org/10.5004/dwt.2020.25571

Maleki, A., Gharibi, F., Alimohammadi, M., Daraei, H., & Zandsalimi, Y. (2013). Concentration levels of heavy metals in irrigation water and vegetables grown in peri-urban areas of Sanandaj, Iran. *Journal of Advances in Environmental Health Research*, *1*(2), 81-88. https://doi.org/10.22102/jaehr.2013.40129

Maldonado, C. S., De la Rosa, J. R., Lucio-Ortiz, C. J., Valente, J. S., & Castaldi, M. J. (2017). Synthesis and characterization of functionalized alumina catalysts with thiol and sulfonic groups and their performance in producing 5-hydroxymethylfurfural from fructose. *Fuel*, *198*(1), 134-144. https://doi.org/10.1016/j.fuel.2016.10.004

Mallinger, K., & Mergili, M. (2022). The global iron industry and the Anthropocene. *The Anthropocene Review*, *9*(1), 52-70. https://doi.org/10.1177/2053019620982332

Matori, K. A., Wah, L. C., Hashim, M., Ismail, I., & Zaid, M. H. M. (2012). Phase transformations of α-alumina made from waste aluminum via a precipitation

technique. *International journal of molecular sciences*, *13*(12), 16812-16821. https://doi.org/10.3390/ijms131216812

Mayordomo, N., Missana, T., & Alonso, U. (2023). Cadmium Sorption on Alumina Nanoparticles and Mixtures of Alumina and Smectite: An Experimental and Modelling Study. *Minerals, 13*(12), 1534.

McAneney, J. (2005). *Characteristics of thin and ultrathin ferroelectric capacitor structures* [Doctoral thesis, Queen's University]. https://www.researchgate.net/publication/263555725_Characteristics_of_Thin_and_Ultrathin_Ferroelectric_Capacitor_Structures

Melnyk, I. V., Pogorilyi, R. P., Zub, Y. L., Vaclavikova, M., Gdula, K., Dąbrowski, A., ... & Kessler, V. G. (2018). Protection of thiol groups on the surface of magnetic adsorbents and their application for wastewater treatment. *Scientific Reports*, *8*(1), 8592.

Memon, J. R., Memon, S. Q., Bhanger, M. I., Memon, G. Z., El-Turki, A., & Allen, G. C. (2008). Characterization of banana peel by scanning electron microscopy and FT-IR spectroscopy and its use for cadmium removal. *Colloids and Surfaces B: Biointerfaces*, *66*(2), 260-265. https://doi.org/10.1016/j.colsurfb.2008.07.001

Meor, Y. M. S., & Masliana, M. (2007). Synthesis of Alumina using the solvo thermal method. *Malaysian Journal of Analytical Sciences*, *11*(1), 262-268. https://www.ukm.my/mjas/v11_n1/39_493C4_IR_Iz-1.pdf

Mohammadnia, E., hadavifar, M., & Veisi, H. (2020). Adsorption of Cadmium (II) onto Thiolated Graphene Oxide and Kinetic Investigations. *Amirkabir Journal of Civil Engineering*, *52*(1), 275-286. 10.22060/ceej.2018.14660.5710

Morgan, D. J. (2023). XPS insights: Asymmetric peak shapes in XPS. *Surface and Interface Analysis.* https://doi.org/10.1002/sia.7215

Moungomo, J. M., Nganga-Kouya, D., Songmene, V., Kouam, J., & Kenné, J. P. (2016). Machinability study of recycled aluminum cans and machining chips. *The International Journal of Advanced Manufacturing Technology*, *87*(1), 2551-2566. https://doi.org/10.1007/s00170-016-8564-x

Muhaidin, M., Naning, F. H., Saad, J. M., Wahi, R., & Zangina, T. (2024). Heavy metal ion adsorbent in aqueous solution: A review on chitosan and chitosan composites. *Journal of Advanced Research in Micro and Nano Engineering*, *18*(1), 78-102.

Muhamad, E. N., Irmawati, R., Abdullah, A. H., Taufiq-Yap, Y. H., & Hamid, S. A. (2007). Effect of number of washing on the characteristics of copper oxide nanopowders. *Malaysian J. Anal. Sci*, *11*(1), 294-301.

Murty, K. V. G. K., Venkataramanan, M., & Pradeep, T. (1998). Self-assembled monolayers of 1,4-benzenedimethanethiol on polycrystalline silver and gold films: An investigation of structure, stability, dynamics, and reactivity. *Langmuir, 14*(19), 5446-5456. https://doi.org/10.1021/la980249i

Mustapha, S., Shuaib, D. T., Ndamitso, M. M., Etsuyankpa, M. B., Sumaila, A., Mohammed, U. M., et al. (2019). Adsorption isotherm, kinetic and thermodynamic studies for the removal of Pb (II), Cd (II), Zn (II) and Cu (II) ions from aqueous solutions using Albizia lebbeck pods. *Applied water science*, *9*(6), 1-11. https://doi.org/10.1007/s13201-019-1021-x

Muttakin, M., Mitra, S., Thu, K., Ito, K., & Saha, B. B. (2018). Theoretical framework to evaluate minimum desorption temperature for IUPAC classified adsorption isotherms. *International Journal of Heat and Mass Transfer*, *122*(1), 795-805. https://doi.org/10.1016/j.ijheatmasstransfer.2018.01.107

Naihi, H., Baini, R., Yakub, I., & Lai, J. (2022). Cadmium adsorption from aqueous solution using alkali modified oil palm empty fruit bunch. *Biocatalysis and Agricultural Biotechnology*, *44*(1), 102480. https://doi.org/10.1016/j.bcab.2022.102480

Nath, J., Dror, I., Landa, P., Vanek, T., Kaplan-Ashiri, I., & Berkowitz, B. (2018). Synthesis and characterization of isotopically-labeled silver, copper and zinc oxide nanoparticles for tracing studies in plants. *Environmental Pollution*, *242*(Part B), 1827-1837. https://doi.org/10.1016/j.envpol.2018.07.084

New Straits Times. (2023, July 31). Malaysia's population to grow 2.1 percent this year. *New Straits Times.* https://www.nst.com.my/news/nation/2023/07/937061/malaysias-population-grow-21-cent-year

Nieto, M. I., Tallon, C., & Moreno, R. (2006). Synthesis of gamma-alumina nanoparticles by freeze drying. *Advances in Science and Technology*, *45*(1), 223-230. http://dx.doi.org/10.4028/www.scientific.net/AST.45.223

Nishijo, M., Nakagawa, H., Suwazono, Y., Nogawa, K., & Kido, T. (2017). Causes of death in patients with Itai-itai disease suffering from severe chronic cadmium poisoning: a nested case–control analysis of a follow-up study in Japan. *BMJ open*, *7*(7), e015694. https://doi.org/10.1136/bmjopen-2016-015694

Norrman, K. E. (2023). World Population Growth: A Once and Future Global Concern. *World*, *4*(4), 684-697. https://doi.org/10.3390/world4040043

Norvivor, F. A., Azizi, S., Fuku, X., Atibu, E. K., Idris, A. O., Sibali, L., ... & Kamika, I. (2024). Ecological and human health risk of heavy metals in Nubui River: a case of rural remote communities. *Frontiers in Water*, *6*, 1397853.

Ochedi, F. O., Liu, Y., & Hussain, A. (2020). A review on coal fly ash-based adsorbents for mercury and arsenic removal. *Journal of cleaner production*, *267*(1), 122143. https://doi.org/10.1016/j.jclepro.2020.122143

Okon Recycling. (2023, July 5). *HOW MANY ALUMINUM CANS AND PLASTIC WATER BOTTLES ARE NOT RECYCLED EACH YEAR?*. https://www.okonrecycling.com/how-many-aluminum-cans-and-plastic-water-bottles-are-not-recycled-each-year/#:~:text=It's%20estimated%20that%20we%20use,30%20billion%20cans%20to%20landfills

Osman, A. I., Abu-Dahrieh, J. K., Rooney, D. W., Halawy, S. A., Mohamed, M. A., & Abdelkader, A. (2012). Effect of precursor on the performance of alumina for the dehydration of methanol to dimethyl ether. *Applied Catalysis B: Environmental*, *127*(1), 307-315. https://doi.org/10.1016/j.apcatb.2012.08.033

Ouellette, R.J. & Rawn, J.D. (2015). *Organic Chemistry Study Guide.* Elsevier. https://doi.org/10.1016/B978-0-12-801889-7.00003-0.

Oyekanmi, A. A., Latiff, A. A. A., Daud, Z., Mohamed, R. M. S. R., Aziz, N. A. A., Ismail, N., Rafatullah, M., Ahmad, A., & Hossain, K. (2019). Adsorption of pollutants from palm oil mill effluent using natural adsorbents: Optimization and isotherm studies. *Desalin. Water Treat*, *169*(1), 181-190. https://dx.doi.org/%2010.5004/dwt.2019.24689

Oyewo, O. A., Mutesse, B., & Leswifi, T. Y. (2019). Highly efficient removal of nickel and cadmium from water using sawdust-derived cellulose nanocrystals. *Journal of Environmental Chemical Engineering*, 7(4), 103251. https://doi.org/10.1016/j.jece.2019.103251

Pandey, K. (2024, August 26). *81 Indian rivers, tributaries have extremely high concentration of one or more heavy metals*. *Down To Earth*. https://www.downtoearth.org.in/rivers/81-indian-rivers-tributaries-have-extremely-high-concentration-of-one-or-more-heavy-metals

Pang, Y., Zhao, C., Li, Y., Li, Q., Bayongzhong, X., Peng, D., & Huang, T. (2022). Cadmium adsorption performance and mechanism from aqueous solution using red mud modified with amorphous MnO_2. *Scientific Reports*, *12*(1), 4424. https://doi.org/10.1038/s41598-022-08451-2

Parida, K. M., Pradhan, A. C., Das, J., & Sahu, N. (2009). Synthesis and characterization of nano-sized porous gamma-alumina by control precipitation method. *Materials Chemistry and physics*, *113*(1), 244-248. https://doi.org/10.1016/j.matchemphys.2008.07.076

Park, Y., Ayoko, G. A., & Frost, R. L. (2011). Characterisation of organoclays and adsorption of p-nitrophenol: environmental application. *Journal of colloid and interface science*, *360*(2), 440-456. https://doi.org/10.1016/j.jcis.2011.04.085

Pasquali, L., Terzi, F., Zanardi, C., Pigani, L., Seeber, R., Paolicelli, G., Suturin, S. M., Mahne, N., & Nannarone, S. (2007). Structure and properties of 1,4-benzenedimethanethiol films grown from solution on Au(111): An XPS and NEXAFS study. *Surface Science, 601*(5), 1419-1427. https://doi.org/10.1016/j.susc.2007.01.007

Pawlas, J., Svensson, T., & Rasmussen, J. H. (2019). 1,4-Benzenedimethanethiol (1,4-BDMT) as a scavenger for greener peptide resin cleavages. *RSC Advances, 9*(67), 38928-38934. https://doi.org/10.1039/C9RA08553J

Perez-Catán, S., & Guraya, M. (2015). High porous gamma-alumina synthesized by a modified sol-gel technique. *Int. J. Mater. Sci*, *5*(2), 33-39.

Pohl, A. (2020). Removal of heavy metal ions from water and wastewaters by sulfur-containing precipitation agents. *Water, Air, & Soil Pollution*, *231*(10), 503. https://doi.org/10.1007/s11270-020-04863-w

Prabhu, P. P., & Prabhu, B. (2018). A review on removal of heavy metal ions from waste water using natural/modified bentonite. In *MATEC Web of conferences* (Vol. 144, p. 02021). EDP Sciences. https://doi.org/10.1051/matecconf/201814402021

Prins, R. (2020). On the structure of γ-Al_2O_3. *Journal of Catalysis*, *392*(1), 336-346. https://doi.org/10.1016/j.jcat.2020.10.010

Puthirath Balan, A., Radhakrishnan, S., Woellner, C. F., Sinha, S. K., Deng, L., Reyes, C. D. L., Rao, B.M., Paulose, M., Neupane, R., Apte, A., Kochat, V., Vajtai., R., Harutyunyan, A.R., Chu, C.W., Costin, G., Galvao, D.S., Martí, A.A., van Aken, P.A., Varghese, O.K., ...Ajayan, P. M. (2018). Exfoliation of a non-van der Waals material from iron ore hematite. *Nature nanotechnology*, *13*(7), 602-609. https://doi.org/10.1038/s41565-018-0134-y

Radi, S., El Abiad, C., Moura, N. M., Faustino, M. A., & Neves, M. G. P. (2019). New hybrid adsorbent based on porphyrin functionalized silica for heavy metals removal: synthesis, characterization, isotherms, kinetics and thermodynamics studies. *Journal of hazardous materials*, *370*(1), 80-90. https://doi.org/10.1016/j.jhazmat.2017.10.058

Raevskaya, A., Rozovik, O., Novikova, A., Selyshchev, O., Stroyuk, O., Dzhagan, V., Goryacheva, I., Gaponik, N., Zahn, D. R. T., & Eychmuller, A. (2018). Luminescence and photoelectrochemical properties of size-selected aqueous copper-doped Ag–In–S quantum dots. *RSC advances*, *8*(14), 7550-7557. https://doi.org/10.1039/C8RA00257F

Rahman, R., & Upadhyaya, H. (2021). Aluminium toxicity and its tolerance in plant: A review. *Journal of Plant Biology*, *64*(2), 101-121. https://doi.org/10.1007/s12374-020-09280-4

Rajabi, M., Najafi, F., Moradi, O., Mirza, B., & Thakur, V. K. (2018). Chapter 8 - Nanopolymers: Graphene and functionalization. In V. K. Thakur (Ed.), *Biopolymer grafting: Synthesis and properties* (pp. 365-407). Elsevier. https://doi.org/10.1016/B978-0-323-48104-5.00008-1

Rehman, M., Liu, L., Wang, Q., Saleem, M. H., Bashir, S., Ullah, S., & Peng, D. (2019). Copper environmental toxicology, recent advances, and future outlook: a review. *Environmental science and pollution research*, *26*(1), 18003-18016. https://doi.org/10.1007/s11356-019-05073-6

Ren, B., Weitzel, K. A., Duan, X., Nadagouda, M. N., & Dionysiou, D. D. (2022). A comprehensive review on algae removal and control by coagulation-based processes: mechanism, material, and application. *Separation and Purification Technology*, *293*(1), 121106. https://doi.org/10.1016/j.seppur.2022.121106

Rozita, Y., Brydson, R., & Scott, A. J. (2010). An investigation of commercial gamma-Al_2O_3 nanoparticles. In *Journal of Physics: Conference Series* (Vol. 241, No. 1, p. 012096). IOP Publishing. 10.1088/1742-6596/241/1/012096

Rustagi, N., & Singh, R. (2010). Mercury and health care. *Indian Journal of Occupational and Environmental Medicine*, *14*(2), 45-48. 10.4103/0019-5278.72240

Ruzi, I. I., Ishak, A. R., Abdullah, M. A., Zain, N. N. M., Tualeka, A. R., & Aziz, M. Y. (2023). Assessment of Heavy Metal Concentrations in Penang, Malaysia's Wastewater Treatment Plants: A Wastewater-Based Epidemiology Approach. *Trends in Sciences*, *20*(5), 6523-6523. https://doi.org/10.48048/tis.2023.6523

Ryu, J., Lee, M. Y., Song, M. G., Baeck, S. H., Shim, S. E., & Qian, Y. (2020). Highly selective removal of Hg (II) ions from aqueous solution using thiol-modified porous polyaminal-networked polymer. *Separation and purification technology*, *250*(1), 117120. https://doi.org/10.1016/j.seppur.2020.117120

Saadatkhah, N., Carillo Garcia, A., Ackermann, S., Leclerc, P., Latifi, M., Samih, S., et al. (2020). Experimental methods in chemical engineering: Thermogravimetric analysis—TGA. *The Canadian Journal of Chemical Engineering*, *98*(1), 34-43. https://doi.org/10.1002/cjce.23673

Sadraei, R. (2020). Fast, green and easy adsorption of dye and emerging contaminants by functionalized γ-AACH. *Journal of Environmental Chemical Engineering*, *8*(4), 103616.

Saeed, A. A. H., Harun, N. Y., Nasef, M. M., Al-Fakih, A., Ghaleb, A. A. S., & Afolabi, H. K. (2022). Removal of cadmium from aqueous solution by optimized rice husk biochar using response surface methodology. *Ain Shams Engineering Journal*, *13*(1), 101516. https://doi.org/10.1016/j.asej.2021.06.002

Sahmoune, M. N. (2019). Evaluation of thermodynamic parameters for adsorption of heavy metals by green adsorbents. *Environmental Chemistry Letters*, *17*(2), 697-704. https://doi.org/10.1007/s10311-018-00819-z

Said, S., Mikhail, S., & Riad, M. (2020). Recent processes for the production of alumina nano-particles. *Materials Science for Energy Technologies*, *3*, 344-363.

Sáiz, L. M., Prolongo, M. G., Bonache, V., Jiménez-Suárez, A., & Prolongo, S. G. (2023). Self-healing materials based on disulfide bond-containing acrylate networks. *Polymer Testing*, *117(1)*, 107832. https://doi.org/10.1016/j.polymertesting.2022.107832

Salahudeen, N., Ahmed, A. S., Ala'a, H., Dauda, M., Waziri, S. M., & Jibril, B. Y. (2015). Synthesis of gamma alumina from Kankara kaolin using a novel technique. *Applied Clay Science*, *105-106*(1), 170-177. https://doi.org/10.1016/j.clay.2014.11.041

Salam, M. A., Paul, S. C., Zain, R. A. M. M., Bhowmik, S., Nath, M. R., Siddiqua, S. A., Aka, T.D., Iqbal, M.A., Kadir, W.R., Ahamad, R., Khaleque, M. A., Rak, A.E., & Amin, M.F.M.et al. (2020). Trace metals contamination potential and health risk assessment of commonly consumed fish of Perak River, Malaysia. *PLoS One*, *15*(10), e0241320. https://doi.org/10.1371/journal.pone.0241320

Salazar Alarcón, L., Chen, L., Esaulov, V. A., Gayone, J. E., Sánchez, E. A., & Grizzi, O. (2010). Thiol terminated 1,4-benzenedimethanethiol self-assembled monolayers on Au(111) and InP(110) from vapor phase. *The Journal of Physical Chemistry C*, *114*(47), 19993-19999. https://doi.org/10.1021/jp1044157

Salazar Alarcón, L., Cristina, L. J., Jia, J., Chen, L., Giglia, A., Pasquali, L., Sánchez, E. A., Esaulov, V. A., & Grizzi, O. (2017). Adsorption and thermal stability of 1,4-benzenedimethanethiol on InP(110). *Surface Science*, *664*(1), 101-109. https://doi.org/10.1016/j.susc.2017.06.003

Santhamoorthy, M., Thirumalai, D., Thirupathi, K., & Kim, S. C. (2023). Synthesis of dithiol-modified mesoporous silica adsorbent for selective adsorption of mercury ions from wastewater. *Applied Nanoscience*, *13*(9), 6015-6024. https://doi.org/10.1007/s13204-022-02531-5

Santhamoorthy, M., Thirupathi, K., Thirumalai, D., Aldawood, S., & Kim, S. C. (2022). Surface grafted silica adsorbent for efficient removal of Hg^{2+} ions from contaminated water. *Environmental Research*, *212*(Part A), 113211. https://doi.org/10.1016/j.envres.2022.113211

Sengupta, D. (2023, November 17). US aluminium scrap exports to Malaysia record a 7% M-o-M drop in contrast to the hike in total exports. *Recycled Aluminium News – Market.* https://www.alcircle.com/news/us-aluminium-scrap-exports-

to-malaysia-record-a-7-m-o-m-drop-in-contrast-to-the-hike-in-total-exports-102973

Shahbudin, N. R., & Kamal, N. A. (2021). Establishment of material flow analysis (MFA) for heavy metals in a wastewater system. *Ain Shams Engineering Journal*, *12*(2), 1407-1418. https://doi.org/10.1016/j.asej.2020.10.009

Shahidian, Z., Zare, K., & Mousavi Safavi, S. M. (2020). Modification of Mesopore Extrudate Gamma Alumina through Thermal Ammonia Treatment. *Iranian Journal of Chemistry and Chemical Engineering*, *39*(3), 61-69. https://doi.org/10.30492/ijcce.2020.34742

Shaifudin, N. I., Sharif, A. M., & Yahaya, R. (2023). Effect of alumina and thiol's roles for Hg^{2+} adsorption in wastewater–a short review. *Malaysian Journal of Microscopy*, *19*(1), 361-373. https://malaysianjournalofmicroscopy.org/ojs/index.php/mjm/article/view/685/404

Shamsudin, R. (2016). *Kenaf bast fiber filter cartridge for removal of heavy metals and dyes in aqueous solution* [Doctoral dissertation, Universiti Pendidikan Sultan Idris]. UPSI Digital Repository (UDRep). https://ir.upsi.edu.my/doc.php?t=p&id=e09fdb36d03ed32cd1abc259b9b3c776669e7d1cb0202

Sharif, A. M., Wan Mahamod, W. R., Abu Bakar, N., Abdul Rahim, N., Mustafar, S., Rosmi, M. S., & Norazan, M. (2018). The effect of pH on the arrangement of 5CB based liquid crystal containing BDMT-mercury complex using polarized optical microscope. *Chemistry Letters*, *47*(4), 494-496. https://doi.org/10.1246/cl.171169

Sharma, S. K., Das, P., & Sanfui, B. K. (2022). Unveiling the role of structure–property correlation and its validation towards engineering the application potential of sol–gel derived mesoporous gamma-alumina. *Molecular Systems Design & Engineering*, *7*(1), 67-91. https://doi.org/10.1039/D1ME00102G

Sheel, T. K., Poddar, P., Murad, A. B. M. W., Neger, A. J. M. T., & Chowdhury, A. M. S. (2016). Preparation of aluminum oxide from industrial waste can available in Bangladesh environment: SEM and EDX analysis. *J. Adv. Chem. Eng*, *6*(2), 1-5. https://doi.org/10.4172/2090-4568.1000152

Shen, Y., Jiang, N., Liu, S., Zheng, C., Wang, X., Huang, T., et al. (2018). Thiol functionalization of short channel SBA-15 through a safe, mild and facile method and application for the removal of mercury (II). *Journal of environmental chemical engineering*, *6*(4), 5420-5433. https://doi.org/10.1016/j.jece.2018.08.030

Shutthanandan, V., Nandasiri, M., Zheng, J., Engelhard, M. H., Xu, W., Thevuthasan, S., Murugesan, V. (2019). Applications of XPS in the characterization of

Battery materials. *Journal of Electron Spectroscopy and Related Phenomena*, *231*(1), 2-10. https://doi.org/10.1016/j.elspec.2018.05.005

Sifontes, Á. B., Gutierrez, B., Mónaco, A., Yanez, A., Díaz, Y., Méndez, F. J., Llovera, L., Cañizales, E., & Brito, J. L. (2014). Preparation of functionalized porous nano-γ-Al_2O_3 powders employing colophony extract. *Biotechnology Reports, 4*(1), 21-29. https://doi.org/10.1016/j.btre.2014.07.001

Silva-Holguín, P. N., Medellín-Castillo, N. A., Zaragoza-Contreras, E. A., & Reyes-López, S. Y. (2023). Alumina–Hydroxyapatite Millimetric Spheres for Cadmium (II) Removal in Aqueous Medium. *ACS omega*, *8*(47), 44675-44688. https://doi.org/10.1021/acsomega.3c05418

Singh, B. P., Choudhary, V., Teotia, S., Gupta, T. K., Singh, V. N., Dhakate, S. R., & Mathur, R. B. (2015). Solvent free, efficient, industrially viable, fast dispersion process based amine modified MWCNT reinforced epoxy composites of superior mechanical properties. *Adv. Mater. Lett*, *6*(2), 104-113.

Singh, S. (2024, April 2). Eight sick from eating mussels in PD, two in intensive care. *The Star*. https://www.thestar.com.my/news/nation/2024/04/02/eight-sick-from-eating-mussels-in-pd-two-in-intensive-care

Singh, S., Basu, H., Bassan, M. K. T., & Singhal, R. K. (2022). Thiol functionalised silica microsphere loaded polymeric hydrogel: Development of a novel hybrid sorbent for removal of lead and cadmium. *Chemosphere*, *286*(1), 131659. https://doi.org/10.1016/j.chemosphere.2021.131659

Singh, S., Srivastava, V. C., Mandal, T. K., & Mall, I. D. (2014). Synthesis of different crystallographic Al_2O_3 nanomaterials from solid waste for application in dye degradation. *RSC Advances*, *4*(92), 50801-50810. https://doi.org/10.1039/C4RA08842E

Siril, P. F., Shiju, N. R., Brown, D. R., & Wilson, K. (2009). Optimising catalytic properties of supported sulfonic acid catalysts. *Applied Catalysis A: General*, *364*(1-2), 95-100. https://doi.org/10.1016/j.apcata.2009.05.032

Siswoyo, E., Endo, N., Mihara, Y., & Tanaka, S. (2014). Agar-encapsulated adsorbent based on leaf of Platanus sp. to adsorb cadmium ion in water. *Water Science & Technology*, *70*(1), 151-157. https://doi.org/10.2166/wst.2014.190

Smajic, J., Alazmi, A., Wehbe, N., & Da Costa, P. M. (2021). Graphitic Cathodes for Aluminum Batteries with Aqueous Electrolytes. http://dx.doi.org/10.33774/chemrxiv-2021-q1rw1-v2

Sri Priya, S. (2022, June 25). Resolute Recycling. *The Star*. https://www.thestar.com.my/metro/metro-news/2022/06/25/resolute-recycling

Sulaiman, F. R., Ibrahim, N. H., & Syed Ismail, S. N. (2020). Heavy metal (As, Cd, and Pb) concentration in selected leafy vegetables from Jengka, Malaysia, and potential health risks. *SN Applied Sciences*, *2*(8), 1430. https://doi.org/10.1007/s42452-020-03231-x

Sun, J., Li, X., Ai, X., Liu, J., Yin, Y., Huang, Y., Zhou, H., & Huang, K. (2018). Efficient removal of cadmium from soil-washing effluents by garlic peel biosorbent. *Environmental Science and Pollution Research*, *25*(19), 19001-19011. https://doi.org/10.1007/s11356-018-2109-9

Tabereaux, A. T., & Peterson, R. D. (2024). Aluminum production. In S. Seetharaman, R. Guthrie, A. McLean, S. Seetharaman, & H. Y. Sohn (Eds.), *Treatise on process metallurgy* (2nd ed., pp. 625–676). Elsevier. https://doi.org/10.1016/B978-0-323-85373-6.00004-1

Tahoon, M. A., Siddeeg, S. M., Salem Alsaiari, N., Mnif, W., & Ben Rebah, F. (2020). Effective heavy metals removal from water using nanomaterials: A review. *Processes*, *8*(6), 645. https://doi.org/10.3390/pr8060645

Tan, T. L., Nakajima, H., & Rashid, S. A. (2020). Adsorptive, kinetics and regeneration studies of fluoride removal from water using zirconium-based metal organic frameworks. *RSC advances*, *10*(32), 18740-18752. https://doi.org/10.1039/D0RA01268H

Thabet, M. S., & Ismaiel, A. M. (2016). Sol-gel γ-Al_2O_3 nanoparticles assessment of the removal of eosin yellow using: adsorption, kinetic and thermodynamic parameters. *Journal of Encapsulation and Adsorption Sciences*, *6*(03), 70. http://dx.doi.org/10.4236/jeas.2016.63007

The Aluminium Association. (2021). *The Aluminium Can Advantage*. https://www.aluminum.org/canadvantage

Tonlé, I. K., Ngameni, E., Tcheumi, H. L., Tchiéda, V., Carteret, C., & Walcarius, A. (2008). Sorption of methylene blue on an organoclay bearing thiol groups and application to electrochemical sensing of the dye. *Talanta*, *74*(4), 489-497. https://doi.org/10.1016/j.talanta.2007.06.006

Tran, H. N., You, S. J., & Chao, H. P. (2016). Thermodynamic parameters of cadmium adsorption onto orange peel calculated from various methods: A comparison study. *Journal of Environmental Chemical Engineering*, *4*(3), 2671-2682. https://doi.org/10.1016/j.jece.2016.05.009

Tuguhiro, T. A. G. O., Kataoka, N., Tanaka, H., Kinoshita, K., & Kishida, S. (2017). XPS study from a clean surface of Al_2O_3 single crystals. *Procedia engineering*, *216*(1), 175-181. https://doi.org/10.1016/j.proeng.2018.02.081

Tumolo, M., Ancona, V., De Paola, D., Losacco, D., Campanale, C., Massarelli, C., & Uricchio, V. F. (2020). Chromium pollution in European water, sources, health risk, and remediation strategies: An overview. *International journal of*

environmental research and public health, *17*(15), 5438. https://doi.org/10.3390/ijerph17155438

Unsal, V., Dalkıran, T., Çiçek, M., & Kölükçü, E. (2020). The role of natural antioxidants against reactive oxygen species produced by cadmium toxicity: a review. *Advanced pharmaceutical bulletin*, *10*(2), 184. https://doi.org/10.34172%2Fapb.2020.023

Urbonavicius, M., Varnagiris, S., Pranevicius, L., & Milcius, D. (2020). Production of gamma alumina using plasma-treated aluminum and water reaction byproducts. *Materials*, *13*(6), 1300. https://doi.org/10.3390/ma13061300

Velázquez Martí, B., Gaibor-Chavez, J., López Cortés, I., & Olivares Aguilar, L. E. (2023). Evaluation of the Intermediate Values of the TGA Curves as Indicators of the Proximal Analysis of Biomass. *Agronomy*, *13*(10), 2552. https://doi.org/10.3390/agronomy13102552

Velempini, T., & Pillay, K. (2019). Sulphur functionalized materials for Hg (II) adsorption: A review. *Journal of environmental Chemical engineering*, *7*(5), 103350. https://doi.org/10.1016/j.jece.2019.103350

Venkataramanan, M., & Pradeep, T. (2000). Surface resistance investigations of the exchange of 3D monolayers with molecules self-assembled on planar gold surfaces. *Chemical Physics Letters*, *327*(5-6), 299-304. https://doi.org/10.1016/S0009-2614(00)00884-8

Vermeulen, C., Gijs, L., & Collin, S. (2005). Sensorial Contribution and Formation Pathways of Thiols in Foods: A Review. *Food Reviews International*, *21*(1), 69–137. https://doi.org/10.1081/FRI-200040601

Vinayan, B. P., Zhao-Karger, Z., Diemant, T., Chakravadhanula, V. S. K., Schwarzburger, N. I., Cambaz, M. A., Behm, R. J., Kubel, C., Fichtner, M. (2016). Performance study of magnesium–sulfur battery using a graphene based sulfur composite cathode electrode and a non-nucleophilic Mg electrolyte. *Nanoscale*, *8*(6), 3296-3306. https://doi.org/10.1039/C5NR04383B

Wahyono, T., Astuti, D. A., Wiryawan, I. K. G., Sugoro, I., & Jayanegara, A. (2019). Fourier transform mid-infrared (FTIR) spectroscopy to identify tannin compounds in the panicle of sorghum mutant lines. *IOP Conference Series: Materials Science and Engineering*, *546*(4), 042045. https://doi.org/10.1088/1757-899X/546/4/042045

Wahyuhadi, M. E., Kusumadewi, R. A., & Hadisoebroto, R. (2023). Effect of Contact Time on The Adsorption Process of Activated Carbon from Banana Peel in Reducing Heavy Metal Cd and Dyes Using a Stirring Tub (Pilot Scale). In *IOP Conference Series: Earth and Environmental Science* (Vol. 1203, No. 1, p. 012035). IOP Publishing. 10.1088/1755-1315/1203/1/012035

Wang, G., Guo, K., Wang, B., Han, F., Guo, Z., Song, Z., et al. (2021). Mercury adsorption on thiol-modified porous boron nitride: a combined experimental and theoretical investigation. *Industrial & Engineering Chemistry Research*, *60*(35), 12984-12998. https://doi.org/10.1021/acs.iecr.1c01530

Wang, S., Li, X., Wang, S., Li, Y., & Zhai, Y. (2008). Synthesis of γ-alumina via precipitation in ethanol. *Materials Letters, 62*(17-18), 3552-3554. https://doi.org/10.1016/j.matlet.2008.03.048

Wang, T., Jiang, M., Yu, X., Niu, N., & Chen, L. (2022). Application of lignin adsorbent in wastewater treatment: A review. *Separation and Purification Technology, 302*, 122116. https://doi.org/10.1016/j.seppur.2022.122116

Wang, X., Li, W., Harrington, R., Liu, F., Parise, J. B., Feng, X., & Sparks, D. L. (2013). Effect of ferrihydrite crystallite size on phosphate adsorption reactivity. *Environmental Science & Technology, 47*(18), 10322–10331. https://doi.org/10.1021/es401301z

Wang, Y., Wang, J., Shen, M., & Wang, W. (2009). Synthesis and properties of thermostable γ-alumina prepared by hydrolysis of phosphide aluminum. *Journal of Alloys and Compounds, 467*(1-2), 405-412. https://doi.org/10.1016/j.jallcom.2007.12.007

Weerasundara, L., Ok, Y. S., & Bundschuh, J. (2021). Selective removal of arsenic in water: A critical review. *Environmental Pollution*, *268*(1), 115668. https://doi.org/10.1016/j.envpol.2020.115668

White, J. L., Rowberg, A. J., Wan, L. F., Kang, S., Ogitsu, T., Kolasinski, R. D., Whaley, J.A., Baker, A. A., Lee, J. R. I., Liu, Y. S., Trotochaud, L., Guo, J., Stavila, V, Prendergast, D., Bluhm, H, Allendorf, M. D., Wood, B., & Gabaly, F. E. (2019). Identifying the role of dynamic surface hydroxides in the dehydrogenation of Ti-doped $NaAlH_4$. *ACS applied materials & interfaces*, *11*(5), 4930-4941. https://doi.org/10.1021/acsami.8b17650

Wong, C. W., Barford, J. P., & Chen, G. (2014). Kinetics and equilibrium studies for the removal of cadmium ions by ion exchange resin. *Journal of Environmental Chemical Engineering, 2*(1), 698–707

Wu, X., Wang, Z., Shao, G., Qin, B., Wang, Y., Wang, T., Liu, Z., & Fu, Y. (2024). Supramolecular cellulose-based heavy metal adsorbent for efficient and accurate removal of cobalt (II) for water treatment. *Reactive and Functional Polymers*, *194*(1), 105759. https://doi.org/10.1016/j.reactfunctpolym.2023.105759

Xia, Z., Baird, L., Zimmerman, N., & Yeager, M. (2017). Heavy metal ion removal by thiol functionalized aluminum oxide hydroxide nanowhiskers. *Applied Surface Science*, *416*(1), 565-573. https://doi.org/10.1016/j.apsusc.2017.04.095

Yahaya, R., Brydson, R., Comyn, T., Scott, A., Hammond, C., Brown, A., Chauruka, S., Hassanpour, A., Young, N., Kirkland, A., Sawada, H., & Smith, R. (2013). A study of commercial nanoparticulate γ-Al_2O_3 catalyst supports. *ChemCatChem*, *5*(9), 2695-2706. https://doi.org/10.1002/cctc.201200880

Yahaya, R., Brydson, R., Scott, A., Comyn, T., Hammond, C., Brown, A., Ward, M., Hondow, N., Young, N., Kirkland, A., Paglia, G., Buckley, C., Brown, G., Kirkland, R., & Bleloch, A. (n.d.). High resolution transmission electron microscopy study of surface reconstruction on faceted cubeoctahedral γ-Al_2O_3 nanoparticles. https://www.researchgate.net/publication/267408211_High_resolution_transmission_electron_microscopy_study_of_surface_reconstruction_on_faceted_cubeoctahedral_g-Al_2_O_3_nanoparticles

Yahaya, R., Zainol, I., Ul-Hamid, A., Bahruji, H., Shah, R. M. R. A., Jasinih, M. H., & Salleh, R. (2021). Synthesis of facetted gamma alumina nanoparticles from waste beverage aluminium cans for potential catalyst support applications. *Malaysian Journal of Microscopy*, *17*(2). https://malaysianjournalofmicroscopy.org/ojs/index.php/mjm/article/view/564/290

Yang, D., Paul, B., Xu, W., Yuan, Y., Liu, E., Ke, X., ... & Zhu, H. (2010). Alumina nanofibers grafted with functional groups: a new design in efficient sorbents for removal of toxic contaminants from water. *Water research*, *44*(3), 741-750.

Yi, J. H., Sun, Y. Y., Gao, J. F., & Xu, C. Y. (2009). Synthesis of crystalline γ-Al_2O_3 with high purity. *Transactions of Nonferrous Metals Society of China*, *19*(5), 1237-1242. https://doi.org/10.1016/S1003-6326(08)60435-5

Yu, Y., Liu, J., Yang, Y., Ding, J., & Zhang, A. (2021). Experimental and theoretical studies of cadmium adsorption over Fe_2O_3 sorbent in incineration flue gas. *Chemical Engineering Journal*, *425*(1), 131647. https://doi.org/10.1016/j.cej.2021.131647

Yunus, K., Zuraidah, M. A., & John, A. (2020). A review on the accumulation of heavy metals in coastal sediment of Peninsular Malaysia. *Ecofeminism and Climate Change*, *1*(1), 21-35. https://doi.org/10.1108/EFCC-03-2020-0003

Yusuff, A. S**.** (2019). Adsorption of hexavalent chromium from aqueous solution by *Leucaena leucocephala* seed pod activated carbon: Equilibrium, kinetic, and thermodynamic studies. *Arab Journal of Basic and Applied Sciences, 26*(1), 1–14. https://doi.org/10.1080/25765299.2019.1567656

Yusuff, A. S., Popoola, L. T., & Babatunde, E. O. (2019). Adsorption of cadmium ion from aqueous solutions by copper-based metal organic framework: equilibrium modeling and kinetic studies. *Applied water science*, *9*(4), 1-11. https://doi.org/10.1007/s13201-019-0991-z

Zainal, F. (2024, January 2). 39,000 tonnes of solid waste daily. *The Star*. https://www.thestar.com.my/news/nation/2024/01/02/39000-tonnes-of-solid-waste-daily

Zanon, M. R., Ishak, A. R., Waras, M. N., & others. (2023). *Assessment of Potential Health Risks Associated with Heavy Metal Contamination in Drinking Water in the Kulim Hi Tech Park (KHTP) Region of Malaysia* (Version 1). Research Square. https://doi.org/10.21203/rs.3.rs-2641089/v1

Zhang, H., Gao, S., Cao, X., Lin, J., Feng, J., Wang, H., Pan, H., Yang, Q., Lou, Y., & Zhuge, Y. (2023). Cd Removal from Aqueous Solutions Using a New Modified Zeolite Adsorbent. *Minerals*, *13*(2), 197. https://doi.org/10.3390/min13020197

Zhang, H., Ma, J., Wang, F., Chu, Y., Yang, L., & Xia, M. (2020). Mechanism of carboxymethyl chitosan hybrid montmorillonite and adsorption of Pb (II) and Congo red by CMC-MMT organic-inorganic hybrid composite. *International journal of biological macromolecules*, *149*(1), 1161-1169. https://doi.org/10.1016/j.ijbiomac.2020.01.201

Zhang, J., Xiong, Z., Li, C., & Wu, C. (2016). Exploring a thiol-functionalized MOF for elimination of lead and cadmium from aqueous solution. *Journal of Molecular Liquids*, *221*(1), 43-50. https://doi.org/10.1016/j.molliq.2016.05.054

Zhang, L., Zhao, Y.-H., & Bai, R. (2011). Development of a multifunctional membrane for chromatic warning and enhanced adsorptive removal of heavy metal ions: Application to cadmium. *Journal of Membrane Science*, 379(1-2), 69–79. https://doi.org/10.1016/j.memsci.2011.05.044

Zhao, X., Zhao, H., Huang, X., Wang, L., Liu, F., Hu, X., Li, J., Zhang, G., & Ji, P. (2021). Effect and mechanisms of synthesis conditions on the cadmium adsorption capacity of modified fly ash. *Ecotoxicology and Environmental Safety*, *223*(1), 112550. https://doi.org/10.1016/j.ecoenv.2021.112550

Zheng, K., Loh, K. Y., Wang, Y., Chen, Q., Fan, J., Jung, T., Nam, S. H., Suh, Y. D., & Liu, X. (2019). Recent advances in upconversion nanocrystals: Expanding the kaleidoscopic toolbox for emerging applications. *Nano Today, 29(1),* 100797. https://doi.org/10.1016/j.nantod.2019.100797

Zoroddu, M. A., Aaseth, J., Crisponi, G., Medici, S., Peana, M., & Nurchi, V. M. (2019). The essential metals for humans: a brief overview. *Journal of inorganic biochemistry*, *195*(1), 120-129. https://doi.org/10.1016/j.jinorgbio.2019.03.013

APPENDIX

Calibration curve of standard solutions for AAS analysis

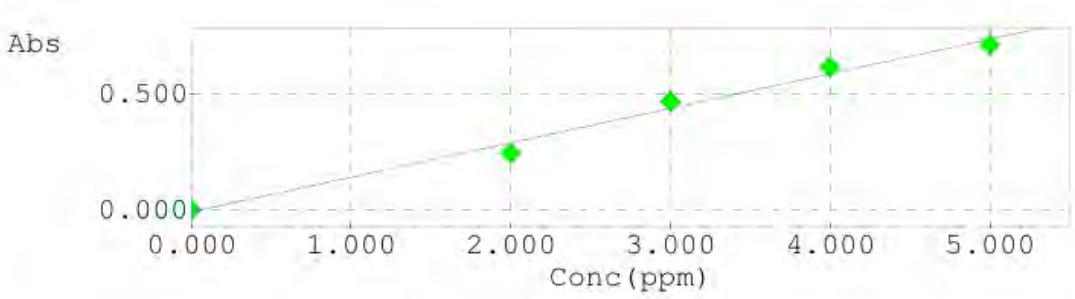

Abs=0.14915Conc-0.0087838

r=0.9936

05-4506832 pustaka.upsi.edu.my Perpustakaan Tuanku Bainun Kampus Sultan Abdul Jalil Shah PustakaTBainun ptbupsi